High-Performance Concrete for Bridge 8F in Frederica

by

Michael J. Chajes
Degang Li
Harry W. Shenton III
Dennis R. Mertz

Department of Civil and Environmental Engineering
University of Delaware

March 2003

DELAWARE CENTER FOR TRANSPORTATION

University of Delaware
355 DuPont Hall
Newark, Delaware 19716
(302) 831-1446

High-Performance Concrete for Bridge 8F in Frederica

by

MICHAEL J. CHAJES
DEGANG LI
HARRY W. SHENTON III
DENNIS R. MERTZ

Department of Civil and Environmental Engineering
University of Delaware
Newark, Delaware 19716

DELAWARE CENTER FOR TRANSPORTATION
University of Delaware
Newark, Delaware 19716

This work was sponsored by the Delaware Center for Transportation and was prepared in cooperation with the Delaware Department of Transportation. The contents of this report reflect the views of the authors who are responsible for the facts and accuracy of the data presented herein. The contents do not necessarily reflect the official views of the Delaware Center for Transportation or the Delaware Department of Transportation at the time of publication. This report does not constitute a standard, specification, or regulation.

The Delaware Center for Transportation is a university-wide multi-disciplinary research unit reporting to the Chair of the Department of Civil and Environmental Engineering, and is co-sponsored by the University of Delaware and the Delaware Department of Transportation.

DCT Staff

Ardeshir Faghri
Director

Jerome Lewis
Associate Director

Wanda L. Taylor
Assistant to the Director

Lawrence H. Klepner
T^2 Program Coordinator

DCT Policy Council

Carolann Wicks, Co-Chair
Acting Chief Engineer, Delaware Department of Transportation

Eric Kaler, Co-Chair
Dean, College of Engineering

Timothy K. Barnekov
Acting Dean, College of Human Resources, Education and Public Policy

The Honorable Timothy Boulden
Chair, Delaware House of Representatives Transportation Committee

Michael J. Chajes
Chair, Civil and Environmental Engineering

Kevin Coyle
Representative of the Secretary of the Delaware Department of Natural Resources and Environmental Control

The Honorable Tony DeLuca
Chair, Delaware Senate Transportation Committee

Raymond C. Miller
Director, Delaware Transit Corporation

Donna Murray
Representative of the Director of the Delaware Development Office

Ralph A. Reeb
Director of Planning, Delaware Department of Transportation

Delaware Center for Transportation
University of Delaware
Newark, DE 19716
(302) 831-1446

High-Performance Concrete for Bridge 8F in Frederica

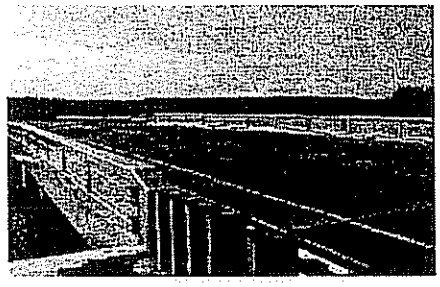

Final Report

by
Michael J. Chajes
Degang Li
Harry W. Shenton III
Dennis R. Mertz

Department of Civil and Environmental Engineering
University of Delaware

March 2003

Table of Contents

EXECUTIVE SUMMARY

Decades of exposure to traffic and the elements have left almost one-third of the nation's 582,000 bridges structurally deficient or functionally obsolete. Although these bridges are not necessarily unsafe, they are often inadequate for carrying the high traffic volumes and heavy traffic loads common on today's highways. Many of these bridges will soon require extensive repair or even replacement.

The condition of our bridges also creates problems for shippers and motorists. As load restrictions are imposed on deficient bridges, vehicles must be diverted to other routes. This can increase trip length, exacerbate congestion, and direct traffic into residential neighborhoods. Projects to repair or replace these bridges create work zones that delay traffic and can endanger workers and motorists.

To prevent such problems, highway agencies need to build bridges that are better able to withstand traffic and environmental demands. These bridges must also be economical to build and maintain. High Performance Concrete (HPC), which is concrete that has been designed to be more durable, and, if necessary, stronger than conventional concrete, can help highway agencies achieve these goals.

The primary objective of this project was to gain an understanding of the actual post-construction performance of HPC bridge structures from both materials and structural behavior perspectives, based on the design and construction of Bridge 8F in Frederica, Delaware.

In 1999, the Delaware Department of Transportation (DelDOT) received funds through the Federal Highway Administration's Innovative Bridge Research and

Construction (IBRC) Program to design and construct an HPC bridge. A two-span, prestressed concrete, adjacent box beam bridge utilizing HPC in both the beams and deck was designed. The beams for the bridge were fabricated by Concrete Building Systems (CBS) in Delmar, Delaware. The bridge replaced a deteriorated four-span structure. Since CBS is a relatively small precast plant with no prior experience with HPC bridges, the outcome of this project is of special interest to DelDOT.

The existing bridge consisted of four 28 ft. 5 in. spans supported by concrete encased I-beams resting on solid concrete piers and abutments. The bridge was built in 1920 and rehabilitated in 1992. It was classified as structurally deficient due to considerable spalling and salt infiltration of the piers, abutments, and fascia beams. Soil conditions (clay layers beneath the marsh) had caused the structure and approach roadway to settle over the years. These problems led DelDOT to pursue bridge replacement.

The HPC replacement bridge comprises two 62 ft. 4 in. spans consisting of adjacent prestressed concrete box beams with a concrete deck to make the structure continuous for live load. The center pier uses 18-in.-square precast concrete piles with a cast-in-place pier cap. Each abutment consists of a continuous wall made of 16 in. by 48 in. precast concrete sheet piles with a cast-in-place abutment cap. HPC is used throughout the bridge (beams, sheet piles, and deck) with low permeability limits to reduce the amount of salt penetrating the concrete over the life of the structure and high strength to optimize structural members and extend the span lengths to minimize the number of intermediate piers.

The use of HPC to eliminate two spans and two piers resulted in an approximate savings of $50,000. These savings resulted from the elimination of two piers from the substructure, elimination of the riprap that would have been necessary to protect the piers from scour, and the elimination of the construction time that would have been required to form and place the piers.

A second novel feature of this bridge is the precast HPC sheet piles used in the abutment walls. Typically, DelDOT uses square precast concrete piles with a cast-in-place concrete cap and backed with A690 steel sheeting to construct abutments for this type of bridge. In 1997, Bethlehem Steel, the only domestic fabricator, stopped rolling A690 steel sheets. This forced the DelDOT design team to look for alternatives and to try domestically available precast prestressed concrete sheeting in lieu of steel sheeting. The sheet piles were designed for bearing as well as retention of fill, eliminating the need for any square piles. HPC provided increased capacity for bending and driving stresses [39].

To assess the performance of the prestressed beams, a combination of vibrating wire strain gages, thermocouples, and a corrosion monitoring system were installed prior to the casting of the beams. In order to assess the properties of the HPC concrete used for the three beams that have been instrumented, a series of material tests were performed at the University of Delaware. During beam fabrication, concrete cylinders and shrinkage beams were cast and allowed to cure at the site along with the beams until the prestressing strands were released and the beams were removed from the bed. The specimens were then brought back to the University of Delaware and cured in a

temperature and humidity controlled room. Using these specimens, tests were conducted to determine the concrete compressive strength, splitting tensile strength, flexural strength, elastic modulus, chloride permeability, and shrinkage behavior.

Based on the test data in this project, the following conclusions can be drawn:

- The test results of compressive strength were compared to predictions made using ACI 209R-92. It is found that ACI 209 does a good job of predicting the HPC strength.
- The elastic modulus test results were compared with the predictions made using AASHTO and ACI 363R-92 formulas. ACI 363R-92 agrees better with the test results than does the AASHTO formula, which overestimate the value of the elastic modulus. It should be noted that in other state projects, ACI 318 was more accurate in some cases, while ACI 363 was more accurate in other cases. Sometimes neither gave good prediction. This may be because the modulus of elasticity of concrete is not a function of compressive strength alone. Other effects on the modulus of elasticity included the type of aggregates and the percentage of coarse aggregates.
- Modulus of rupture test results were compared with predictions made using AASHTO and ACI 363R-92 formulas. In this case, the ACI equation proved to be fairly accurate, while the AASHTO formula underestimated the modulus of rupture for the HPC.
- The equation for the prediction of the splitting tensile strength from AASHTO and ACI 363R-92 both overestimated the splitting tensile strength, from 16% to 52%.

- Low permeability and high strength concrete can be obtained in Delaware with locally available materials.
- Ongoing corrosion monitoring will help to establish the long-term durability of the HPC.

The elevated temperature during curing causes the strand stress to decrease significantly. However, the loss was shown to be recoverable upon cooling. Adherence of the concrete to the strand in a precast girder did not prevent the steel from regaining its thermal loss of stress upon cooling.

The effect on strain measurements of the hydration heat depends upon when the strands are released relative to the heating and cooling cycle.

The strand stress was shown to change with the temperature. In summer, the temperature goes up, and the stress goes down; in winter, the temperature goes down, and the stress goes up. Given the same condition, the thermal loss variation may reach ±2.4%.

In terms of short-term losses (less than 28 days), current AASHTO and PCI equations for conventional concrete underestimated the prestress losses. This may be because creep and shrinkage occur much faster for HPC than they do for conventional concrete.

In terms of long-term losses (after half a year), AASHTO and PCI equations for conventional concrete yield very accurate loss predictions. In the study reported,

the losses occurring after half a year were measured to be between 10 and 12%, reasonably close to the predicted losses (11%).

Vibrating wire strand meters seemed to be a very effective method for monitoring both short- and long-term prestress losses.

From the test result in this case, it can be seen that the thermal loss caused by the elevated temperature during curing is recoverable, and ambient temperature changes can cause fluctuation in losses over time. This phenomenon is not well understood and needs to be investigated further.

Many of the design provisions in the AASHTO Standard Specifications for Highway Bridges are based on knowledge and experience with normal concrete. With the introduction of high-performance concrete, the applicability of these provisions needs to be reassessed. Items that can be investigated with live load tests include impact factors, lateral load distribution, shear lag, and vertical deflections.

To compare the life cycle costs of conventional concrete bridges and with those of HPC bridges, the continued monitoring of Bridge 8F is necessary.

For HPC to be used more extensively, information about HPC and Bridge 8F needs to be widely disseminated.

Increasing emphasis is being placed on the durability, rather than the strength, of HPC. In many applications, high-strength concrete is used only because of its high durability rather than the need for its strength. There has been an enormous amount of research performed on the durability of concrete but without much correlation, largely because the properties are material specific and dependent on test methods. There is

an urgent need for new and improved test methods that would provide more consistent correlation between the laboratory and field results so that the data on durability can be better quantified. More research is needed to develop a rational design methodology for durability.

In New York State, all new and replacement bridge decks built using the HPC concrete from 1995 through early 1998 were inspected. Of the 84 inspected decks, 51 percent exhibited cracking. Of these cracked decks, over 50 percent began cracking within 14 days of the concrete placement. Deck cracking is common in all of the states. There are also many cracks in the deck of Bridge 8F. The reasons for the deck cracking need to be investigated and steps taken to reduce or eliminate the cracking.

ACKNOWLEDGMENTS

The authors would like to acknowledge the financial support of the Delaware Department of Transportation and the Delaware Transportation Institute for this work.

DISCLAIMER

This work was sponsored by the Delaware Transportation Institute and was prepared in cooperation with the Delaware Department of Transportation. The contents of the report reflect the views of the authors, who are solely responsible for the facts and accuracy of the data reported herein. The contents do not necessarily reflect the official views of the Delaware Transportation Institute or the Delaware

Department of Transportation at the time of publication. This report does not constitute a standard, specification, or regulation.

Chapter 1

INTRODUCTION

1.1 Background

Decades of exposure to traffic and the elements have left almost one-third of the Nation's 582,000 bridges structurally or functionally deficient. Although these bridges are not necessarily unsafe, they are often inadequate for carrying the high traffic volumes and heavy traffic loads common on today's highways. Many of these bridges will soon require extensive repair or even replacement. These projects will take a big bite out of the $3.2 billion highway agencies spend each year on bridge construction and maintenance, leaving less money available for other bridge needs [1].

The condition of our bridges also creates problems for shippers and motorists. As load restrictions are imposed on deficient bridges, vehicles must be diverted to other routes. This can increase trip length, exacerbate congestion, and direct traffic into residential neighborhoods. Projects to repair or replace these bridges create work zones that delay traffic and can endanger workers and motorists [1].

To prevent such problems, highway agencies need to build bridges that are better able to hold up to traffic and environmental demands. These bridges must also be economical to build and maintain. High Performance Concrete (HPC), which is concrete that has been designed to be more durable, and, if necessary, stronger than conventional concrete, can help highway agencies achieve these goals [1].

In the fall of 1996, the American Association of State Highway and Transportation Officials (AASHTO) established the Lead States team for HPC. It is made up of States that are ahead of the curve in implementing HPC in bridges and have volunteered to help other States catch up. The members of the team – Missouri, Nebraska, New Hampshire, Texas, and Washington –assembled information on the costs of building and maintaining HPC bridges. FHWA and the team worked hard to address these issues and provided training and technical assistance on the use of HPC in bridge projects. Judging from the steady increase in the number of States building HPC bridges, these efforts payed off [1].

1.2 Research Significance

The enhanced performance characteristics of HPC (higher strength and improved durability) are usually obtained by adding chemical admixtures to conventional concrete mix designs and by modifying curing procedures. Changes in mixes also affect other material properties, such as modulus of elasticity, creep, shrinkage, modulus of rupture, splitting tensile strength, etc. The first three will strongly affect the prestress losses in a prestressed girder. Because current design codes have their roots in the 1970s, and were based on empirical results of tests on members made with conventional concrete (28-day compressive strengths less than 6 ksi), they may not be suitable for HPC. In this project, both the HPC properties and structural behavior are investigated, and compared to predictions made using the current codes.

1.3 Organization of the Study

This report is organized as follows:

- Chapter 2 describes HPC, presents its benefits, and discusses the relevant literature.
- Chapter 3 describes the experimental program, and the instrumentation used, as well as presenting details of Bridge 8F.
- Chapter 4 presents the material test results (compressive strength, elastic modulus, modulus of rupture, splitting tensile strength and shrinkage), their comparison to current code equations and structural response (temperature, corrosion, concrete strain, and strand strain).
- Chapter 5 presents methods for predicting prestress losses.
- Chapter 6 presents a comparison of measured and calculated losses.
- Chapter 7 presents the conclusions of the research and recommendations for future work.

Chapter 2

AN OVERVIEW OF HPC

2.1 The Definition of HPC

Any concrete which satisfies certain criteria proposed to overcome limitations of conventional concrete may be called High Performance Concrete (HPC). It may include concrete which provides either substantially improved resistance to environmental influences (durability in service) or substantially increased structural capacity while maintaining adequate durability. It may also include concrete which significantly reduces construction time to permit rapid opening or reopening of roads to traffic, without compromising long-term serviceability. Therefore it is not possible to provide a unique definition of HPC without considering the performance requirements of the intended use of the concrete [2].

Forster [3] defined HPC as "a concrete made with appropriate materials combined according to a selected mix design and properly mixed, transported, placed, consolidated, and cured so that the resulting concrete will give excellent performance in the structure in which it will be exposed, and with the loads to which it will be subjected for its design life." In discussing the meaning of HPC, Aitcin and Neville [4] stated that "in practical application of this type of concrete, the emphasis has in many cases gradually shifted from the compressive strength to other properties of the material, such as a high modulus of elasticity, high density, low permeability, and resistance to some forms of attack."

The American Concrete Institute defines HPC as concrete that meets special performance and uniformity requirements that can not always be obtained using conventional ingredients, normal mixing procedures, and typical curing practices. These requirements may include the following enhancements [5]:

- Ease of placement and consolidation without affecting strength,
- Long-term mechanical properties,
- Early high strength,
- Toughness,
- Volume stability, and
- Longer life in severe environments.

Zia [2] defined HPC in terms of certain target strength and durability criteria as shown in Table 2.1. In this definition, the target minimum strength should be achieved in the specified time after water is added to the concrete mixture. The compressive strength is determined from 4 × 8 in. cylinders tested with neoprene caps. The water cement ratio (w/c) is based on all of the cementitious materials used. The minimum durability factor should be achieved after 300 cycles of freezing and thawing according to ASTM C 66, procedure A.

Zia's definition uses the w/c ratio as a mixture proportion criterion to define HPC. The ACI cites fresh concrete properties, and both cite long-term performance parameters. By restricting the definition to long-term performance parameters, concrete mix designers may be more willing to incrementally modify the use of ingredients, change concrete curing procedures, and use admixtures and alternate hydraulic cements such as granulated ground blast furnace slag. However use of a performance definition alone can not address all deterioration mechanisms.

There is insufficient experience to relate laboratory test results with resistance to the wide range and combination of field conditions. Deterioration stemming from poor quality materials subjected to an adverse environment can also represent a quality control and quality assurance problem. For bridge engineers to adopt an HPC performance definition, it must include adequate durability and strength parameters [5].

The Federal Highway Administration (FHWA) has proposed criteria for four different performance grades of HPC given by Goodspeed et al. [5]. The criteria are expressed in terms of eight performance characteristics including strength, elasticity, freezing/thawing durability, chloride permeability, abrasion resistance, scaling resistance, shrinkage, and creep as shown in Table 2.2. Depending on a specific application, a given HPC may require a different grade of performance for each performance characteristics. For example, a bridge located in an urban area with moderate climate may require Grade 3 performance for strength, elasticity, shrinkage, creep, and abrasion resistance, but only Grade 1 performance for freezing/thawing durability, scaling resistance, and chloride permeability [2].

Table 2.1 Definition of HPC According to Zia et al.

Category of HPC	Minimum Compressive Strength	Maximum Water/ Cement Ratio	Minimum Frost Durability Factor
Very early strength (VES)			
Option A (with Type III cement)	2,000 psi in 6 hours	0.40	80%
Option B (with PBC-XT cement)	2,500 psi in 4 hours	0.29	80%
High early strength (HES) (with Type III cement)	5,000 psi in 24 hours	0.35	80%
Very high strength (VHS) (with Type I cement)	10,000 psi in 28 hours	0.35	80%

Table 2.2 Definition of HPC According to Federal Highway Administration

Performance Characteristics	Standard test method	FHWA HPC performance grade			
		1	2	3	4
Freeze-thaw durability (X = relative dynamic modulus of elasticity after 300 cycles)	AASHTO T 161 ASTM C 666 Procedure A	60%≤X<80%	80%≤X		
Scaling resistance (X = visual rating of the surface after after 50 cycles)	ASTM C 672	X=4, 5	X=2, 3	X=0, 1	
Abrasion resistance (X = avg. depth of wear in mm)	ASTM C 944	2.0>X≥1.0	1.0>X≥0.5	0.5>X	
Chloride penetration (X = coulombs	AASHTO T 277 ASTM C 1202	3000≥X>2000	2000≥X>800	800≥X	
Strength (X = compressive strength)	AASHTO T 2 ASTM C 39	6≤X<8 ksi	8≤X<10 ksi	10≤X<14 ksi	14 ksi≤X
Elasticity (X = modulus)	ASTM C 469	4≤X<6x10^{6}psi	6≤X< 7.5x10^{6}psi	7.5x10^{6}psi≤X	
Shrinkage (X = microstrain)	ASTM C 157	800>X≥600	600>X≥400	400>X	
Specific creep (X = microstrain per MPa)	ASTM C 512	0.52≥X> 0.41/psi	0.41≥X> 0.31/psi	0.31≥X> 0.21/psi	.21/psi≥X

2.2 Advantages of HPC

Conventional concrete is designed to provide the compressive strength required for a job and to resist damage caused by freezing temperatures and deicing chemicals. HPC is concrete that has been designed to be more durable and, if

necessary, stronger than conventional concrete. HPC mixes are composed of essentially the same materials as conventional concrete mixes, however the proportions are designed, or engineered, to provide the strength and durability needed for the structural and environmental requirements of the project [1].

High strength can increase bridge span lengths and spacing of bridge girders. The increased span lengths enable greater underpass clearance widths resulting in fewer supports or bridge piers. In addition more slender, shallower, long span members can be used to replace deeper members. This facilitates the transportation and placement of the members (lower loads on equipment transporting and erecting the girders). Using shallower members also enables reduced embankment heights or increased underpass clearance heights. The latter option can be used to retrofit bridges with deficient underpass clearances by replacing deeper members with shallower members. Increasing the bridge girder spacing results in economic savings through requiring fewer girders per bridge. Savings are realized in material reductions and reduced transportation and erection costs involved with fewer required girders.

Another benefit is that HPC bridge components are far less permeable than conventional concrete bridge components and are therefore expected to be more resistant to damage caused by freeze-thaw cycles, salts in seawater and deicing chemicals, and other environmental conditions. This means that HPC bridges may have much longer service lives than conventional bridges, and reduced long-term maintenance [1].

Prestressed concrete bridges made with conventional concrete have only been in use since the 1950s making it difficult to accurately determine their eventual

service life. However, Federal Highway Administration (FHWA) figures show that the average time before reconstruction is needed is 42 years for all types of bridges. HPC bridges may be capable of lasting much longer – the current estimate is that HPC bridges may have a useful service life of 75 to 100 years [1].

HPC bridges are not necessarily more expensive than conventional bridges. While the materials used in High Performance Concrete mixes may be more expensive than the materials in conventional concrete, an HPC bridge that has longer spans and smaller or fewer structural components than a conventional concrete bridge can be built faster and with less concrete, thereby saving money on labor and at least partially offsetting any increase in materials costs. Furthermore HPC bridges should have lower life-cycle costs as a result of their longer service lives. The savings in life-cycle costs will far outweigh any increase in costs for raw materials [1].

Even though HPC has many advantages over conventional concrete, there are several reasons why it isn't being used more extensively. For one, information about HPC and its benefits for bridge projects has not been widely disseminated. Another reason is that there are always risks in using a new technology, which can cause highway agencies to hesitate in implementing it. In addition, HPC that is suited to bridges is a relatively new technology. Although high strength HPC has been used in buildings for about 20 years, it has taken longer to develop the highly durable HPC needed for bridge applications [1].

For bridge applications increasing emphasis is being placed on concrete durability as opposed to its strength. In many applications, high strength concrete is used only because of its high durability quality rather than the need for its strength [2].

2.3 Disadvantages of HPC

Despite the numerous benefits associated with the use of HPC, there are also some potential disadvantages, including high early age autogenous shrinkage, and increased risk for early age cracking, etc. The early age autogenous shrinkage of HPC is much bigger than that of normal strength concrete (NSC). Early age cracking is a serious problem that has been estimated to occur in nearly half the monitored bridges in the United States. Cracks reduce durability, decrease service life, and increase maintenance costs [6]. While this can occur with even conventional concrete, it is more of a concern with HPC.

Some additional concerns are listed below.

1. Quality control concern [7]

An article in Engineering News Record (ENR) stated "Lack of confidence in test methods may be slowing acceptance, increasing costs." Henry G. Russell [8] said "My perspective is the availability and development of higher strength concretes has outpaced testing capabilities." In many cities where high-strength concrete is novel and difficult to achieve, sloppy testing procedures and undersized testing machines are threatening progress. The higher-strength concrete is far more sensitive to sloppy preparation, improper curing, rough handling and imprecise testing. Despite greater sensitivity of high-strength concrete to testing errors, no special testing standards exist. All structural concrete is subject to the same testing standards established by ASTM. The four factors (Cylinder End Condition, Cylinder Mold Material, Testing Machine Stiffness and Loading Rate) may have insignificant effects on tests for normal concrete, but they can significantly affect results for HPC. As concrete strengths continue to increase, the significance of good quality control

procedures becomes increasingly important and is a critical factor influencing the overall success of a project.

2. High bid price [7]

Another disadvantage of HPC can be higher bid prices, at least initially. As with any new technology, some risk is inherent. This may be reflected in bid prices for HPC members until the technology becomes part of everyday use.

3. Instability caution [7]

As promising as high strength concretes are in providing increased strength and reduction in weight, there is a price for these advantages in the form of reduced flexural stiffness of beam due to smaller section. The designer must be aware of the potential for global and local instabilities resulting from decreased stiffness.

4. Thicker deck for wider beam spacing

One of the advantages listed for HPC was increased beam spacing. It should be noted that if increased beam spacing are used, they may result in slightly thicker decks.

5. The lack of ductility [9]

The lack of ductility of plain high strength concrete (HSC) has been a major concern regarding the safety of HSC columns. While this type of behavior can be much improved by adequate detailing of the lateral steel, it has been reported that confinement is less effective for HSC than for NSC.

6. The concern of thermal hydration [10]

The general trend indicates a nearly linear decrease in compressive strength with an increase in maximum concrete temperature during hydration at later ages. While higher concrete temperatures during hydration allow the fabricator to

release prestressing strands sooner, the detrimental effect at later ages on the compressive strength development may be noted. Beyond a concrete temperature of 170 ^{0}F, there appears to be no benefits to early-age property development. For conventional mix designs and standard shapes, excessive concrete temperatures during hydration are generally not a major concern. However, as the use of HPC with high cementitious contents becomes more prevalent in highway structures, specifications must address the concerns.

7. The concern about resistance to fire [11]

While the strength and durability of HPC are often greatly superior to conventional concrete under ambient conditions, their failure is sometimes rapid and dramatic during exposure to a fire, characterized by the explosive spalling of layers from the exposed concrete surface. This failure mode is rarely encountered in conventional concretes of high w/c ratios.

2.4 HPC Bridges

The Louetta Road Overpass (two adjacent bridges), completed in 1997, located on Texas State Highway 249 near Houston, was the first bridge project in the U.S. to use HPC in all aspects of design and construction. Designed by the Texas Department of Transportation (TxDOT), these bridges use simple span, pretensioned concrete beams with composite, cast-in-place concrete decks. Ramon Carrasquillo and Ned Burns from the University of Texas at Austin provided guidance with HPC mixes and structural details. The contractor for the overpass was Williams Bros., Houston, and the precaster was Texas Concrete Co., Victoria, Tex [12].

Texas State Highway 249 was upgraded from a four-lane, at-grade road to a limited access freeway. Consequently, two overpass structures have been built at Louetta Road to carry three lanes in each direction plus shoulders and ramp transitions. The bridges are three spans each, nominally 130 ft. per span. The beams are pretensioned and U-shaped. At the interior bents, each beam is supported by a single post-tensioned pier. All beams and piers were designed and fabricated using high performance/high-strength concrete. The composite decks are precast concrete subdeck panels with cast-in-place concrete topping. For comparison purposes, the southbound main-lane bridge has a high-performance/high-strength cast-in-place concrete deck, whereas the northbound main-lane bridge has a high performance/normal-strength cast-in-place concrete deck. The Texas Department of Transportation (TxDOT) conducted the project in cooperation with the University of Texas at Austin [13].

- **Outline of HPC Features [13]**

The concrete strength of the bridge elements varies according to the demand of the particular application. The design strengths were specified at 28 days for the deck and piers. The design strength for the beams was specified at 56 days to account for the strength gain with time that is typical of many higher strength concretes. Table 2.3 summarizes the design concrete strengths for various bridge elements.

Table 2.3 The Design Strengths for Louetta Road Overpass

Element	Compressive Strength
Beams @ Transfer	6,900-8,800 psi
Beams @ 56 Days	10,000-13,000 psi
Piers	10,000 psi
Deck - Southbound	8,000 psi
Deck - Northbound	4,000 psi
Subdeck Panels	8,000 psi

Due to the large number of closely spaced prestressing strands, placement of the concrete in the U-shaped beams required superior workability and the use of a set retarder and high-range water-reducing admixture. No accelerated curing was used. Cement was partially replaced with fly ash in all mixes.

- **Pretensioned Beams [13]**

The pretensioned beams were fabricated using a newly developed cross-section. The TxDOT U54 beams are trapezoidal in cross-section, but open at the top with flanged stems (thus referred to as U-shaped). The width of the beams across the top of the stems is 8 ft.; the beams are 54 in. deep. The beam stems are 5 in. thick and the thickness of the bottom flange can be varied to accommodate either two or three rows of strands. Except for the interior beams of the shortest span where 0.5 in. diameter strand was used, 0.6 in. diameter strand spaced at 2 in. on center was used for pretensioning. Transfer and development length tests were conducted in this project to obtain FHWA approval for the use of 0.6 in. diameter pretensioned strands at 2 in. spacing.

- **Piers [13]**

The piers are hollow, 3.25 ft. square segments with chamfered corners. Two walls are 7.5 in. thick to accommodate three 1.38 in. diameter post-tensioning bars. The other two walls are 4 in. thick. The use of this pier system allowed for speedy construction in the field to provide beam supports and the effective utilization of high-performance concrete in the substructure.

- **Deck [13]**

The deck is composite, cast-in-place, reinforced concrete with precast, prestressed concrete subdeck panels. One task in this project was to accumulate field experience on the use of high strength versus normal strength high performance concrete in cast-in-place concrete deck construction.

- **Construction [13]**

Construction of the Louetta Road Overpass began in February 1994. The overpass was completed in May 1997.

- **Benefits [13]**

The use of the high-strength, high-performance concrete in the beam design allowed simple-span construction for this overpass. Otherwise, a more complicated and costly superstructure and/or substructure design would have been required due to the underneath-roadway constraints. Aesthetics were a consideration, and the U-beams with a single pier per widely-spaced beam offer an attractive alternative to typical designs.

Following the Louetta Road Overpass in Texas, many HPC bridges have been built, including US 87 & South Orient Railroad Overpass in San Angelo Texas, U.S 30 Bridge in Crawford Country Ohio, 120th Street and Giles Road Bridge in Sarpy County Nebraska, Eastbound State Route 18 over State Route 516 in King County Washington, and Route 104 bridge over the Newfound River in Bristol New Hampshire. Now nearly every state has at least one HPC bridge. Support of FHWA's Innovative Bridge Research and Construction (IBRC) program has greatly aided the implementation of HPC bridges.

2.5 Material Performance

HPC has eight performance characteristics, including freezing/thawing, durability, scaling resistance, abrasion resistance, chloride permeability, strength, elasticity, creep, and shrinkage.

2.5.1 Freeze-Thaw Durability

Kriesel et al. [14] investigated freeze-thaw durability of high performance concrete in prestressed bridge girders. This study included a total of 30 concrete mixes and more than 130 specimens, with the following variables: aggregate type (round river gravel, partially-crushed gravel, granite, high-absorption limestone, and low-absorption limestone); cementitious material composition (Type III portland cement only, 20 percent fly ash, 7.5 percent silica fume, and a combination of 20 percent fly ash with 7.5 percent silica fume replacement by weight of cement); and curing condition (heat-cured or seven-day moist-cured). No air-entraining agents were used in the study's initial phase to simulate the production of precast/prestressed

bridge girders. Results indicate that it is possible to produce Portland cement concrete with high strength and freeze thaw durability without the use of air-entraining agents. Overall, the moist-cured concrete specimens exhibited better freeze-thaw durability than the heat-cured concrete specimens. The reference concrete mixes, containing only portland cement, performed better than the concrete containing pozzolan material of fly ash or silica fume. The low-absorption limestone aggregate concrete mixes exhibited the best freeze-thaw durability performance, in some cases enduring more than 1,500 freeze-thaw cycles without failing. The study found that the moisture content of the coarse aggregate at the time of mixing had a significant impact on the concrete's freeze-thaw durability.

In Crouch et al.'s test [15], there was no variability in the freezing and thawing test results from specimens at different ages. The specimens achieved a durability factor (defined in ASTM C 666-92) of 100 after 600 freezing and thawing cycles.

Carrasquillo [16] showed that the use of air entrainment in high performance concrete reduces the compressive strength of the concrete. However, if the concrete is to be exposed to freezing and thawing conditions, the incorporation of entrained air within the concrete is a must if the concrete is to exhibit adequate performance. Tests have indicated that 3 to 4 percent entrained air will render high strength concrete that is resistant to freezing and thawing.

During placement, the concrete should be deposited close to its final position. Contractors find pumping a convenient way of delivering concrete. Using this method care should be exercised, since pumping can cause segregation and a change in the air content. Loss of air content in concrete undergoing free fall in a

pump with an elevated bend line was documented. The greater the free fall, the larger was the loss of air. Loss of air can lead to deterioration in the air-void system, resulting in poor resistance to freezing and thawing. To evaluate the adequacy of the air-void system, either a test for resistance to freezing and thawing or the petrographic determination of the air-void system must be conducted [17].

2.5.2 Scaling Resistance

Scaling is another durability issue, which is caused by repeated application of deicing salts. A concrete surface damaged by salt scaling becomes roughened and pitted as a result of the spalling and flaking of small pieces of mortar near the surface. Even high–quality concrete with adequate air entrainment can still suffer scaling due to deicing chemicals. The exact cause of scaling is not well understood, but it is recognized that when deicing chemicals are applied to melt ice, the heat consumption causes a rapid drop in the temperature of the concrete just below the surface resulting in damage from the effects of rapid freezing or differential thermal strains. Furthermore, deicing chemicals can accumulate in the surface layer of the concrete, forming relatively concentrated solutions. When water stays on the concrete surface, it flows towards the concentrated chemical solution causing an osmotic action accompanied by hydraulic pressures. These pressures may, in turn, cause salt scaling. Scaling is most likely to occur where there is a weak layer of paste or mortar at or near the concrete surface. The best way to prevent scaling is to eliminate the weak layer of material by proper mix design and good construction practice in placing, finishing, and curing. Over vibration, too much trowelling, and excessive bleeding should all be avoided. Well-cured concrete pavements, allowed to

dry for a period before deicing salts are applied, generally will have good scaling resistance [2].

2.5.3 Abrasion Resistance

Abrasion is wearing due to repeated rubbing and friction. For pavements, abrasion results from traffic wear. Adequate abrasion resistance is important for pavements and bridge decks from the standpoint of safety. Excessive abrasion leads to an increase in accidents as the pavement becomes polished reducing its skid resistance. There is no generally accepted criterion for evaluating the abrasion resistance of conventional concrete. The lack of an abrasion resistance criteria is due to the fact that surface wear normally is not a controlling factor in pavement performance. If the pavement surface is provided with an adequate texture depth during construction, its design is dictated by other requirements. An exception is in areas where the use of studded tires is permitted. Abrasion resistance of concrete is a direct function of its strength, and thus its water-cement ratio and constituent materials. High quality paste and strong aggregates are essential to produce an abrasion resistant concrete [2].

After investigating the resistance to abrasion of concrete produced with different sources of fly ash and different fly ash contents, Carrasquillo [16] found that the depth of wear, or abrasion resistance, of the concrete is best described by its compressive strength, rather than by the materials which make up the cementitious fraction of the concrete.

2.5.4 Chloride Permeability

A standard procedure for measuring the movement of chloride ions through concrete is the AASHTO T 277 "Rapid Determination of the Chloride Permeability of Concrete" test method. In this procedure, the specimens are conditioned first by one hour of air dry, three hours of vacuum (pressure < 1 mm Hg), one hour of additional vacuum with specimens under de-aired water, and followed by 18 hours of soaking in water. The test consists of monitoring the amount of electrical current passing through a 4 in. diameter by 2 in. long vacuum-saturated concrete specimen when one side of the specimen is immersed in an NaCl solution and the other side in an NaOH solution and a potential difference of 60V dc is maintained on the specimen for 6 hours. The total charge passed, in coulombs, is related to chloride permeability of the specimen. The lower the total charge, the less permeable and more durable the concrete is [2].

Carrasquillo [16] found that the permeability of concrete containing no fly ash decreases significantly during the first 60 days after casting of the concrete, however, no significant decreases in permeability occur at later ages beyond 60 days. On the other hand, the permeability of concrete containing fly ash continues to decrease with time even after 300 days. The permeability of concrete is a very important factor affecting the durability of the concrete. In general, permeability is affected by the water to cementitious material ratio, use of mineral admixtures, and the use of high-range water-reducing admixtures. Other studies have shown that the use of silica fume results in extremely low values for permeability of concrete. For concrete having compressive strengths in the 6,000 to 9,000 psi range, permeability is more dependent on the use of mineral admixtures than on compressive strength. For

high performance concrete having compressive strengths from 9,000 psi to 15,000 psi, the use of high range water-reducing admixtures results in a significant reduction in concrete permeability. However, for these concrete, permeability is still affected by the use of mineral admixtures. Water to cementitious material ratio is not a good predictor of the permeability of concrete. Use of mineral admixtures has a more significant effect on concrete permeability than reductions in the water to cementitious material ratio.

2.5.5 Compressive Strength

ACI 209 [18] gives a general equation (2-1) for predicting compressive strength at any time for NSC.

$$(f_c')_t = \frac{t}{a + \beta t}(f_c')_{28} \qquad (2\text{-}1)$$

where α and β are constants with α in days (see Table 2.4), $(f_c')_{28}$ is the 28-day compressive strength, and t is the age of concrete in days. The compressive strength is determined in accordance with ASTM C39 from 6×12 in. standard cylindrical specimens, made and cured in accordance with ASTM C192.

Table 2.4 Values of the Constants α and β

Type of curing	Cement Type	Constants α and β
Moist cured	I	α=4.0 β=0.85
	III	α=2.3 β=0.92
Steam cured	I	α=1.0 β=0.95
	III	α=0.7 β=0.98

Ahmad et al. [19] found that the use of a corrosion inhibitor has the effect of retarding the compressive strength gain of young concretes ($t \leq 3$ days). After the age of 3 days, the effect of the retarder is relatively small for steam-cured concretes as compared to concrete that is not steam cured. ACI 209 prediction underestimates the strength of steam cured high early strength (HES) concrete at early ages ($t \leq 3$ days). For HES concrete that is not steam cured, and with and without DCI-S corrosion inhibitor, ACI 209 underestimated the measured values at each age tested.

Carrasquillo [16] found that cements produced at different plants and meeting the same ASTM specification for a given type of cement do not necessarily mean that concrete produced with each of the different types of cement will perform similarly. Concrete produced with different types of cement can have significantly different compressive strength. He also showed that the maximum temperature achieved by the concrete had a great influence on the strength of the concrete achieved. In fact, it was found that as the maximum temperature of the concrete increased beyond 152 ^{0}F, the strength of the concrete decreased.

The most significant property of an HPC prestressed beam is the compressive strength of the concrete at release. Allowable compression at release has the most impact on span capacity, while allowable tension at service has minor impact [20].

2.5.6 Modulus of Elasticity

The elastic modulus of concrete depends on factors including the strength, stiffness, fraction of the coarse aggregate, unit weight of concrete, and matrix of the

concrete. Generally the modulus of elasticity is expressed as proportional to the square root of the compressive strength of the concrete [19].

ACI 318 [21] gives an equation (2-2) for the prediction of Modulus of Elasticity (Ec) for values of (Wc) between 90 and 155 lb/cf.

$$E_c = W_c^{1.5} 33\sqrt{f_c'} psi \tag{2-2}$$

The equation for predicting the elastic modulus in ACI 363R-92 [22] for strengths over 3,000 psi but lower that 12,000 psi is given by

$$E_c = 40000\sqrt{f_c'} + 1.0 \times 10^6 \, psi \tag{2-3}$$

Ahmad and Shah suggested equation (2-4) for the prediction of elastic modulus.

$$E_c = W_c^{2.5} (f_c')^{0.325} \tag{2-4}$$

where, E_c is the elastic modulus, and f_c' is the concrete compressive strength.

After comparing the experimental results with these equations, Ahmad et al. [19] came to the following conclusions.

At all test ages, ACI 318 predictions overestimated the results except for concrete with DCI-S and without steam curing. The predictions were within ±8% of the observed values for 80% of the specimens tested. The test results show that the equation proposed by Ahmad and Shah predicts the value within 10% at all ages for concrete without steam curing and at ages greater than 3 days for concrete with steam curing. At the age of 17 hours, all equations overestimated the elastic modulus of the steam cured concrete by a minimum of 12%. It appears that for steam cured concrete,

the predictions as per the equation of ACI 363 are closest to the observed strengths. The use of corrosion inhibitor has no significant influence on the elastic modulus (Ec), since Ec is primarily a function of the aggregate type and its percent content. Furthermore, it was shown that steam curing had much less effect on the increase in the elastic modulus with time as compared to the increase in compressive strength with time.

Shing et al. [23] investigated a 215 ft. long, four-span bridge in Denver, Colorado. The concrete mix design is shown in Table 2.5. They found that the ACI 318 yields values that are higher than the test data.

Table 2.5 Girder Concrete Mix Design

Material	Quantity (lb./cy)
Type III Cement	800
Water	263
Coarse Aggregate (3/8" Colley)	1570
Fine Aggregate (Sand, Cooley)	1320
Silica Fume	30
Water Reducer (Polyheed 997)	100 oz/cy
Water Reducer (Rheo 1000)	120-200 oz/cy

After testing air entrained HPC using Tennessee materials, Crouch et al. found that ACI 363 proved to be a good approximation for the 28-day static modulus of elasticity data with differences less than 2%. On the other hand ACI 318 greatly overestimated the 28-day static modulus of elasticity [15].

In tests by Roller et al. [24], the calculated values for concrete modulus of elasticity using AASHTO and ACI 318 correlated well with the measured values.

In some tests, ACI 318 is more accurate. In some tests, ACI 363 works well. In some tests, neither yield good predictions. This may be because the modulus of elasticity of concrete is not a function of compressive strength alone. Other effects on the modulus of elasticity included the type of aggregate and the content percentage of the coarse aggregates [25].

Zia [26] showed that both ACI 318 and ACI 363 can be used to predict the modulus of elasticity of HPC.

Carrasquillo [16] found that the modulus of elasticity of the concrete is mostly dependent upon the coarse aggregate content. For a fairly high coarse aggregate content (44 percent), the modulus of elasticity of the concrete is fairly accurately predicted by the use of the equation contained in ACI 318.

2.5.7 Modulus of Rupture

The empirical equations used to predict the modulus of rupture from ACI 318-89 (Eq. 2-5), ACI 363 (Eq. 2-6), and Ahmad and Shah (Eq. 2-7) are shown.

Ahmad et al. [19] found that ACI 318 provided a better prediction of the observed results than the other two equations, however, the difference at all test ages ranged as high as 21%. The differences between predictions and experimental results ranged from –5% to 7% for 70% of the specimens tested. Differences between measured and predicted values were almost 90% for some specimens with the ACI 363 equation, and up to 66% for the equation proposed by Ahmad and Shah.

$$f_r = 7.5\sqrt{f_c'} \tag{2-5}$$

$$f_r = 11.7\sqrt{f_c'} \tag{2-6}$$

$$f_r = 2.3(f_c')^{2/3} \tag{2-7}$$

Shing et al. [23] found ACI 318 expression for the modulus of rupture to be somewhat conservative.

Based on results of modulus of rupture tests performed by Roller et al. [24], it appears that the AASHTO and ACI 318 may slightly underestimated the modulus of rupture of high strength HPC.

In the investigation of Zia [26], it was found that ACI 318 matches the test data very well, and ACI 363 greatly overestimates the modulus of rupture.

2.5.8 Splitting Tensile Strength

The empirical equations for estimating the splitting tensile strength from ACI 318-89 (Eq. 2-8), ACI 363 (Eq. 2-9), Oluokun [27] (Eq. 2-10) and Ahmad and Shah (Eq. 2-11) are shown below.

$$f_{ct} = 6.7\sqrt{f_c'}psi \tag{2-8}$$

$$f_{ct} = 7.4\sqrt{f_c'}psi \tag{2-9}$$

$$f_{ct} = 1.38(f_c')^{0.69}\ psi \tag{2-10}$$

$$f_{ct} = 4.34(f_c')^{0.55}\ psi \tag{2-11}$$

Test by Ahmad et al. [19] indicated that the empirical equations of ACI 318 and ACI 363 significantly overpredicted the splitting tensile strength of high early strength at all ages. The equations of Ahmad and Shah, and Oluokun are quite similar,

and in this investigation the predictions yielded by Oluokun's equation are compared with the observed results since Oluokun's equation was developed for early age concrete. In this investigation the equation proposed by Oluokun was used with a correction factor of 0.94 to convert the 4×8 in. cylinder strengths to 6×12 in. cylinder strengths. The predictions for the non-steam cured specimens at very early ages were close to observed values, but the predictions overestimated the observed values for the steam cured specimens at early ages. The equation also overpredicted the results for cylinders at 28 days of age.

In test by Crouch et al. [15], the average 28-day splitting tensile strength exceeded ACI 363 by only 7.8%.

In the investigation by Zia [26], it was found that both ACI 318 and ACI 363 match the test data of splitting tensile strength very well.

2.5.9 Creep

Creep is the time-dependent increase in strain of hardened concrete subjected to sustained stress. It is usually determined by subtracting from the total measured strain in a loaded specimen, the sum of the initial instantaneous strain (usually considered elastic) due to sustained stress, the shrinkage, and any thermal strain in an identical load-free specimen, subjected to the same history of relative humidity and temperature conditions. Creep is closely related to shrinkage and both phenomena are related to the hydrated cement paste. As a rule, concrete that is resistant to shrinkage also has a low creep potential. The principal parameter influencing creep is the load intensity as a function of time; however, creep is also influenced by the composition of the concrete, the environmental conditions, and the

size of the specimen. The composition of concrete can essentially be defined by the w/c ratio, aggregate and cement types and quantities. Therefore, as with shrinkage, an increase in w/c ratio and an increase in cement content generally result in an increase in creep. Also, as with shrinkage, the aggregate induces a restraining effect so that an increase in aggregate content and stiffness reduces creep [2].

ACI 209 gives equation (2-12) for predicting a creep coefficient v_t for a loading age of 7 days, for moist cured concrete, and for 1-3 days steam cured concrete.

$$v_t = \frac{t^{0.6}}{10 + t^{0.6}} v_u \tag{2-12}$$

where, t is time in days after loading. In the absence of specific creep and shrinkage data for local aggregates and conditions, the average values suggested for v_u are $2.35\gamma_c$, where γ_c represents the product of the applicable correction factors. Aggregates affect creep and shrinkage principally because they influence the total amount of cement-water paste in the concrete [18].

Creep correction factors for steam cured concrete is given as follow.

Loading age:

$$\gamma_{la} = 1.13(t_{la})^{-0.094} \tag{2-13}$$

where, t_{la} is the loading age in days.

Ambient relative humidity:

$$\gamma_{\lambda} = 1.27 - 0.0067\lambda \tag{2-14}$$

where, λ is relative humidity in percent (greater than 40 percent)

Volume-surface ratio other than 1.5 in:

$$\gamma_{vs} = \frac{2}{3}[1 + 1.13\exp(-0.54\frac{v}{s})] \quad (2\text{-}15)$$

where, v/s is the volume-surface ratio of the member in inches.

The effect of slump, percent of fine aggregate, cement and air content also needs to be corrected. It should be noted that for slumps less than 5 in., fine aggregate percentage between 40-60 percent, cement contents of 470 to 750 lbs/cy, and air contents less than 8 percent, the correction factor is approximately equal to 1. The principal disadvantage of the concrete composition correction factors is that concrete mix characteristics are unknown at the design stage and have to be estimated. Since these correction factors are normally not excessive and tend to offset each other, in most cases, they may be neglected for design purposes.

Ahmad et al. [19] conducted creep testing using two replicate 4×8 in. cylinders. The cylinders were loaded to 1,035 psi and the measurements recorded. The average of the creep values for cylinders showed an initial strain of 300×10^{-6} in./in. and a final strain 950×10^{-6} in./in. at an age of 104 days. The ultimate creep coefficient was determined to be 3.17 which is within the range of 1.3 to 4.15 reported by ACI 209. The higher than average creep strains observed could be attributed to the high cement content (870 pcy) used for HES concretes

Burns et al. [28] showed that creep was observed to be substantially less and occur at a much faster rate than predicted by ACI 209 procedures. After regression curves to fit the data, they suggested an equation $C_{ct}=1.81\times t^{0.6}/(7+t^{0.6})$ for standard conditions of 40% relative humidity and a v/s ratio equal to 1.5.

Zia [26] showed that creep strains of the different groups of very high strength (VHS) concrete ranged from only 20% to 50% of that of conventional concrete, due to low w/c ratios and higher compressive strength. Specific creep of

concrete with marine marl was higher than concrete with other aggregates because marine marl was a softer aggregate.

After research conducted on over 6,000 specimens to determine the mechanical properties and time-dependent effects of high-strength concrete, Mokhtarzadeh and French found that the recommended form of ACI 209 equation: $V_t=[t^{0.6}/(10+t^{0.6})]V_u$, is suitable for predicting the creep coefficient of high strength concrete at any time t. The range of ultimate creep coefficients V_u predicted in this study varied between 0.92 to 2.46, as compared with the 1.30 to 4.15 range reported by ACI 209 for normal strength concrete. The specific creep of specimens heat cured at lower temperatures was less than companion specimens cured at higher temperatures [29].

2.5.10 Shrinkage

Shrinkage is the decrease of concrete volume with time. This decrease is due to changes in the moisture content of the concrete and physicochemical changes which occur without stress. Shrinkage of high performance concrete may be expected to differ from conventional concrete in three broad areas: plastic shrinkage, drying shrinkage, and autogenous shrinkage. Plastic shrinkage occurs during the first few hours after fresh concrete is placed. During this period, moisture may evaporate faster from the concrete surface than it is replaced by bleed water from lower layers of the concrete mass. Paste-rich mixes, such as high performance concrete, will be more susceptible to plastic shrinkage than conventional concrete. Drying shrinkage occurs after the concrete has already attained its final set and a good portion of the chemical hydration process in the cement gel has been accomplished. Drying shrinkage of high

strength concrete, although perhaps potentially larger due to higher paste volumes, does not, in fact, appear to be appreciably larger than conventional concrete. This is probably due to the increase in stiffness of the stronger mixes. Shrinkage should not be confused with thermal contraction which occurs as concrete loses the heat of hydration. Shrinkage is unaffected by the w/c ratio but is approximately proportional to the percentage of water by volume in concrete. Laboratory and field studies have shown that shrinkage of higher strength concrete is similar to that of lower-strength concrete. Higher strength concrete exhibits a higher initial rate of shrinkage, but after drying for 180 days, there is little difference between the shrinkage of high strength concrete and lower strength concrete made with dolomite or limestone [2].

ACI 209 gives equation (2-16) for the prediction of shrinkage for steam cured concrete with 1-3 days of age.

$$(\varepsilon_{sh})_t = \frac{t}{55+t}(\varepsilon_{sh})_u \tag{2-16}$$

$$(\varepsilon_{sh})_u = 780\gamma_{sh} \times 10^{-6} in/in \tag{2-17}$$

where, t is the time after shrinkage is considered, that is, after the end of the initial wet curing and γ_{sh} represents the product of the applicable correction factors. Correction factors for ambient relative humidity and volume surface ratio are shown below.

Ambient relative humidity:

$$\gamma_\lambda = 1.40 - 0.010\lambda, for 40 <= \lambda <= 80 \tag{2-18}$$

$$= 3.00 - 0.030\lambda, for 80 < \lambda <= 100 \tag{2-19}$$

where λ is relative humidity in percent.

Volume surface ratio (v/s) other than 1.5 in:

$$\gamma_{vs} = 1.2\exp(-1.12v/s) \tag{2-20}$$

Correction factors for concrete composition can be neglected for the same reasons as the creep.

Ahmad et al. [19] tested the shrinkage and creep behavior for air cured high early strength concrete without DCI-S corrosion inhibitor. The shrinkage value was determined using two companion 4×8 in. cylinders. The average of the measurements from both sides of each cylinder was used to calculate the shrinkage strain for the specimen. The average shrinkage strain was determined to be $1{,}060\times10^{-6}$ in./in. for steam cured concrete. The observed shrinkage was higher than the mean value of 730×10^{-6} in./in. as per the recommendation of ACI Committee 209. It should be noted that the specimens for shrinkage testing were stored in an area with a relative humidity below 40%. Since the specimens were tested under conditions with lower humidity than those generally existing in service and reported by ACI 209, this could have attributed to larger measured shrinkage strains for these tests.

Burns et al. [28] showed that shrinkage was observed to be substantially less and to occur much faster than predicted by ACI 209 procedures. After fitting regression curves to the data, they gave an equation for standard conditions of 40% relative humidity and a v/s ratio of 1.5, $\varepsilon_{sh}=(433\times10^{-6})\times t^{0.6}/(3+t^{0.6})$.

Zia [26] showed that shrinkage of the HPC was considerately less than that of conventional concrete due to very low w/c ratio. It is opposite to his former conclusion: shrinkage is unaffected by the w/c ratio [2].

Mokhtarzadeh and French showed that the time to achieve ½ of the ultimate shrinkage strain was longer for the high strength concrete specimens observed in this study in comparison with the values presented in ACI 209. Drying shrinkage strains observed in this study ranged between 63 to 83% of values predicted by ACI 209 equations. Based on the data collected, the following two equations were suggested for predicting the shrinkage strain of high strength concrete, for moist cured concrete $(\varepsilon_{sh})_t=[t/(45+t)]\times(\varepsilon_{sh})_u$ and for heat cured concrete $(\varepsilon_{sh})_t=[t/(65+t)]\times(\varepsilon_{sh})_u$ where, $(\varepsilon_{sh})_u = 530\ \mu\varepsilon$.

A lower w/c and denser matrix of high strength concrete were believed to be the main reasons for the observed smaller ultimate shrinkage of high strength concrete and its increased time to the ½ ultimate shrinkage strain value. Specimens heat-cured at lower temperatures had slightly higher drying shrinkage strains than companion specimens cured at higher temperatures [29]. The ultimate value of creep and shrinkage for HPC were found to be less than those for conventional concrete. Creep occurs at the same rate of conventional concrete, and shrinkage occurs at a lower rate than conventional concrete.

2.6 Structural Performance

2.6.1 Shear Capacity

Cumming et al. conducted an experimental program to investigate production techniques and mechanical properties of high-strength concrete and to provide recommendations for using these concretes in the manufacturing of precast/prestressed bridge girders [30].

As part of a project at the University of Minnesota to investigate the application of high-strength concrete in prestressed girders, four shear tests were performed on high-strength concrete prestressed girders. The girders were originally constructed in August 1993. The girders are classfied as Minnesota Department of Transportation (Mn/DOT) 45M sections and 45 inches deep. Each girder utilized 46 0.6-inch diameter prestressing strands spaced 2-inch on center. The girders were designed assuming a 28-day compressive strength of 10,500 psi. Later, a 4-foot-wide, 9-inch-thick composite concrete deck was added to each girder using unshored construction techniques. The shear test results were compared with predicted results using the ACI 318-95 Simplified Method, the ACI 318-95 Detailed Method (AASHTO 1989), the Modified ACI 318-95 Procedure, the Modified Compression Field Theory (AASHTO LRFD 1994), the Modified Truss Theory, the Truss Theory, the Horizontal Shear Design Method (AASHTO 1989), and the Shear Friction Method (AASHTO LRFD 1994). The calculated shear capacities were in all cases conservative compared to the actual shear capacity.

French et al. [31] found the observed shear capacities were much greater than predicted. The increased capacities were attributed to the large amount of prestressing strands in the bottom flange which confined each other and the stirrups. The aggregate type was found to have a significant effect on the shear capacity (attributed to aggregate interlock). In the case of the limestone concrete mix, the crack plane tended to be much smoother than in the glacial gravel mix.

2.6.2 Temperature

Burns et al. [28] monitored temperatures during casting through the depth of the cross section for several instrumented beams. As hydration takes place, the top portions of the section get significantly hotter than the lower portions. The presence of this temperature gradient as the beam is forming may have a significant impact on beam camber. One consequence of the high hydration temperatures in the beams is the formation of thermal cracking prior to release. On most pours, vertical cracks were observed at several locations along the length of the beams. All of these cracks closed upon release of prestress and are not likely to pose any long-term structural problem. In a completed bridge, temperature gradients, which are nonuniform vertical distributions of temperature, develop in the composite beam due to uneven heating and cooling. Heat energy is provided to the bridge superstructure by means of solar radiation. Additional heat may be gained or lost due to convection to or from the surrounding atmosphere. The amount of temperature change created by these heat sources depends upon wind speed, ambient temperature, relative humidity, weather conditions (clear or cloudy), material properties of the bridge, surface characteristics, the time of day, and the time of year.

Internal concrete temperature is not always monitored for normal concrete. The internal concrete temperature should be monitored for HPC because: (1) it can reach high temperatures (over 200 ^{o}F has been measured) which could harm the concrete; and (2) it may affect concrete strength [7].

2.6.3 Camber

Camber is an important property of prestressed concrete beams that can greatly influence the construction and service states of typical highway bridge structures. Inadequate camber prior to casting of the deck slab may make it difficult, if not impossible, for the contractor to satisfy minimum thickness requirements for the deck slab without creating a sagging (downward deflecting) bridge. Camber differences between adjacent girders may cause similar problems during construction. Excessive camber, though less undesirable than inadequate camber, can result in an uneven riding surface for vehicles traveling across the bridge. Considering these and other potential problems, accurate prediction of camber is very important. A large number of parameters can affect the camber and deflection behavior of bridge girders. Concrete material properties which influence the deformation behavior include modulus of elasticity, unit weight, and creep. Composite and noncomposite girder section properties, especially the cross sectional moment of inertia, have a significant impact on camber and deflection. The span length of a girder will affect its camber and deflection behavior dramatically [32].

Gross et al. [32] investigated the cambers of the Louetta Road Overpass (Houston, Texas). Camber was measured for all beams immediately after release of prestress force and long time after deck casting. At release the ratios of measured to predicted cambers changed from 0.68 to 0.99. In the long term, the ratios changed from 0.07 to 0.92. They drew the following conclusions.

1. Prediction of camber and deflection is highly sensitive for long span beams.

2. Errors in estimation of prestress loss, member self weight, and modulus of elasticity could contribute to the low observed camber.

3. Thermally induced deflection prior to release may contribute to low camber. This deflection is due to the cooling of the member after hydration, at which a temperature gradient exists, to a uniform temperature state.

4. Errors in prediction of camber growth over time are likely due to the difference between the creep model used for prediction and the actual creep history experienced by the member.

Shing et al. [23] also investigated camber. Bolts were attached to one side of each girder at both ends at the level of the center of gravity of the girder section. A fishing line was stretched tight between these bolts and a reference mark was made on the girder at midspan. The tension in the line was maintained the same in measuring camber. Camber was measured for each girder immediately after prestress release, immediately before and after the topping slab casting, 14 and 28 days after girder casting, and on the day of development length testing. A time step procedure was used to estimate the camber of the girders, based on the creep and shrinkage properties, and the calculated camber was compared to the measured values. The calculated camber at 28 days using these values was 2.2 in., which is significantly higher than the average measured value of 1.2 in. Creep was the prime contributor to increases in camber and it is suspected that the measured creep values might have been too high.

In the investigation of Roller et al. [24] measured early-age camber values correlated well with deflections calculated using conventional methods and the measured material properties and prestress losses.

2.6.4 Transfer Length

In a pretensioned member, the prestressing force imparted by the strand is transferred to the concrete by bond in the end region of the member. The distance over which the effective prestress is developed in the strand is called the transfer length [33].

ACI 318 gives equation (2-21) for predicting the transfer length.

$$L_t = \frac{f_{se}}{3} d_b \tag{2-21}$$

where, d_b is the nominal diameter of the prestressing strand; and f_{se} is the effective stress in the prestressing steel after losses in ksi.

Zia and Mostafa [33] proposed equation (2-22) for the transfer length of prestressing strands.

$$L_t = 1.5 \frac{f_{si}}{f_{ci}} d_b - 4.6 \tag{2-22}$$

where, f_{si} is initial stress in the strand before losses in ksi; f_{ci} is compressive strength of concrete at transfer in ksi; and d_b is the nominal diameter of prestressing strand in inches.

Cousins, Zia and Johnston [34] proposed equation (2-23) for computing the transfer length of uncoated strands. This equation is not intended for high early strength concrete.

$$L_t = 0.5 \frac{U_t' \sqrt{f_{ci}}}{B} + \frac{f_{se} A_s}{\pi d U_t' \sqrt{f_{ci}}} \tag{2-23}$$

where, U_t' is plastic transfer bond stress coefficient; B is bond modulus (slope of bond stress curve in the elastic zone) in psi/in; f_{ci} is compressive strength of the concrete at transfer in psi; f_{se} is effective prestress in psi; A_s is area of prestressing strand in in^2; and d is nominal strand diameter in inches.

Ahmad et al. [19] cast a prestressed beam to determine the transfer length of the prestressing strands. The beam had a length of 84 in. and a cross section of 12 in. by 5.5 in. with a 3.5 in. effective depth. Four 0.5 in. Grade 270 low relaxation strands were cast in the beam. The observed transfer length of about 30 in. is a little greater than the prediction of 25 inches given by ACI 318 and falls between the predictions of 26.6 inches given by equation 2-22 and 39.5 inches given by equation 2-23. Therefore, it appears that a reasonable estimate of the transfer length of prestressing strands can be made by use of the ACI 318, and other equations available in the literature.

Shing et al. [23] determined transfer lengths by measuring strains on girder surfaces with a Whittemore gage. This gage had a 7.87 in. gage length. Threaded target points were cast into both sides of each girder at the same level as the tendon center of gravity. These target points were located at 3.94 in. spacings over the first 63 in. from each end of the girder, and at 7.87 in. spacings in the rest of the girder. The average transfer length for the three girders tested was determined to be 23.4 in. The development length for these girders was determined to be about 60 in. The AASHTO specifications overestimated the transfer length by 18% and the development length by 53% for these girders. However, these results can't be generalized to all 0.6 in diameter strands as the bond quality may vary depending on the surface condition and manufacturing process of the strand.

Roller et al. [24] showed that measured transfer lengths interpreted from Whittemore gauge readings were in reasonable agreement with expected values from ACI 318.

French et al. [31] determined transfer lengths graphically from the measured surface strains using the "95% Average Maximum Strain Method," and "Final Average Method." The measured transfer lengths were all less than those predicted using the AASHTO relationship of $50d_b$. This indicates that the AASHTO estimated transfer length relationship was a conservative predictor for the high strength concrete girders for the arrangement of 0.6 in. diameter strands.

2.6.5 Prestress Losses

Stanton et al. ever talked about the prestress loss caused by temperature changes during fabrication [25]. The strand is stressed in cold weather, then it is heated by the curing of the surrounding concrete, which causes the strand stress to drop. During the time at high temperature, the strand bonds to the concrete, after which the concrete and steel cool and shorten together. If the two materials have the same coefficient of thermal expansion, no mechanical strain change, and so no stress change, would be induced by the cooling. Therefore, temperature changes during fabrication would induce a permanent prestressing loss.

After an experimental study carried out to specifically determine the thermal loss, Huang found that steam curing causes the steel pretension to decrease significantly under elevated temperature [35]. However, this thermal loss was found to be almost completely recovered upon cooling after the termination of curing. Huang suggested that there is no need to consider long-term losses due to the

excursion into high temperatures. Adherence of concrete to steel in a pretensioned member does not prevent the steel from regaining its thermal loss of stress upon cooling [35].

In the investigation of Roller et al. [24], concrete strains measured at a concrete age of 28 days indicated that prestreess losses were significantly less than the losses calculated using the provisions from AASHTO and PCI. After nine months of being subjected to design dead load, the prestress losses measured were only slightly greater than the losses determined at 28 days and significantly less than the total long term prestress losses predicted using AASHTO.

Burns et al. [28] investigated the prestress losses in beams of an HPC bridge in San Angelo. Relaxation, temperature changes, and concrete drying shrinkage contributed to prestress losses prior to release. Total losses prior to release were estimated to be between 4 and 6 percent. A large component of the total loss was due to the high heat of hydration observed in all beams. Measured elastic shortening losses were significantly higher than predicted. It is probable that the difference is caused by an unavoidable measurement error due to restraint from the prestress bed. Measured long-term losses for all beams were reasonably close to predicted values.

In the experiment of French et al. [31], they found that at release the measured losses were greater than predicted; whereas at later ages the predicted losses exceeded the measured losses. The early age losses tend to be underpredicted due to an overestimate in the girder stiffness. Conventional modulus of elasticity relations overpredict the stiffness of high strength concrete which causes an underestimation of the girder elastic shortening at release. At later ages, conventional concrete creep

relations overpredict the concrete creep which results in an overprediction of the long-term losses.

2.7 Price Evaluation

The cost of HPC/HSC has been found to be lower than that of NSC. For T-shaped beams, the cost benefit of using HPC was low since it was not possible to reduce the size of the upper flange. However, using HPC in I-shaped beams decreased the weight by about 35% given constant span and loading. This means that the cost of an I-girder was reduced substantially, especially when taking into account the reduced number of strands and thus the reduced labor cost required to install the strands in the beam. For the I-shaped beams, the cost benefit becomes about 15% when compared with NSC. Due to the high cementitious material content of HPC, the heat of hydration must be controlled. This may also create a savings opportunity by eliminating steam curing. About 7% of the production of carbon dioxide in the world comes from the manufacturing of cement. Using HPC for I-girders reduces the total required amount of cement, since cement is performing more efficiently in HPC. Also much less aggregate is required to produce the same type of structure due to smaller member sections. The use of HPC in prefabrication also lowers the energy consumption of transport of aggregate and element fabrication. For example, the same type of transport truck may carry 10 HPC beams instead of 6 NSC members, given constant length and capacity. Lower crane capacity requirements, smaller foundations, and strand reduction are also positive environmental factors of HPC use. In total, the requried release of carbon dioxide to produce an I-girder with a given span and load-carrying capacity was reduced by 35% over NSC, which is substantial [36].

When the Route 104 Bridge over the Newfound River, Bristol 14 was built, a cost comparison between the HPC bridge and several NPC bridges in New Hampshire was made [37]. The HPC bridge had an approximate initial superstructure cost of $59/sf. Compared to the average superstructure cost of the NPC bridges, approximately $48/sf, the HPC cost is 23% higher. There are several possible explanations for this outcome. One possibility is that HPC is a new material in the region and because of its unknown nature, contractors assume a higher risk level and subsequently submit higher bids. Another possibility is HPC requires additional mix development and testing which increases cost. Since these costs were distributed over a small volume of concrete (the bridge had five girders and a relatively short span length) this could have inflated the concrete cost. Another possible factor contributing to the higher HPC cost was the winning low bidder was a road contractor. The bridge work had to be sublet which would inflate the road contractor's bid. The second low bidder was a bridge contractor who had a 10% lower bid for the superstructure than the winning bidder. Lastly, two girders were instrumented for testing purposes. Although the instrumentation was provided by FHWA and installed by the University of New Hampshire, the contractor could have included additional costs associated with potential coordination delays during the girder fabrication and bridge construction.

Another example is the HPC bridge at 120th Street and Giles Road in Omaha, Nebraska. This bridge is a stream overpass with an overall length and width of 225 ft. and 84.5 ft., respectively. A bridge of similar geometry, but using conventional concrete, had been built in the close vicinity of this HPC bridge on the same road. Having two bridges with almost identical layouts, traffic volume, and

environment provides an excellent opportunity to compare the initial and life-cycle economics, as well as, the overall structural and functional performance of the HPC bridge with that of a conventional concrete bridge. The initial cost comparison between the two bridges (similar geometry and function with different concrete and girder section) is shown in Table 2.6 [38].

Table 2.6 Comparison in the Cost Between the Conventional and HPC Bridges

Item	Conventional Bridge			HPC Bridge		
	Quantity	Unit Price($)	Total ($)	Quantity	Unit Price($)	Total ($)
Prestressed Concrete (cy)	334	511	170,674	280	742	207,760
Concrete (cy)	494	245	121,030	517	245	126,665
Epoxy coated steel (lb)	171,401	0.58	99,180	127,200	0.58	73,660
Total			390,884			408,085

The cost figures used were taken from the contract bids of each bridge. Only the items which are different in the two bridges were considered. Although the unit cost of the HPC was slightly higher, the overall cost of the superstructure was about the same, not including the labor savings for erecting fewer girder lines. Considering the differences between the various bids at different times, the difference in cost as shown is almost negligible and is expected to be even lower as contractors get more familiar with HPC. If experience from observation of this bridge indicates a longer service life and less maintenance, more significant life-cycle savings will result.

Chapter 3

EXPERIMENTAL PROGRAM

3.1 Introduction

This study is jointly sponsored by Federal Highway Administration (FHWA) and Delaware Department of Transportation (DelDOT). The primary objective is to gain an understanding of the actual post-construction performance of HPC bridge structures from both a materials and structural behavior perspective, based on the design and construction of Bridge 8F in Frederica, Delaware. To address the critical issues associated with evaluating the performance of HPC in bridge structures, a cross disciplinary team of University of Delaware (UD) researchers, working in cooperation with the bridge and materials staff at DelDOT was assembled. The team's expertise ranged from concrete materials to structural design and testing to structural monitoring and instrumentation. The DelDOT staff members involved in this project included several bridge design staff members, and several materials staff members. While Bridge 8F makes good use of the performance characteristics of HPC, it has not necessarily been optimized to make use of all HPC benefits. UD has also investigated design issues that DelDOT may consider on future HPC bridges.

It should be noted that only monitoring while beams were in the yard is reported here. Upon the finishing of this report, the monitoring is still going on. The monitoring in the field will be reported in other papers.

3.2 Bridge 8F

In 1999, the Delaware Department of Transportation (DelDOT) received funds through the Federal Highway Administration's Innovative Bridge Research and Construction Program (IBRC) to design and construct an HPC bridge. A two-span, prestressed concrete, adjacent box beam bridge utilizing HPC in both the beams and deck was designed. The beams for the bridge were fabricated by Concrete Building Systems (CBS) in Delmar, Delaware. The bridge replaced a deteriorated four-span structure. Since CBS is a relatively small precast plant with no prior experience with HPC bridges, the outcome of this project is of special interest to DelDOT.

The existing bridge consisted of four 28 ft. 5 in. spans supported by concrete encased I-beams resting on solid concrete piers and abutments. The bridge was built in 1920 and rehabilitated in 1992. It was classified as structurally deficient due to considerable spalling and salt infiltration of the piers, abutments, and fascia beams. Soil conditions (clay layers beneath the marsh), have caused the structure and approach roadway to settle over the years. These problems led DelDOT to pursue bridge replacement.

The HPC replacement bridge consists of two 62 ft. 4 in. spans consisting of adjacent prestressed concrete box beams with a concrete deck to make the structure continuous for live load (see Figure 3.1). The center pier uses 18 in. square precast concrete piles with a cast-in-place pier cap. Each abutment consists of a continuous wall made of 16 in. by 48 in. precast concrete sheet piles with a cast-in-place abutment cap. HPC is used throughout the bridge (beams, sheet piles, and deck) with low permeability limits to reduce the amount of salt penetrating the concrete over the life

of the structure and high strength to optimize structural members and extend the span lengths to minimize the number of intermediate piers (reduced from three to one).

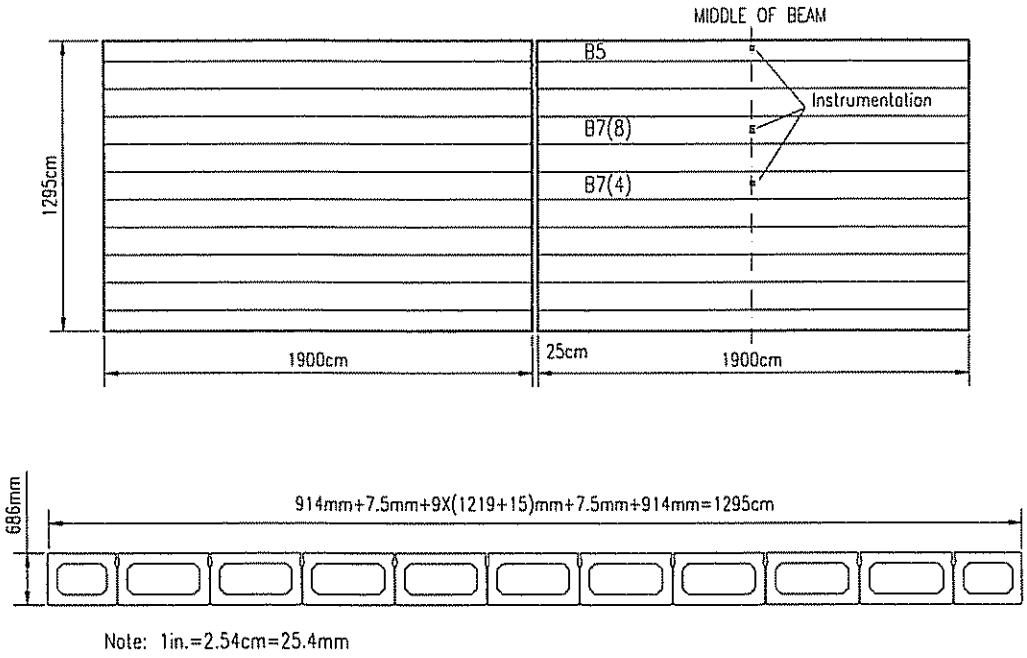

Figure 3.1 Plan and Cross-Section of HPC Bridge 8F

The reduction in the number of piers from three to one improves the hydraulics of the bridge, minimizes the effects of scour, and reduces the overall cost. To accomplish this, much longer span lengths had to be designed. The beam depth had to be optimized to fit within the constraints of maintaining the existing clearance under the bridge and minimizing the need to raise the roadway elevation (and thereby potentially causing future settlement problems). High strength concrete with a 28-day strength of 8 ksi was used for the design of the precast beams. By utilizing the higher

compressive stress limits, a 27 in. deep beam was able to span the required distance. A cast-in-place deck using 6.1 ksi concrete also helped to increase the efficiency of the composite section. In the final design, the roadway elevations were maintained and the under clearance was slightly improved.

The use of HPC to eliminate two spans and two piers resulted in an approximate savings of $50,000. These savings resulted from the elimination of two piers from the substructure, elimination of the riprap that would have been necessary to protect the piers from scour, and the elimination of the construction time that would have been required to form and place the piers.

A second novel feature of this bridge is the precast HPC sheet piles used in the abutment walls. Typically, DelDOT uses square precast concrete piles with a cast-in-place concrete cap and backed with A690 steel sheeting to construct abutments for this type of bridge. In 1997, Bethlehem Steel, the only domestic fabricator, stopped rolling A690 steel sheets. This forced the DelDOT design team to look for alternates and to try domestically available precast prestressed concrete sheeting in lieu of steel sheeting. The sheet piles were designed for bearing as well as retention of fill, eliminating the need for any square piles. HPC provided increased capacity for bending and driving stresses [39].

Each of the 22 adjacent prestressed concrete box beams used in the bridge are 62 ft. 4 in. long and 27 in. deep. The beams were fabricated by Concrete Building Systems (CBS) in Delmar, Delaware, and were all produced in the same bed. The test program focuses on three particular beams and the HPC associated with those particular pours. Standard test data for all of the other pours is also being studied. The three beams being studied here are referred to as B5, B7(4), and B7(8) and can be

seen in Figure 3.1. Each beam was prestressed using 0.5 in. diameter, Grade 270, seven-wire low relaxation strands. Beams B5, B7(4), and B7(8) have 16, 18, 18 straight strands respectively. The strands were jacked to an initial tensile force of 31 kips. Beam B5 was cast on August 30, 1999, while beams B7(4) and B7(8) were cast on October 4, 1999 and October 14, 1999, respectively. Approximately 16-hours after casting, the strands for each beam were released. Prior to casting, long-term monitoring instrumentation was installed in each beam. Furthermore, during the casting, standard test specimens were made for the material testing program.

3.3 Instrumentation

In order to assess the performance of the prestressed beams, a combination of vibrating wire strain gages, thermocouples, and a corrosion monitoring system were installed prior to the casting of the beams. In total for the three beams, four vibrating wire strand meters, six vibrating wire rebar strain meters, eighteen thermocouples, and eight corrosion monitoring systems were installed. This instrumentation will allow the research team to evaluate the prestress losses over time, as well as monitor the live load performance of the beams. The instrumentation also allows the evaluation of the heat of hydration during the curing of the beams. Finally, the corrosion monitoring system will allow an assessment of the HPC beams resistance to corrosion (i.e. low permeability). The DataTaker 615 was used to measure the gages.

3.3.1 Vibrating Wire Strandmeter [40]

The Geokon Vibrating Wire Strandmeter used are designed to measure change in deformation in wire strands. The instrument consists of a vibrating wire

sensing element in series with a heat treated, stress relieved spring which is connected to the wire at one end and a connecting rod at the other. The unit is fully sealed and operates at pressures of up to 250 psi. As the connecting rod is pulled out from the gage body, the spring is elongated causing an increase in tension which is sensed by the vibrating wire element. The tension in the wire is directly proportional to the extension. Hence, the change in deformation can be determined very accurately by measuring the strain change. A thermistor is enclosed in the strandmeter. The cable of the strandmeter is connected to a DataTaker 615. This instrument provides the necessary excitation to pluck the vibrating wire element so that it vibrates at its resonant frequency. This frequency is then measured by the DataTaker, displayed and stored in memory. Strain in the strand causes the same strain in the strandmeter and a corresponding change in the resonant frequency of the vibrating wire.

The basic units utilized by Geokon for measurement and reduction of data from Vibrating Wire Strandmeters are "digits". Calculation of digits are based on the following equation:

$$Digits=(1/Period)^2 \times 10^{-3}$$

or

$$Digits = Hz^2 \times 10^{-3} \tag{3.1}$$

To convert digits to deformation the following equation applies;

Deformation=(Current Reading – Initial Reading) ×Calibration Factor×Conversion Factor

or

$$D = (R1 - R0) \times C \times F \tag{3.2}$$

where, R1 is the Current Reading; R0 is the Initial reading (usually obtained at installation); C is the Calibration Factor (usually millimeters or inches per digit); and F is an engineering units conversion factor (optional). See Table 3.1 for applicable engineering units and conversion multipliers.

Table 3.1 Engineering Units Conversion Multipliers

From → To ↓	Inches	Feet	Millimeters	Centimeters	Meters
Inches	1	12	0.03937	0.3937	39.37
Feet	0.0833	1	0.003281	0.03281	3.281
Millimeters	25.4	304.8	1	10	1000
Centimeters	2.54	30.48	0.10	1	100
Meters	0.0254	0.3048	0.001	0.01	1

The Model 4410 Vibrating Wire Strandmeters have a very small coefficient of thermal expansion so in many cases correction is not necessary. However, if maximum accuracy is desired or the temperature changes are extreme (> 50^0C) a temperature correction may be applied. The total strandmeter deformation (including mechanical deformation and thermal deformation) is given by,

$$Dcorrected = ((R1 - R0) \times C) + ((T1 - T0) \times K) \qquad (3.3)$$

where, R1 is the Current Reading; R0 is the Initial Reading; C is the Calibration Factor; T1 is the Current Temperature; T0 is the Initial Temperature; and K is the Thermal Coefficient.

Tests have determined that the Thermal Coefficient, K, changes with the position of the transducer shaft. Hence, the first step in the temperature correction

process is the determination of the proper Thermal Coefficient based on the following equation;

Thermal Coefficient = ((Reading in Digits×0.000295)+1.724)
×Calibration Factor

or

$$K = ((R1 \times 0.000295) + 1.724) \times C \tag{3.4}$$

where, R1 is the Current Reading; and C is the Calibration Factor supplied with the instrument.

In this study, the Calibration Factors C of strandmeters 15667, 15668, 15669, 15670 are 0.000024071, 0.000024238, 0.000024266, 0.000024467 Inches/Digit respectively.

3.3.2 VW Rebar Strain Meters [41]

The Model 4911 Rebar Strain Meter used is designed for direct embedment in concrete. These instruments are commonly used for measuring strains. Various units are available to match all sizes of concrete reinforcing bars. The smallest size utilizes No.4 rebar (1/2 in. diameter) and is commonly called a "Sister Bar" since it is intended to be attached alongside existing rebar of all sizes. The larger models are intended to be welded at their ends into the rebar system and so the size is chosen to match the existing rebar. The Rebar Strain Meters consist of two lengths of rebar welded onto each end of a central steel section, which includes along its axis a miniature vibrating wire strain gage element complete with an electronic "plucking" coil. This coil is connected to an electrical cable which extends out of the strain meter close to its midpoint. In order to read the gages the cable is connected to a DataTaker

615. This instrument provides the necessary excitation to pluck the vibrating wire element so that it vibrates at its resonant frequency. This frequency is then measured by the DataTaker, displayed, and stored in memory. Strain in the concrete causes the same strain in the rebar (perfect bond assumed) and a corresponding change in the resonant frequency of the vibrating wire.

Each strain meter is individually calibrated at the factory so that the relationship between strain and frequency is known and presented as a calibration factor. Since the vibrating wire element is axially located the strain meter is not affected by bending moments.

The advantage of the Vibrating Wire Rebar Strain Meter over more conventional electrical resistance types lies mainly in its long-term stability and its use of a frequency, rather than a voltage, as the output signal. Frequencies may be transmitted over long cable lengths without appreciable degradation caused by variations in cable resistance, contact resistance, or leakage to ground. A thermistor is included in each strain meter as a standard feature and permits measurement of temperature at the strain meter location.

The basic units utilized by Geokon for measurement and reduction of data from Vibrating Wire Rebar Strain Meters are "digits". Calculation of digits are based on the following equation;

$$Digits = (1/T)^2 \times 10^{-3} \tag{3.5}$$

or

$$Digits = Hz^2 / 1000$$

where, T is the period in seconds; and Hz is the frequency in cycles per second.

To convert digits to strain the following equation applies;

$$\varepsilon_{uncorrected} = (R1 - R0) \times C \tag{3.6}$$

where, R0 is the initial reading in digits (usually obtained at installation); R1 is the current reading in digits; and C is the calibration factor from the supplied calibration sheet.

Rebar strain meters are usually embedded in concrete and strained by the concrete, the assumption being that the strain in the meter is equal to the strain in the concrete. When the temperature changes, the concrete expands and contracts at a rate slightly less than the rate of the steel of the vibrating wire. Assuming that the thermal coefficients of steel and concrete are 6.7 ppm/^{0}F and 5.5 ppm/^{0}F respectively, the difference K is therefore 1.2 ppm/^{0}F. Hence a correction is required to the observed strains equal to the difference of these two coefficients.

$$\varepsilon_{corrected}=((R1-R0) \times C)+((T1-T0) \times K) \tag{3.7}$$

where, T0 is the initial temperature recorded at the time of installation; T1 is the current temperature; and K is the thermal coefficient difference.

In this study, the calibration factors C of sister bars 17375, 17376, 17377, 17378, 17379, 17380 are 0.35648, 0.34913, 0.35873, 0.35493, 0.35596, 0.37136 Microstrain/Digit respectively.

3.3.3 Corrosion Monitoring Systems

VETEK V2000 uses a unique patented measuring electrode system to determine the actual electrochemical condition of steel embedded in cement grout or concrete. The V2000 is able to detect a single corrosion site of less than 1 mm, as

well as monitor for subsequent corrosion progression (or lack there of), without destructive examinations or tests of any kind.

The V2000 monitoring system consists of an electrode of silver-silver chloride wire which is inside a plastic braid. The braid prevents the wire from coming into contact with the steel strand. The porewater of the grout performs the function of an electrolyte between the strand and electrode. It is therefore possible to measure the electrical potential between the anchor and the electrode, and thus know the condition of the steel.

On-site, embedded electrodes within a 30 meter area can be wired to a junction box, making it possible to test all locations in that area at one central location. Alternatively a voltmeter can easily take readings of each of the locations one at any time. The readings on the voltmeter will indicate one of the following series of ranges (see Table 3.2).

Table 3.2 The Meaning of Readings from VETEK

Range 1 **V < 270mv**	The steel is not actively corroding.
Range 2 **270mv <V< 370mv**	The passivation layer of the steel is damaged, and corrosion is possible. It is possible to do current measurements to determine if corrosion has actually started.
Range 3 **V > 370mv**	The steel is actively corroding.

3.3.4 Data Acquisition System [42]

Data acquisition and data logging are not the same. Traditionally, data acquisition has been defined as the regular collection of data — scanning sensors, making instantaneous measurements, then feeding these to a recorder or computer. Data logging has two possible definitions:

- It is considered by some to be simply making a permanent record of data that has been collected: printing or plotting it, writing it on a sheet of paper, or storing it on a computer's hard disk or in electronic memory.
- Others perceive data logging as the total operation of collecting data and making a permanent record of it — they see data acquisition as a subset of data logging.

With Datataker (in this project DataTaker 615 was used), any distinction between these two terms has become even more blurred because the Datataker combines acquisition, logging, and more in a single instrument about the size of a standard house brick. It scans sensors and transducers, takes measurements, processes the data by performing conversions and calculations, records and/or displays the data, and raises alarms — all according to schedules which you define.

One of the Datataker's two basic functions is to "read" ("sample," "scan," or "measure") sensors and present the values on a computer screen or on the Datataker's built-in display (if it has one). Although these readings can be used, say, to trigger an alarm, they are temporary: the Datataker has not recorded, stored or remembered them anywhere — that is, the data has not been "logged" by the Datataker. To "log" ("record," "store," or "remember") data one must issue the Logon

command to the Datataker after having commanded it to acquire data. Logging is a separate and distinct operation.

Being microprocessor-based, one sends instructions ("commands") to the Datataker (from a computer terminal) telling it which sensors to read, when and how often to read them, how to interpret the readings, and what to do with the data. Then one lets the Datataker do the work.

More specifically, the Datataker can perform any or all of the following tasks:

- acquire data (scan sensors, make instantaneous measurements and forward them to a computer);
- log data (store measurements in the internal memory and/or one a removable memory card);
- convert measurements according to your requirements (voltages to °C or °F, for example);
- carry out calculations on the measurements (average, standard deviation, maximum, minimum,...);
- log the converted measurements and the results of calculations to its internal memory and/or a removable memory card, or transfer them to a computer;
- display all of the above information on a computer screen, or locally (on the logger's built-in display or panel-mount display, if there is one);
- return data directly to a computer in real time (that is, as each measurement is made) as well as, or instead of, logging it;

- raise alarms when data is outside specified ranges. Alarms can trigger outside events (turn on a warning light or siren, for example), or making the Datataker carry out additional tasks (scan more frequently, stop logging, or scan and log additional sensors, for example).

In order to start the DataTaker, one must use a computer. Once the Datataker is running one can disconnect the computer and the Datataker will continue to operate as programmed since the software which controls the logger is inside the logger itself. This is called "stand-alone" operation.

We often want to know the time and date each measurement was made. As a result, the Datataker can automatically log this information along with the measurements. Thus every reading from every sensor can be "time- and date-stamped".

Here are some typical ways one can operate the Datataker:

- connected permanently to a computer, transferring data to the computer continuously or periodically;
- connected temporarily to a portable computer for transferring data or programming the Datataker;
- periodically transferring data to a distant computer via a pair of modems (the data transfer can be initiated by the Datataker or from the computer);
- periodically recovering data and/or programming the Datataker via a removable memory card.

The thermistor type encapsulated in strandmeter and sister bar is YSI 44005 (YS05), Dale #1C3001-B3, Alpha#13A3001-B3. Thermistors are

semiconductor devices that change their electrical resistance with temperature. Thermistors measure temperatures from –80 ^{0}C up to 250 ^{0}C. They are sensitive but highly nonlinear. Datatakers support all two wire YSI* thermistors. The response is :

$$T = \frac{1}{A + B(LnR) + C(LnR)^3} - 273.2^o C \tag{3.8}$$

where, T is Temperature in ^{0}C; LnR is Natural Log of Thermistor Resistance; A, B, and C are constant terms recommended by YSI*.

3.4 Material Tests

In order to assess the properties of the HPC concrete used for the three beams that have been instrumented, a series of material tests were performed at the University of Delaware. During beam fabrication, concrete cylinders and shrinkage beams were cast and allowed to cure at the site along with the beams until the prestressing strands were released and the beams were removed from the bed. The specimens were then brought back to the University of Delaware and cured in a temperature and humidity controlled room.

Using these specimens, tests were conducted to determine the concrete compressive strength, splitting tensile strength, flexural strength, elastic modulus, chloride permeability, and shrinkage behavior. The tests were performed at concrete ages of 1, 7, 28 and 56, 91 and 365 days (shrinkage tests were conducted at 1, 4, 7, 14, 28, 56, 112, 224, and 448 days). The compression tests were conducted in accordance with ASTM C39-96 [43], the splitting tension tests according to ASTM C496-96 [43], the flexural tests according to ASTM C78-94 [43], the elastic modulus tests according

to ASTM C469-94 [43], and the shrinkage tests according to ASTM C157-93 [43]. The test results were compared to predictions derived from both ACI [18, 22] and AASHTO [44] formulae. The test results were also compared to the results of tests conducted by CBS for the same three beams, as well as results from the tests from the other beams. This allowed the research team to assess the ability of the contractor to produce a consistent mix. Since CBS is a relatively small plant with no prior experience with HPC bridge beams, their ability to work effectively with HPC is of considerable interest.

3.5 Structural Tests

In order to assess the performance of the prestressed beams, a combination of vibrating wire strain gages, thermocouples, and a corrosion monitoring system were installed prior to the casting of the beams. In total for the three beams, four vibrating wire strand meters, six vibrating wire rebar strain meters, eighteen thermocouples, and eight corrosion monitoring sensors were installed. This instrumentation allowed the research team to evaluate the prestressing losses over time, as well as monitor the live load performance of the beams. The instrumentation also allows the evaluation of the heat of hydration during the curing of the beams. Finally, the corrosion monitoring system allows an assessment of the HPC beams resistance to corrosion (i.e. low permeability).

In terms of strain monitoring, two types of gages were used. Vibrating wire strand meters were selected to directly measure any change in strain in the prestressing strands. These gages were clamped onto the strands after they were stressed. The gages also include a thermistor that allows one to measure temperature

in the concrete at the gage location. A second type of vibrating wire stain gage was used for redundancy. These gages are referred to as vibrating wire rebar strain meters. These consist of a vibrating wire strain gage attached to a piece of standard rebar "Sister Bar" that is then embedded into the concrete. Like the strandmeter, these include a thermistor as well.

In order to get the temperature changes versus time (especially the temperature changes caused by hydration heat) and the thermal gradient, many thermocouples were installed in the beams in addition to the thermistors of the vibrating wire gages. Furthermore, thermocouples where placed in some cylinders, and one was used to measure the ambient temperature.

A corrosion monitoring system consisting of an electrode of silver-silver chloride wire which is protected by plastic braid was installed to help monitor any onset of corrosion. By measuring the electrical potential between the strand and the electrode, the existence of active corrosion can be evaluated. Furthermore, the strand and silver wire form a transmission line. By using Time Domain Reflectometry (TDR), the location of corrosion can be determined. Detailed information about the use of TDR is available in reference 45.

The beam instrumentation layout in B5, B7(4) and B7(8) is shown in Figure 3.2, Figure 3.3, Figure 3.4 respectively. Sensors are located at the middle of the beams (except for Beam B7(8) for which some thermocouples were located in the end block). All of the instrumentation was tested and verified prior to field installation.

A data logger is being used to record the data. All data was measured and logged automatically every half-hour when beams were in the yard. Because the three

beams were fabricated and cast at different times, monitoring was conducted for each one from the time of casting, until the time that the next instrumented beam was cast. After three beams were finished, they were put together and the Datataker was used to monitor all of them. After they were erected in the bridge site, the monitoring is still going on.

Because the construction lagged behind schedule, the time between girder casting and girder erection was much longer than had been scheduled. Casting of B7(8) was completed in October 1999, while the beams were erected in September 2000. This provided a very good opportunity to take relatively long-term strain readings on the bare girders.

It should be noted that two situations caused delays to the construction schedule. The first one, not related to the use of HPC, was the delay of pile construction due to unexpected geometric condition. The second one, caused by the use of HPC, was that some beams didn't have enough concrete protection cover. Two beams were rejected.

Figure 3.2 Beam Instrumentation Layout in B5

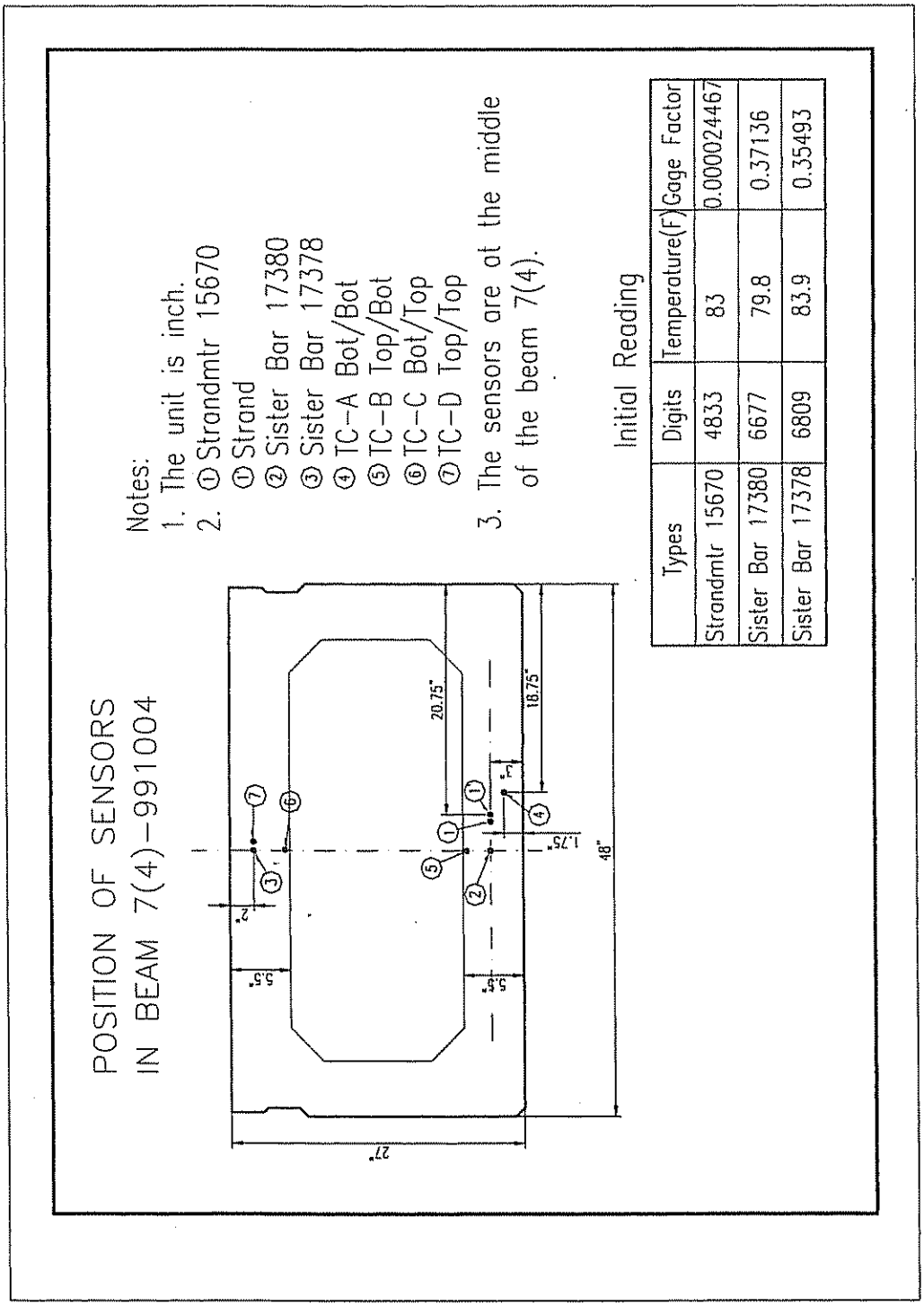

Types	Digits	Temperature(F)	Gage Factor
Strandmtr 15670	4833	83	0.000024467
Sister Bar 17380	6677	79.8	0.37136
Sister Bar 17378	6809	83.9	0.35493

Figure 3.3 Beam Instrumentation Layout in B7(4)

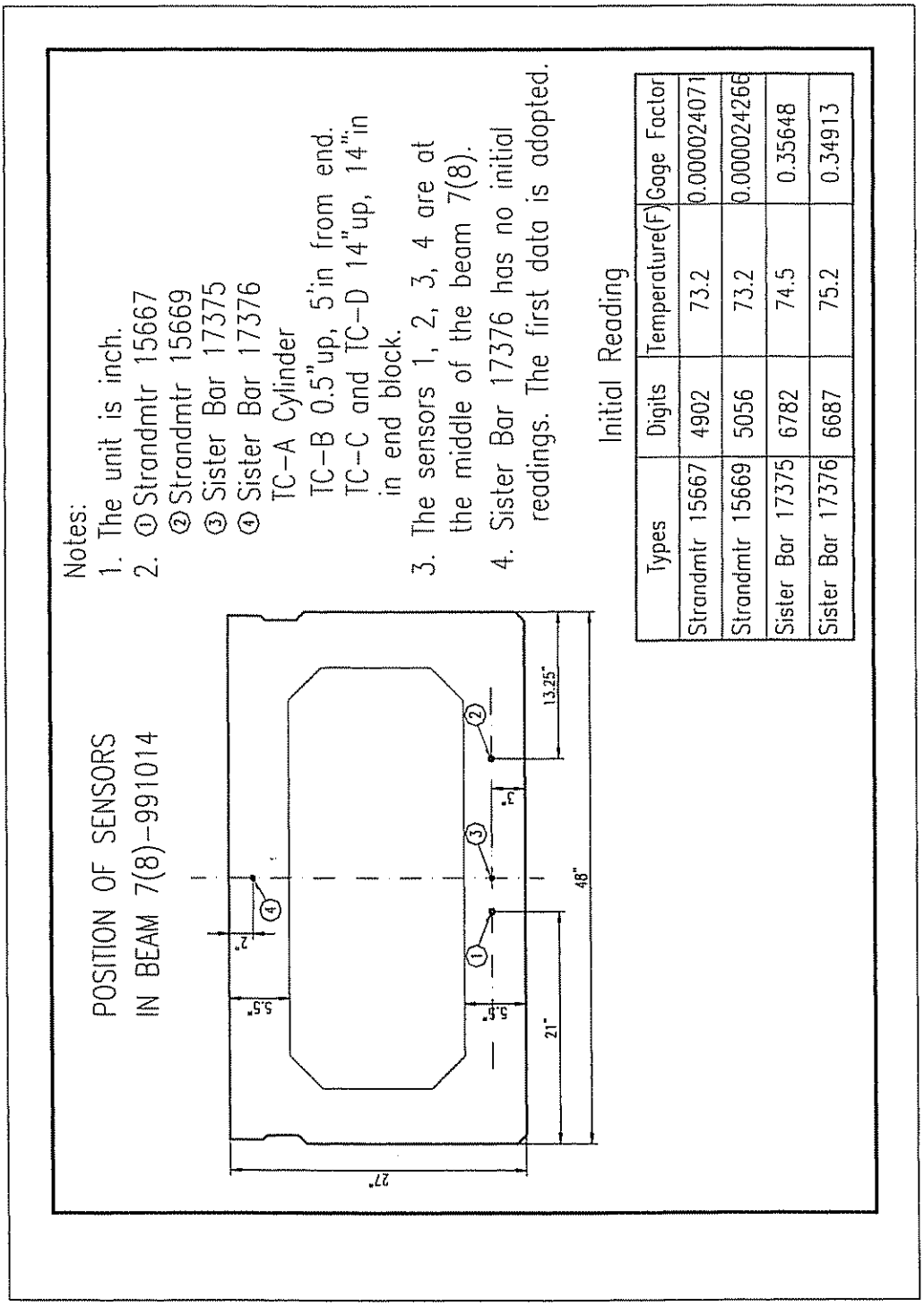

Figure 3.4 Beam Instrumentation Layout in B7(8)

Chapter 4

EXPERIMENTAL RESULTS

4.1 Material Properties

By testing 4 by 8 inch cylinders to failure in compression, we got the corresponding compressive strength of the concrete using formula (4.1).

$$\sigma = P/(\pi r^2) \tag{4.1}$$

where, P is the maximum load; r is the radius of the cylinder.

The formula used to calculate the splitting tensile strength is given by equation (4.2).

$$T=2P/\pi ld \tag{4.2}$$

where, T is the splitting tensile strength; P is the maximum applied load indicated by the testing machine; l is the length of the specimen; and d is the specimen diameter.

Like the compressive strength, every splitting tensile strength value in Table 4.1 is the average of 3 cylinders.

Formula (4.3) was used to calculate the modulus of rupture.

$$R=PL/bd^2 \tag{4.3}$$

where, R is the modulus of rupture; P is the maximum applied load indicated by the testing machine; L is the span length; b is the average width of specimen at the fracture location; d is the average depth of specimen at the fracture location.

Shrinkage was calculated using equation (4.4).

$$\Delta L_x = (CRD\text{-}initial\ CRD)/G \times 100 \tag{4.4}$$

where, ΔL_x is the percentage change in length of the specimen at any age; CRD is the difference between the comparator reading of the specimen and the reference bar at any age; and G is the gage length.

The modulus of elasticity of the concrete was calculated to the nearest 50 kips using equation (4.5):

$$E = (S_2 - S_1)/(\varepsilon_2 - 0.000050) \tag{4.5}$$

where, E is the chord modulus of elasticity; S_2 is the stress corresponding to 40% of the ultimate load; S_1 is the stress corresponding to a longitudinal strain, ε_1, of 50 microstrain; and ε_2 is the longitudinal strain produced by stress S_2.

Equations (4.1) to (4.5) are all standard ASTM test procedures [44].

A summary of the HPC material test results is given in Table 4.1. All results are average values of three specimens, except for the elastic modulus which is the average of two specimens. Based on the number of samples cast, some tests were not performed at each interval. Recall that the HPC design release strength was 6.4 ksi. One can see from the 1-day strength results of 7.6 ksi, 7.0 ksi, and 6.8 ksi that release could be performed the day after casting. Furthermore, the 28-day strengths of 8.8 ksi, 10.7 ksi, and 10.6 ksi exceeded the design value of 8 ksi in all cases.

Table 4.1 HPC Material Test Results

Concrete Property		1 day	7 day	28 day	56 day
B5	Compressive Strength (ksi)	7.6	8.4	8.8	8.8
	Modulus of Rupture (ksi)	-	1.08	1.19	-
	Modulus of Elasticity (ksi)	-	4546	4992	-
	Splitting Tensile Strength (ksi)	-	0.44	0.57	0.52
B7(4)	Compressive Strength (ksi)	7.0	9.3	10.7	10.9
	Modulus of Rupture (ksi)	-	1.1	1.33	-
	Modulus of Elasticity (ksi)	-	5134	5261	-
	Splitting Tensile Strength (ksi)	-	0.6	0.59	0.59
B7(8)	Compressive Strength (ksi)	6.8	9.2	10.6	-
	Modulus of Rupture (ksi)	-	-	1.42	-
	Modulus of Elasticity (ksi)	-	-	5158	-
	Splitting Tensile Strength (ksi)	-	-	0.65	-

The results of the shrinkage tests at different times are shown in Table 4.2. The initial reading for specimens for beam B5 wasn't measured, so shrinkage results for B5 are unavailable. The values given for beam B7(4) are the average of two specimens, while the values given for beam B7(8) are from one specimen.

Table 4.2 Shrinkage (ppm) vs. Time

Items	4 day	7 day	14 day	28 day	56 day
B7(4)	195	236	323	368	395
B7(8)	191	282	345	391	-

4.2 Comparison of Test Results to Code Equations

In the following sections, material test results are compared to selected formulae from ACI 209R-92 [18], ACI 363R-92 [22], and the AASHTO LRFD Bridge Design Specifications [44].

4.2.1 Compressive Strength

The test results of compressive strength were compared to predictions made using ACI 209R-92 which states that

$$(f_c')_t = \frac{t}{\alpha + \beta t}(f_c')_{28} \tag{4.6}$$

where, $(f_c')_t$ is the compressive strength at age t days, $(f_c')_{28}$ is the 28-day compressive strength, and α and β are parameters that depend on the curing method and concrete type. In this case, $\alpha = 0.7$ and $\beta = 0.98$ (specified in code). A comparison of the test results with Eq. 4.6 is shown in Figure 4.1. As one can see, Eq. 4.6 does a good job of predicting the concrete strength.

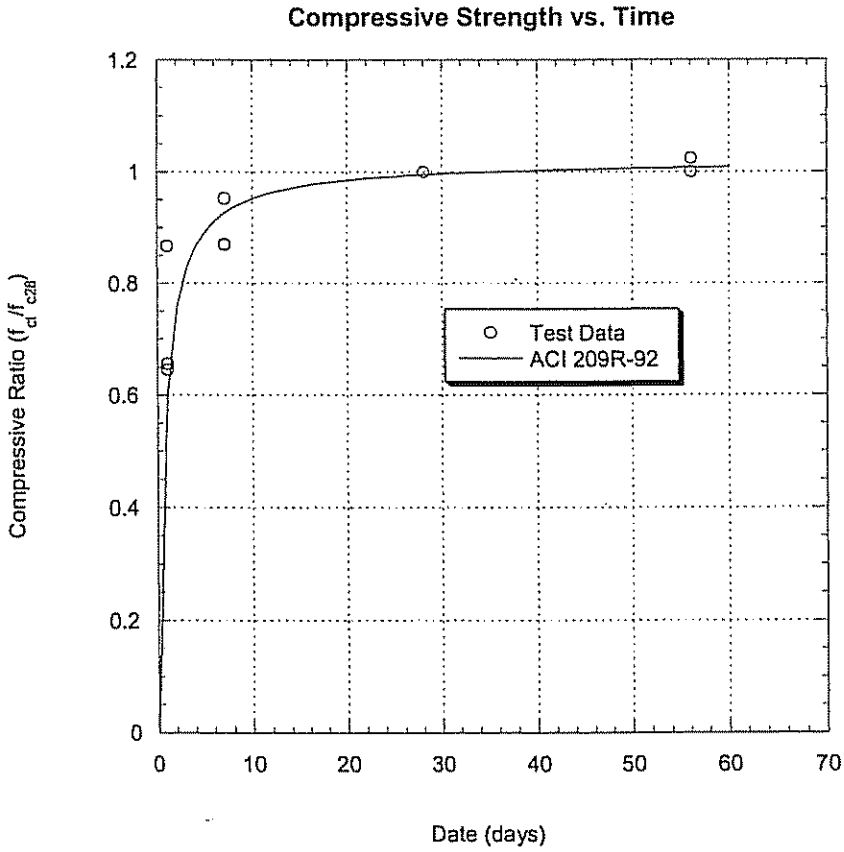

Figure 4.1 Compressive Strength Test Results Compared to ACI Predictions

4.2.2 Elastic Modulus

The elastic modulus test results were compared with the predictions from AASHTO and ACI 363R-92. AASHTO 5.4.2.4 gives the following equation,

$$E_c = 33{,}000 W_c^{1.5} \sqrt{f_c'} ksi \tag{4.7}$$

where, E_c is the elastic modulus, W_c is the unit weight of concrete, and f_c' is the concrete compressive strength. According to ACI 363R-92, AASHTO 5.4.2.4 overestimates the modulus of elasticity for concrete with compressive strengths over 6 ksi. The equation for predicting elastic modulus in ACI 363R-92 for strengths over 3 ksi but lower that 12 ksi is given by

$$E_c = 40{,}000\sqrt{f_c'} + 1.0x10^6\ psi$$
$$\text{For } 3{,}000 \text{ psi} < f_c' < 12{,}000 \text{ psi} \qquad (4.8)$$

where, E_c is the elastic modulus, and f_c' is the concrete compressive strength. A comparison of test results to predictions using AASHTO and ACI formulae are shown in Figure 4.2. It can be seen that ACI 363R-92 agrees quite well with the test results and that AASHTO 5.4.2.4 does indeed overestimate the value of the elastic modulus.

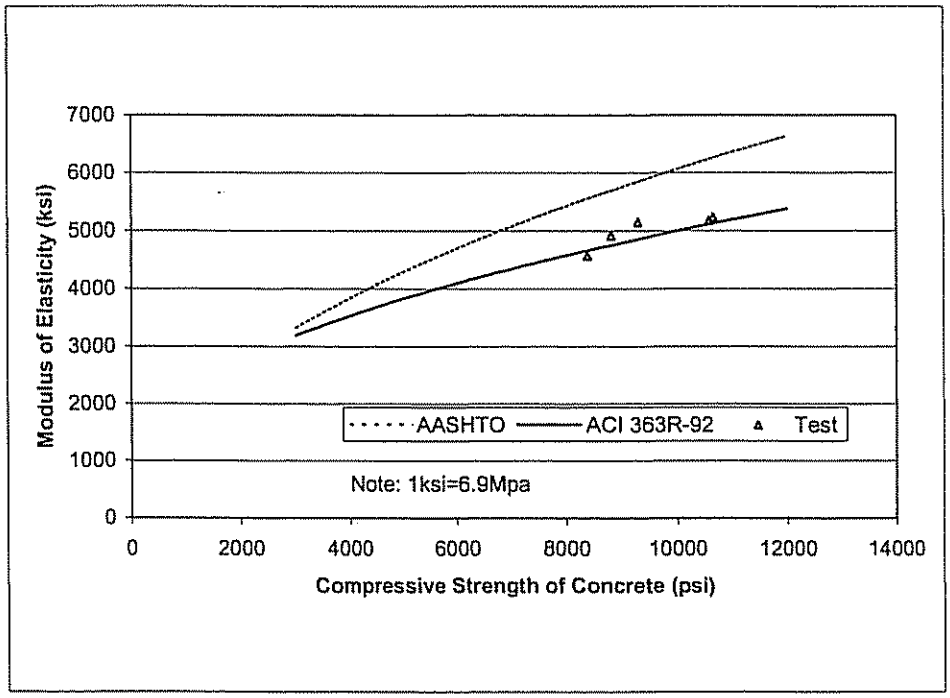

Figure 4.2 Elastic Modulus Test Results Compared to AASHTO and ACI

4.2.3 Modulus of Rupture

The modulus of rupture computed from the test results were compared with predications made using AASHTO and ACI 363R-92 formulae. AASHTO 5.4.2.6 gives the following equation,

$$f_r = 0.24\sqrt{f_c'}ksi \tag{4.9}$$

where, f_r is the modulus of rupture, and f_c' is the concrete compressive strength. ACI 363R-92 gives the following equation for the predication of modulus of rupture of concrete

$$f_r' = 11.7\sqrt{f_c'}psi \quad \text{for } 3{,}000 \text{ psi} < fc < 12{,}000 \text{ psi} \tag{4.10}$$

where, f_r'is the modulus of rupture, and f_c' is the concrete compressive strength. A comparison of the test data and the two predictions is shown in Fig. 4.3. In this case the ACI equation is again fairly accurate while the AASHTO formula underestimates the modulus of rupture for the HPC.

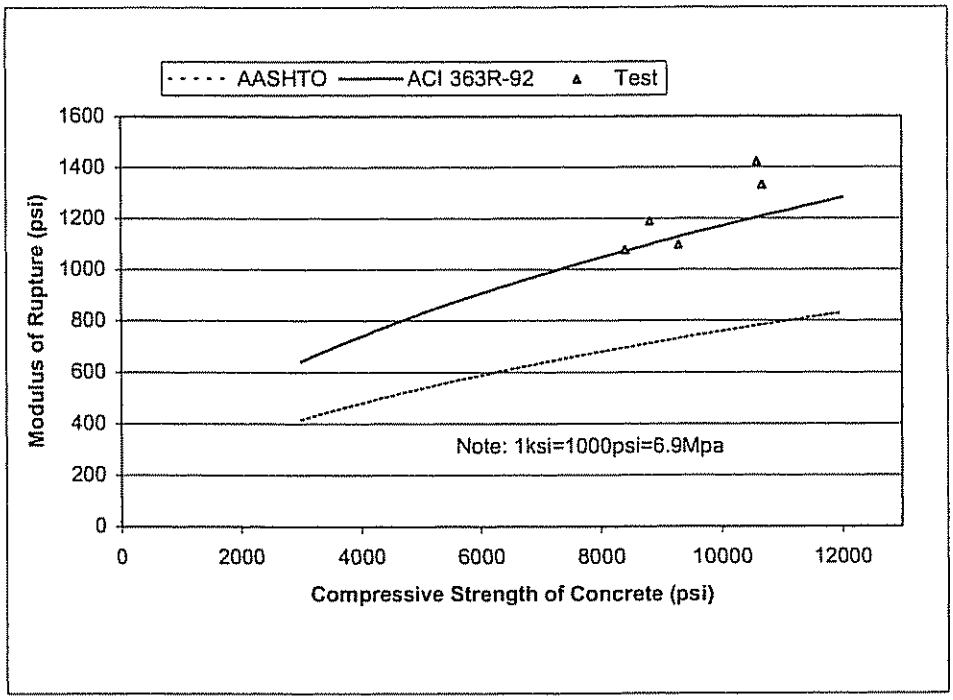

Figure 4.3 Modulus of Rupture Test Results Compared to AASHTO and ACI

4.2.4 Splitting Tensile Strength

The equation for the prediction of the splitting tensile strength based on AASHTO 5.4.2.7 is given by

$$f_r = 0.23\sqrt{f_c'}ksi \tag{4.11}$$

where, f_r is the concrete tensile strength, and f_c' is the concrete compressive strength. The equivalent equation from ACI 363R-92 is

$$f_{sp}' = 7.4\sqrt{f_c'}psi$$
$$\text{for } 3{,}000 \text{ psi} < fc < 12{,}000 \text{ psi} \tag{4.12}$$

In this case, the two equations are very similar. However, for the tests conducted so far, Equations. (4.11) and (4.12) both overestimate the splitting tensile strength from 16% to 52%.

4.2.5 Creep and Shrinkage

AASHTO LRFD 5.4.2.3.3 gives the following shrinkage prediction equation for steam-cured concrete devoid of shrinkage-prone aggregates,

$$\varepsilon_{sh} = -k_s k_h \left(\frac{t}{55.0+t}\right) 0.56 \times 10^{-3} \tag{4.13}$$

$$k_s = \left[\frac{\frac{t}{26e^{0.36(v/s)}+t}}{\frac{t}{45+t}}\right]\left[\frac{1064-94(v/s)}{923}\right]$$

For $H < 80\%$ $\quad k_h=(140-H)/70$

For $H \geq 80\%$ $\quad k_h=3(100-H)/70$

where, t is the drying time (days); k_s is the size factor; k_h is the humidity factor; v/s is the volume to surface ratio; and H is the relative humidity.

Based on this formula, ε_{sh} is not a function of the concrete compressive strength. If two beams made up of concrete having different compressive strengths have the same size factor and are cured and stored under the same condition, they would theoretically have the same ε_{sh}.

After assigning a relative humidity, H of 50% and a volume-to-surface ratio v/s of 0.65, we get the following formula

$$\varepsilon_{sh} = \varepsilon_u \times \frac{45+t}{32.88+t} \times \frac{t}{55+t} \tag{4.14}$$

$\varepsilon_u = 782 \times 10^{-6}$ *in/in*

A plot of shrinkage vs. time is shown in Figure 4.4. From this figure, it can be seen clearly that the shrinkage of HPC in the first month occurs much faster than is predicted by the AASHTO LRFD formula.

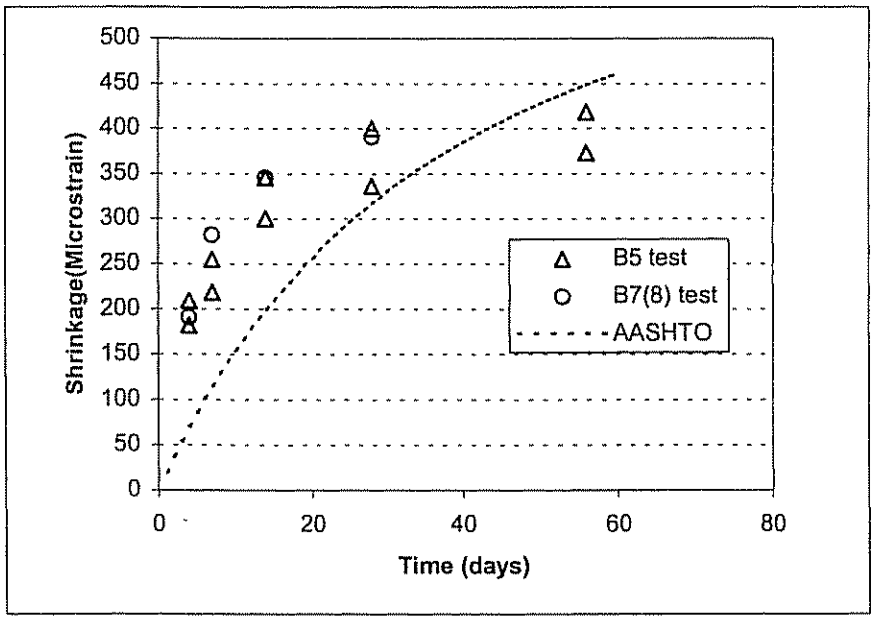

Figure 4.4 Shrinkage vs. Time

AASHTO LRFD 5.4.2.3.2 gives the following equation for creep prediction.

$$\Psi(t,t_j) = 3.5 k_c k_f (1.58 - \frac{H}{120}) t_j^{-0.118} \frac{(t-t_j)^{0.6}}{10.0+(t-t_j)^{0.6}} \tag{4.15}$$

for which:

$$k_f = \frac{1}{0.67 + (\frac{f_c'}{9})}$$

where, H is the relative humidity (%); k_c is the factor for the effect of the volume-to-surface ratio of the component; k_f is the factor for the effect of concrete strength; t is maturity of concrete (days); t_j is age of concrete when load is initially applied (days).

From this formula, it can be seen that when fc' increases, k_f goes down, and the creep coefficient Ψ goes down. Therefore, the creep of HPC will be less than for a conventional concrete.

After assuming a relative humidity, H of 50%, and volume-to-surface ratio v/s of 0.65, and a concrete strength, fc' of 8 ksi, one gets the following formula,

$$\Psi(t) = \Psi u \times \frac{45 + t}{32.88 + t} \times \frac{(t-1)^{0.6}}{10 + (t-1)^{0.6}}, \Psi u = 3.07 \tag{4.16}$$

From the specimens cast from the Louetta HPC beam mix, Burns [28] developed an empirical formula for creep and shrinkage at standard conditions of 40% relative humidity and a volume-to-surface ratio of 1.5,

$$\Psi_{ct} = \frac{t^{0.6}}{7 + t^{0.6}}(\Psi_u), \Psi_u = 1.81 \tag{4.17}$$

$$\varepsilon_{sh} = \frac{t^{0.6}}{3 + t^{0.6}}\varepsilon_u, \varepsilon_u = 433 \times 10^{-6} in/in \tag{4.18}$$

ACI 209 gives equation (4.19) for creep for 1-3 day steam cured conventional concrete. Shrinkage after age 1-3 days for steam cured conventional concrete is given as (4.20). Equation (4.19) and (4.20) are based on 40% relative humidity and a 1.5 volume-to-surface ratio.

$$\Psi_{ct} = \frac{t^{0.6}}{10 + t^{0.6}}(\Psi_u), \Psi_u = 2.35 \tag{4.19}$$

$$\varepsilon_{sh} = \frac{t}{55 + t}\varepsilon_u, \varepsilon_u = 780 \times 10^{-6} in/in \tag{4.20}$$

Comparing equations (4.16), (4.17), and (4.19), it can be seen clearly that creep of HPC occurs much faster than predicted for NSC by AASHTO and ACI. Comparing equations (4.14), (4.18), and (4.20), it can be seen clearly that the shrinkage of HPC also occurs much faster than predicted for NSC by AASHTO and ACI.

4.3 Structural Behavior

The structural behavior, including corrosion vs. time, temperature changes, the effect of concrete maturity, and measured strain will be talked about in the following.

4.3.1 Corrosion

The strand corrosion was monitored using the V2000 monitoring system consisting of an electrode of silver-silver chloride wire inside of a plastic braid. If the reading is less than 270mv, then the strand is not actively corroding. It should be noted that the V2000 only monitors one strand per beam. It is thought to be representative.

Beams B5, B7(4) and B7(8) were monitored for roughly 35 days, 8 days, and 14 days respectively. Plots of the voltages vs. time are shown in Figure 4.5, Figure 4.6, and Figure 4.7. It can be seen that the voltage was high during the

beginning 24 hours. This is due to initial corrosion that occurs when the concrete is wet. As the concrete cures, the voltage goes down quickly with time. After about 530 hours, the voltage in B5 decreased from 700mv to 270mv. It took about 65 hours for the voltage in B7(4) to decrease from 840mv to 270mv. For B7(8), while the voltage was dropping, after about 350 hours the voltage was 440 mv (above 270 mv) indicating that corrosion was still occurring. The continuation of corrosion for a relatively long time (530 hours in B5, over 350 hours in B7(8)) is possibly due to voids in the beam that allow moisture to remain for a long period of time.

The voltages were measured again on March 29, 2000, about 6 months after the beams were cast. The readings were 181.9mv, 118.7mv, and 214.6mv in beams B5, B7(4) and B7(8) respectively. At this time, based on the readings, none of the strands being monitored were actively corroding. Continued monitoring will help to verify the ability of HPC to enhance durability through the prevention of corrosion of the reinforcement.

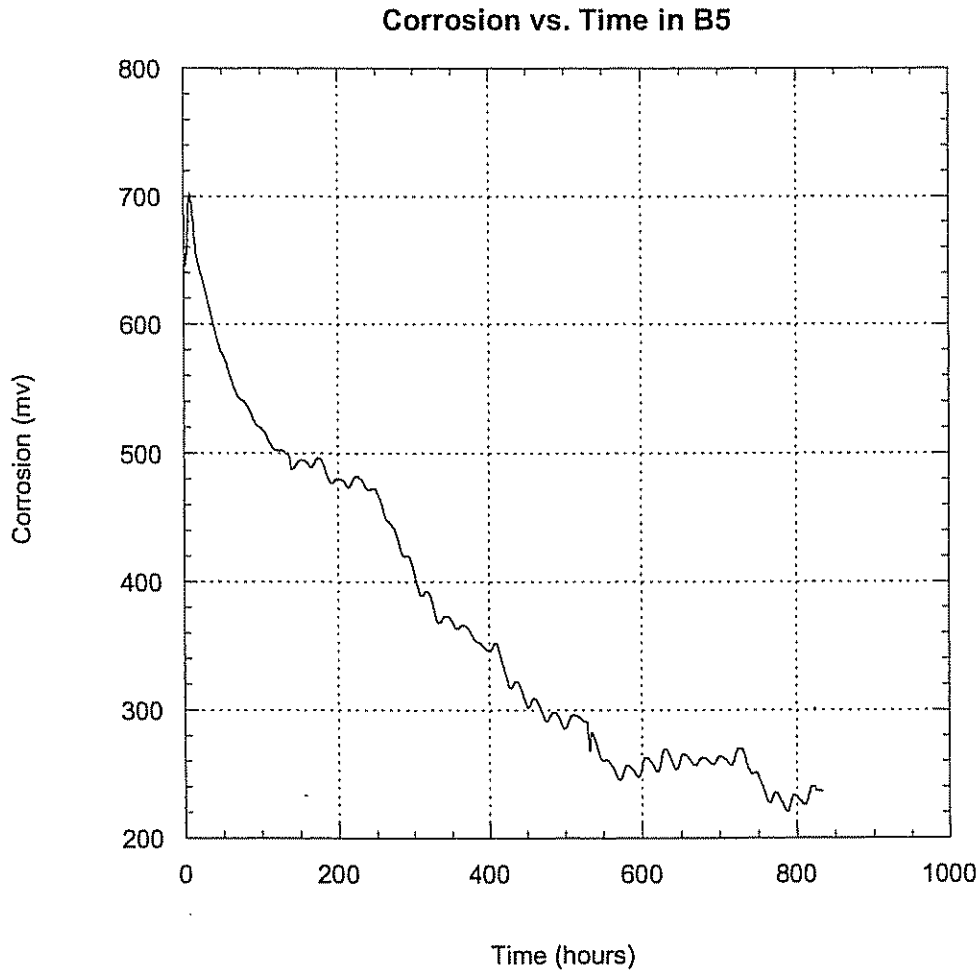

Figure 4.5 Corrosion vs. Time in B5

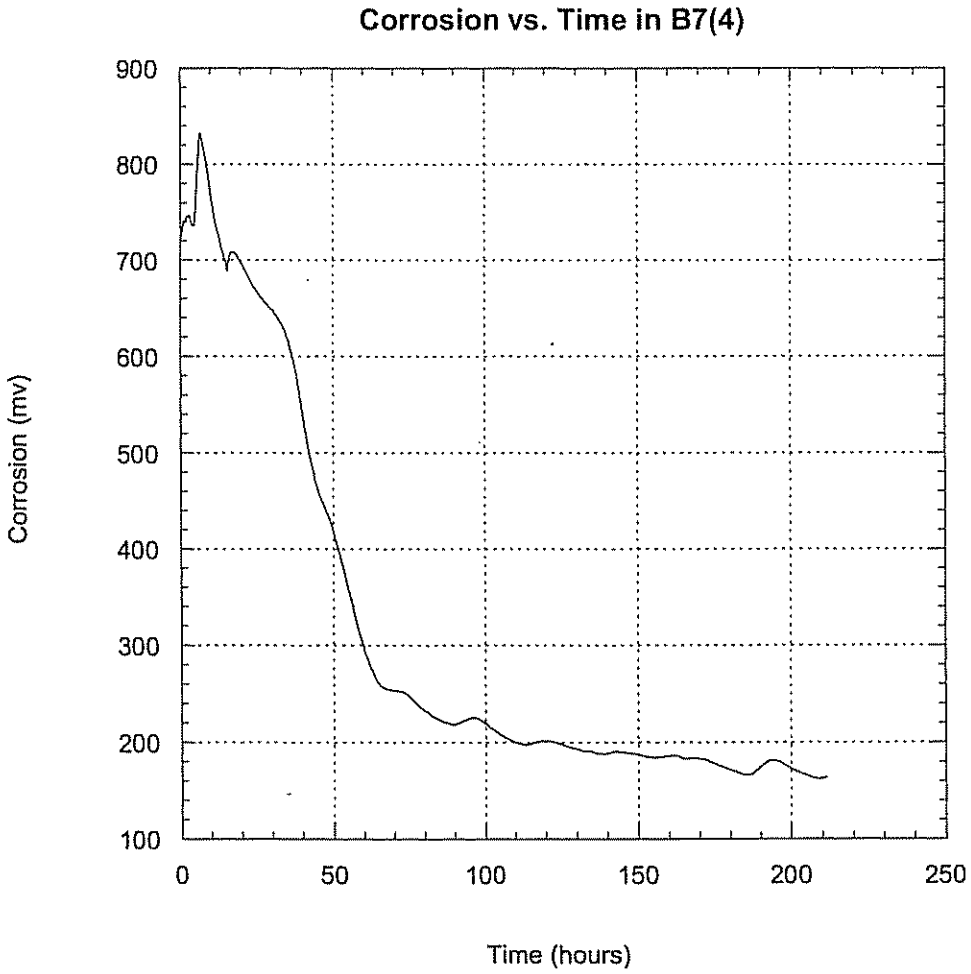

Figure 4.6 Corrosion vs. Time in B7(4)

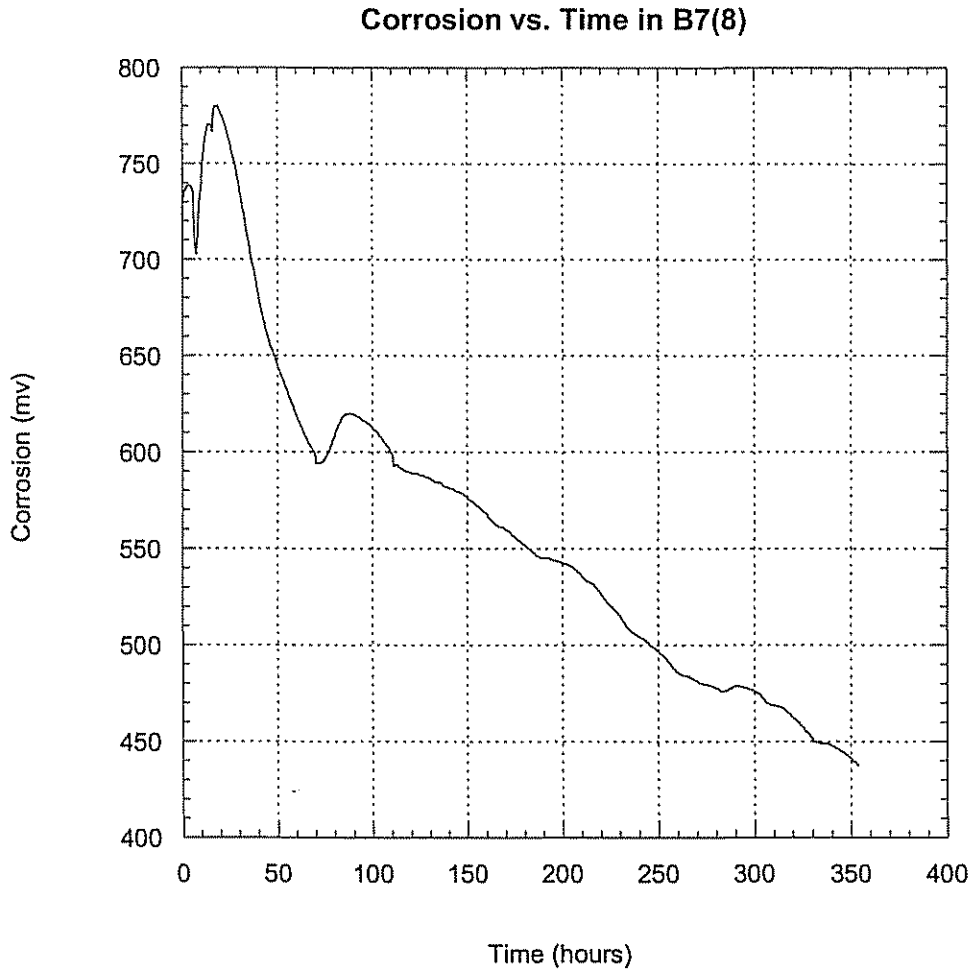

Figure 4.7 Corrosion vs. Time in B7(8)

4.3.2 Temperature

The temperature rise within the concrete due to hydration depends on the cement, water-cement ratio, size of the member, ambient temperature, environment, etc. [22].

The temperature changes vs. time in B5 are shown in Figure 4.8. The temperature change vs. time in B7(4) are shown in Figure 4.9 and Figure 4.10. The temperature changes vs. time in B7(8) are shown in Figure 4.11.

In B5, about 10 hours after casting, the temperature at the top of the beam reached a peak temperature of 150 °F. The temperature at the top was about 20 °F higher than at the bottom. After peaking at 10 hours the temperature went down. The lines between 15 hours and 45 hours represents a time when no data was recorded due to equipment problems. It should be noted that strandmeter 15668 and sister bar 17379 (both in the bottom of the beam) gave very similar temperature readings. They indicated that both were working properly. The sister bar 17377 is in the top of the beam, and this gage recorded larger temperature changes than the other two gages. This is likely due to the solar radiation..

In B7(4), the gages indicate a peak temperature of 160 °F about 10 hours after casting. While all of the temperature readings were somewhat affected by the ambient temperature, the concrete at the top was significantly more affected. In one day, the temperature change could reach 45 °F at the top, while the corresponding temperature change in the beam bottom was relatively stable, only about 5 °F change. The thermal gradient itself can cause significant stresses and strains.

The temperature changes in B7(8) are almost the same as those in B7(4). About 10 hours after casting, the gages reached a peak temperature of roughly 130 °F.

After release, the temperature at the bottom is more stable than at the top. In one day, based on sister bar readings, the temperature change at the top can reach 45 °F. The temperature change at the bottom in one day rarely exceeds 5 °F.

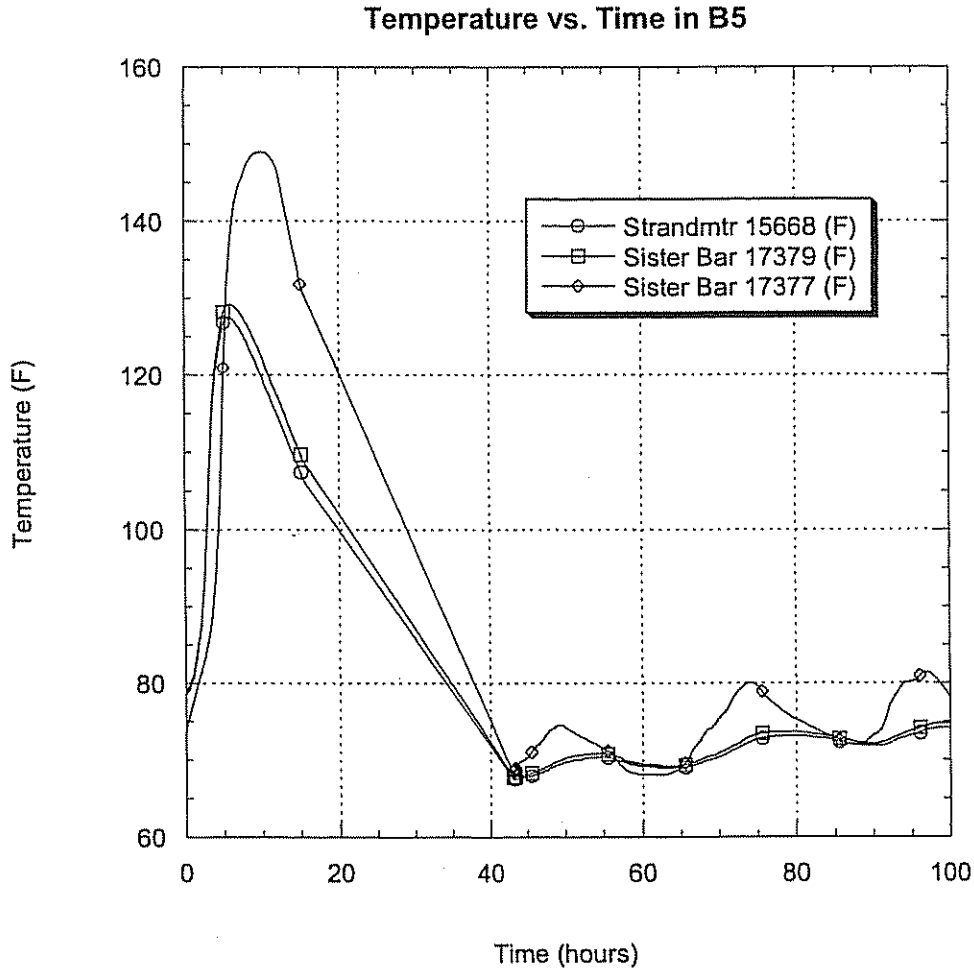

Figure 4.8 Temperature vs. Time in B5

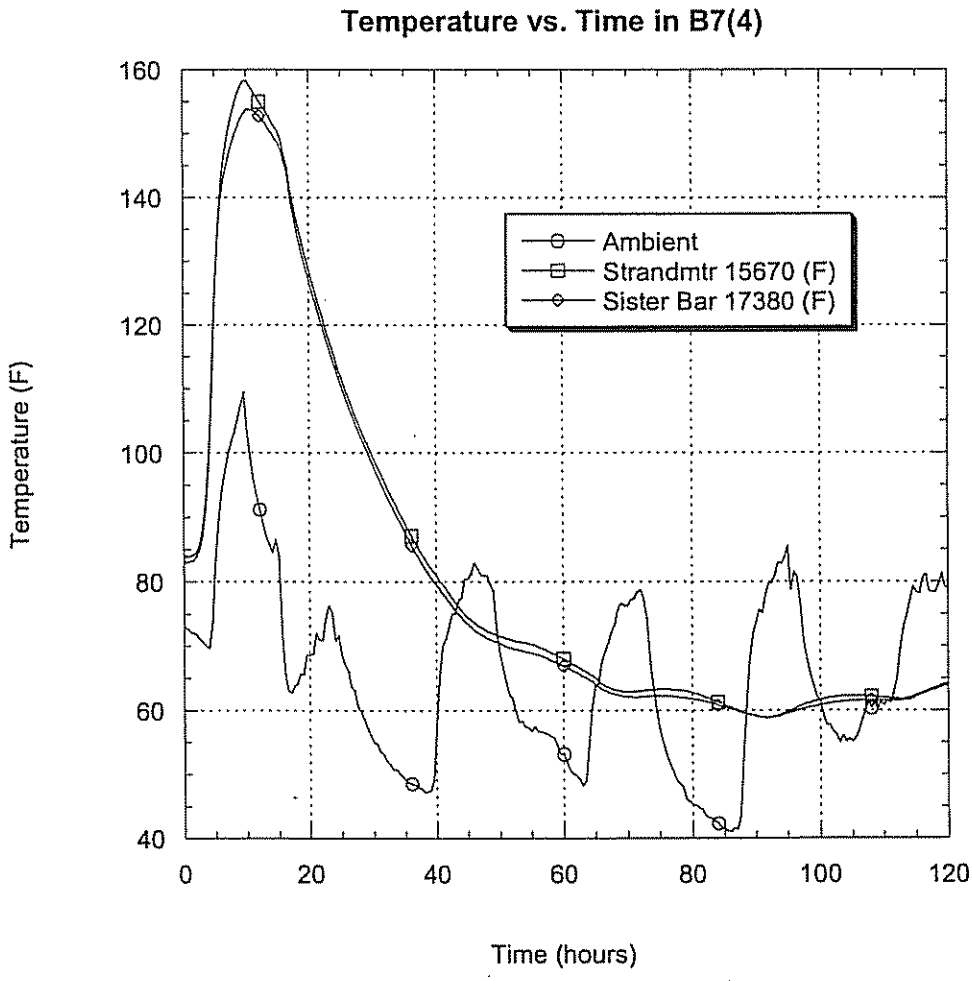

Figure 4.9 Gages Temperature vs. Time in B7(4)

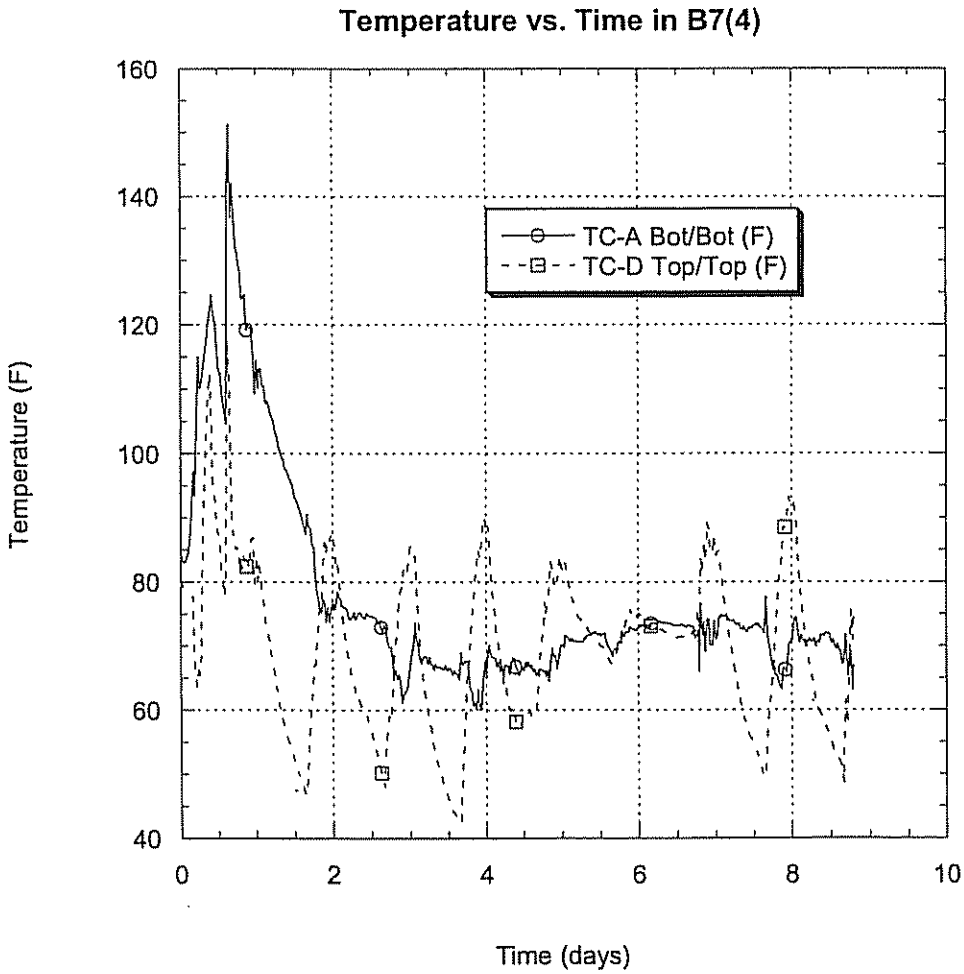

Figure 4.10 Concrete Temperature vs. Time in B7(4)

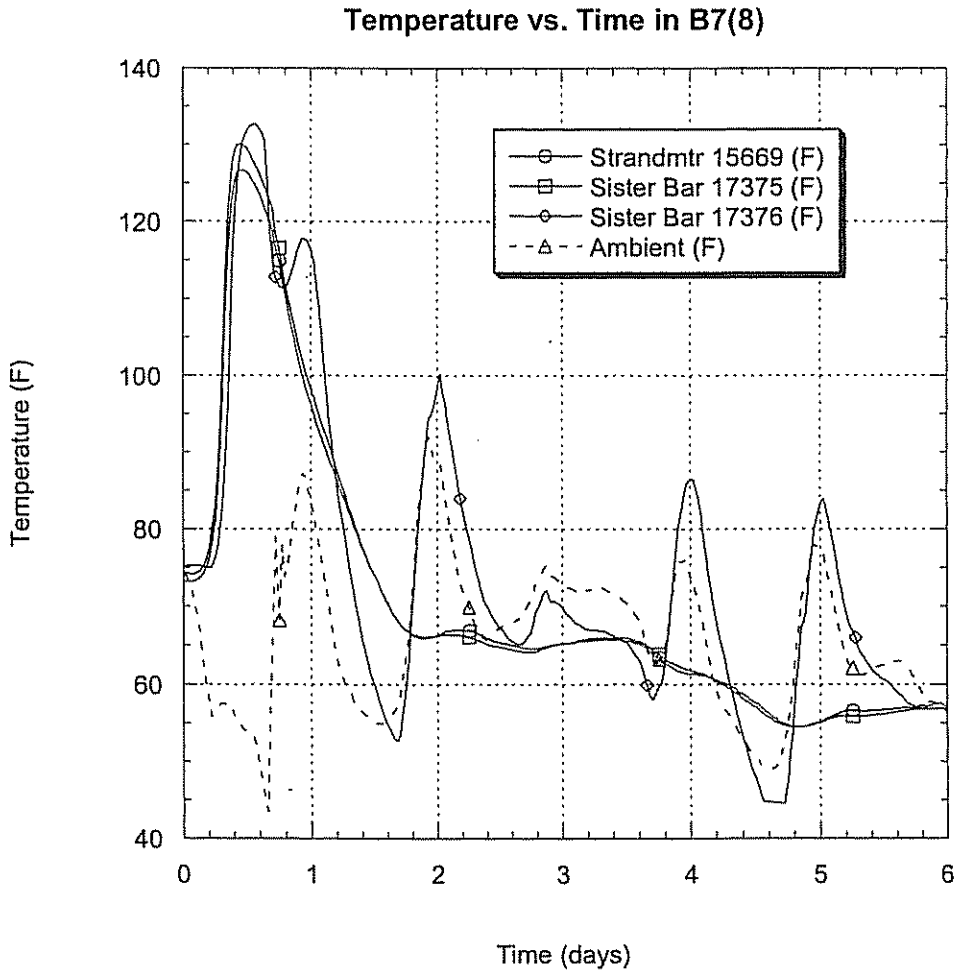

Figure 4.11 Temperature vs. Time in B7(8)

4.3.3 Maturity

The strength gain of concrete is a function of time and temperature when premature drying is prevented. The maturity factor M may be expressed as [46]

$$M=\Sigma (C + 10)\ \Delta t \tag{4.21}$$

where, M is the Maturity factor; C is the Temperature degrees in Celsius; and Δt is the duration of curing at temperature C, in hours or days.

The equation is based on cement hydration ceasing and strength not increasing at temperatures below about –10 °C (14 °F). In the maturity concept, the method of superposition is applied such that the strength is equal to the sum of the contributions from each curing interval. The location giving the lowest values should be the source of the temperature used in the computations.

The maturity M in B5 was calculated using the temperature at TC-B (Top/Bot). The temperature at this location is the lowest. M in B5 was 400 deg-hr at transfer. The maturity M in B7(4) was found using the temperature at TC-A (Bot/Bot). M was 814 deg-hr at transfer. The maturity M in B7(8) was found by using the temperature at TC-B (Top/Bot). M was 737 deg-hr at release.

While B7(4) and B7(8) are the same size, at transfer, the maturity factor M for B7(4) is bigger than for B7(8).

4.3.4 Measured Strain

Figure 4.12 to 4.16 show the measured strains from the sister bars and strandmeters for all three beams during the time they were monitored in the CBS yard prior to the bridge construction. The following sections describe how the data was corrected for thermal effects, as well as providing insights regarding the recorded data.

Recall that when using vibrating wire gages, what one measures directly is frequency, not strain. One needs to use the equations given in section 3.3 to reduce the measured data and get strain values.

In reducing the data from the sister bars, the equations used are shown below,

$$Digits\ R = Hz^2/1000$$

$$\varepsilon_{uncorrected} = (R1-R0) \times C \tag{4.22}$$

$$\varepsilon_{corrected} = ((R1-R0) \times C)+((T1-T0) \times K) \tag{4.23}$$

where Hz is the measured frequency; R is the calculated digit from the measured frequency; C is the calibration factor from the supplied calibration sheet; and K is the thermal coefficient difference.

In this study, the concrete thermal coefficient is assumed to be 5.5 ppm/°F. The sister bars are made of steel. The thermal coefficient is assumed to be 6.7 ppm/°F. Therefore, the factor K is 1.2 ppm/°F. The measured strains from the sister bars vs. time for all three beams are shown in Figure 4.12 to Figure 4.16.

In reducing the data from the strandmeters, the following equations are used.

$$Digits\ R = Hz^2 \times 10^{-3}$$

$$D = (R1\text{-}R0) \times C \tag{4.24}$$

$$Dcorrected = ((R1\text{-}R0) \times C)+((T1\text{-}T0) \times K)$$

$$K=((R1 \times 0.000295)+1.724) \times C \tag{4.25}$$

where R is the calculated digits from the measured frequency; C is the calibration factor; T is the temperature; and K is the thermal coefficient of strandmeter. K has units of Inch/Celsius, which must be converted to Inch/Fahrenheit by multiplying by 5/9. The thermal coefficient of the strandmeter changes with time. When prestressing losses occur, the tension strain goes down, the measured digits goes down and the thermal coefficients decrease as well. The calculated thermal coefficient at the beginning and at 200 days are shown in Table 4.3.

Table 4.3 The Thermal Coefficients of the Strandmeters (ppm/°F)

Items	15668 (in B5)	15670 (in B7(4))	15669 (in B7(8))	15667 (in B7(8))
Beginning	5.3	5.4	5.4	5.3
200 days	5.1	5.3	5.3	5.2

For the strandmeters, one must account for the fact that three materials are acting together, the strandmeter, the strands and the concrete. Each has different thermal coefficient. The measured strain can be found by dividing the strand deformation by the length of strandmeter (8 in.). The total measured strain (mechanical strain + thermal strain) can be found using the following equation,

$$\varepsilon_{total} = ((R1\text{-}R0) \times C+(T1\text{-}T0) \times K1)/8 \tag{4.26}$$

The formula for calculating the strain after temperature correction is shown below. The temperature correction between the strandmeter and the strand is (T1-T0)×(K1-K2); the temperature correction between the strand and the concrete is (T1-T0)× (K2-K3). Therefore, after all corrections, the mechanical strain is given by

$$\varepsilon_{temperature\ correction} = ((R1-R0) \times C+(T1-T0) \times (K1-K2)+(T1-T0) \times (K2-K3))/8$$

or

$$\varepsilon_{temperature\ correction} = ((R1-R0) \times C+(T1-T0) \times (K1-K3))/8 \qquad (4.27)$$

where K1 is the thermal coefficient of the strandmeter; K2 is the thermal coefficient of strand; and K3 is the thermal coefficient of the concrete.

In the first several days after concrete casting, the temperature change may reach 80 °F. However, since the thermal coefficients of the strandmeter and the concrete are very close, the needed temperature correction is very small, between 8 ppm to 16 ppm. Because we don't know K3 with sufficient certainty, we neglect the difference between K1 and K3. After the concrete casting, the difference between K1 and K3 increases with time. At 200 days, the difference reaches 0.3 ppm/°F to 0.4 ppm/°F. However, at this point the temperature change (T1-T0) isn't very big (less than 40 °F). Therefore, the temperature correction is less than 16 ppm. It can be seen that in either the short or long term, no temperature correction is necessary. The measured strain from the strandmeter is found using the following equation,

$$\varepsilon = ((R1-R0) \times C)/8 \qquad (4.28)$$

The measured strains from the strandmeters in B5, B7(4) and B7(8) are shown in Figure 4.12 to Figure 4.16.

After comparing the strains in the three beams, one finds that several days after casting the strains in the bottom of the beam recorded by the sister bars and strandmeter were very similar, and the strain at the top was less than at the bottom.

In B5, the strain from sister bar 17377 at the top was less than the strain at the bottom, and it was close to that of B7(8). These values verified each other. The bottom strain from sister bar 17379 was similar to that of B7(4) and B7(8). strandmeter 15668 in B5 gave strain readings that were too large to be believed. This may have been due to slipping of the clamp.

For beam B7(4), about 2 days after casting, the strains in the bottom of the beam recorded by sister bar 17380 and strandmeter 15670 were similar and they validated each other. In the first two days, the strain from strandmeter 15670 was much bigger than that from sister bar 17380 at the bottom. Another sister bar 17378 at the top did not work well. The reason is unclear.

For beam B7(8), about 2 days after concrete casting, the strains at the bottom of the beam recorded by strandmeter 15669, sister bar 17375 and strandmeter 15667 were all quite similar. Furthermore, the recorded temperatures were almost the same. This validated that the gages were working properly. The strain at the top of the beam from sister bar 17376 was much less than that at the bottom, similar to B5. Like in B7(4), in the first two days, the bottom strains from strandmeters were much bigger than that from the sister bar.

Table 4.4 Strains (ppm) vs. Time in B5

Title	Position	Before Transfer	7 days	14 days	28 days	240 days
Bottom	Sister Bar 17379	-200	-619	-667	-676	-689
Top	Sister Bar 17377	-332	-472	-487	-495	-467

Table 4.5 Strains (ppm) vs. Time in B7(4)

Title	Position	Before Transfer	After Transfer	7 days	180 days	210 days	360 days
Bottom	Strand meter 15670	-607	-816	-482	-500	-521	
	Sister Bar 17380	-227	-466	-527	-535	-536	
	Average	...	...	-505	-518	-529	

Table 4.6 Strains (ppm) vs. Time in B7(8)

Title	Position	Before Transfer	After Transfer	7 days	14 days	180 days	240 days
Bottom	Strand meter 15669(bottom)	-502	-739	-634	-642	-665	
	Strand meter 15667(bottom)	-533	-771	-576	-580	-614	
	Sister Bar 17375(bottom)	-231	-460	-616	-625	-665	
	Average	...	...	-609	-616	-648	
Top	Sister Bar 17376(top)	-208	-368	-458	-472	-472	

The measured strains at different times for the three beams are shown in Table 4.4, Table 4.5 and Table 4.6. It can be seen that at transfer the strains from the sister bars are much less than those from the strandmeters. However, about 40 hours after transfer, when the temperature goes back to ambient levels, the concrete and the strands have almost the same strains. Their deviation from their average value is less than 8%. Before transfer, there were big compressive strains in the sister bars and strandmeters. This could be due to the elevated temperature during curing. During curing the whole bed was covered by a steam blacket.

In B5, the temperature at the top of the girder is about 20 °F higher than at the bottom. As a result, the compressive strain at the top was much larger. Based on the thermal coefficients, a 20 °F increase in temperature can cause $5.5 \times 20 = 110$ ppm compressive strain. The measured difference was 132 ppm. In B7(8), the temperatures at the top and bottom were almost the same. It is therefore reasonable that the strains in sister bars 17375 and 17376 were reasonably close.

In B7(8) from 0-16 hours just before transfer, the bottom concrete strain is –229 ppm. It can be attributed to concrete shrinkage, especially autogenous shrinkage. And the average strand strain is –518 ppm. Temperature increase is 48 °F. Every degree of increasing temperature can cause about 6 ppm compressive strain because the strand was fixed on both ends. Likewise, one can get that every degree of increasing temperature can cause about 5.7 ppm compressive strain in B7(4). They are very close to steel thermal coefficient 6.7 ppm/°F. The difference may be due to the bed which can extend a little under elevated temperature.

One should note that the concrete properties change greatly before transfer. Before the concrete has hardened, the sister bar can expand freely.

Furthermore, the beam end was restrained by wood formwork. Under pressure, the wood formwork can undergo large deformations. Since there is also friction between the beam and the formwork, it is difficult to estimate the sister bar strain before transfer.

Beam B5 is a different size from B7(4) and B7(8). B7(4) and B7(8) are the same size, however they were cured under different conditions. B7(4) was steam cured. B5 and B7(8) were heat cured (naturally cured). Therefore different strains vs. time are to be expected. The strains from B7(8) are larger than those from B7(4). Maturity factor M in B7(4) is 814 deg-hr, larger than that the 737 deg-hr for B7(8),. B7(4) was more mature at release and is expected to exhibit less creep and shrinkage.

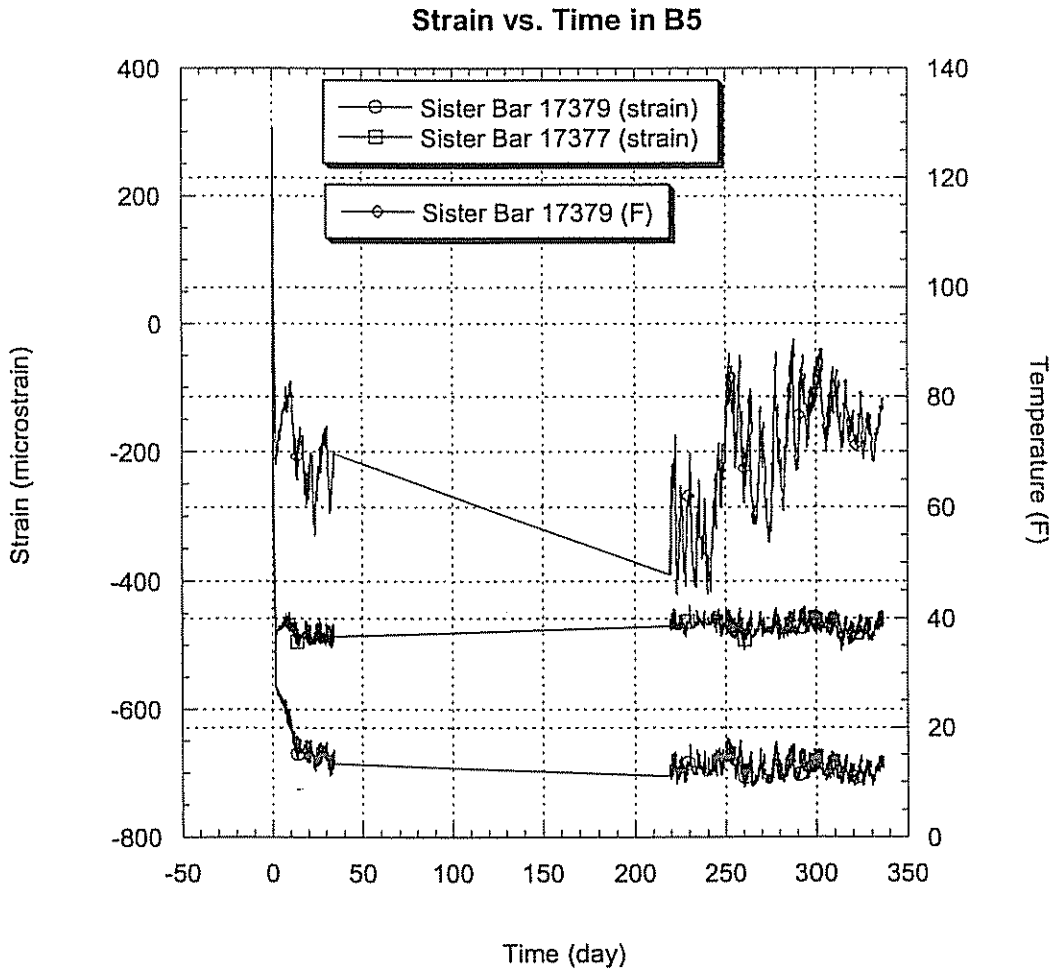

Figure 4.12 Strain vs. Time in B5

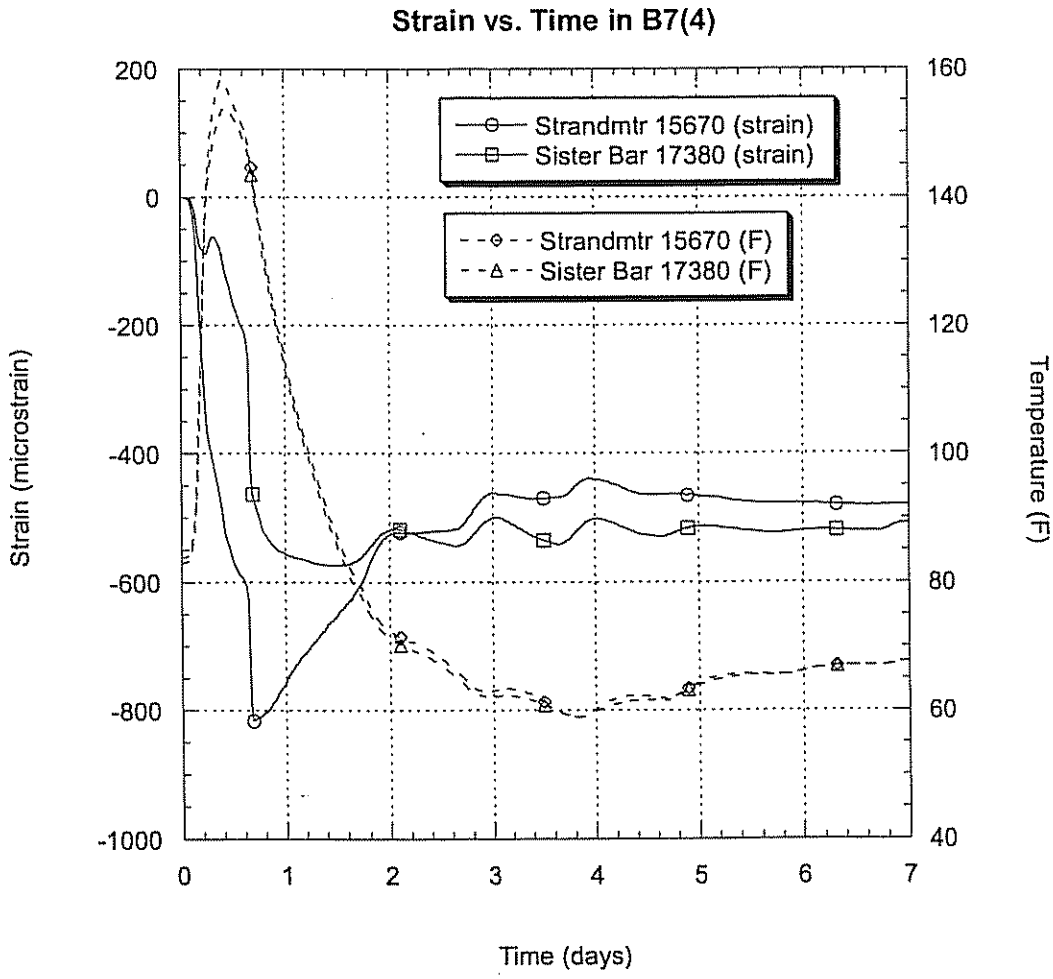

Figure 4.13 Short-Term Strain vs. Time in B7(4)

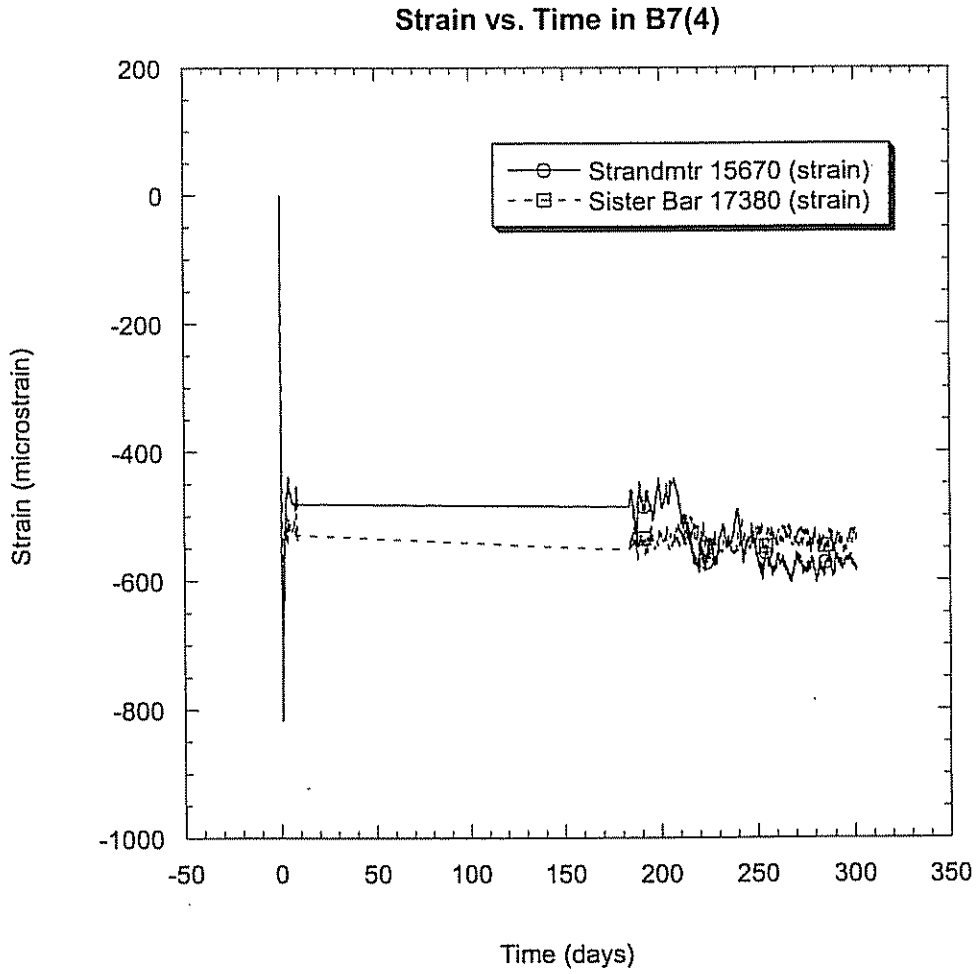

Figure 4.14 Long-Term Strain vs. Time in B7(4)

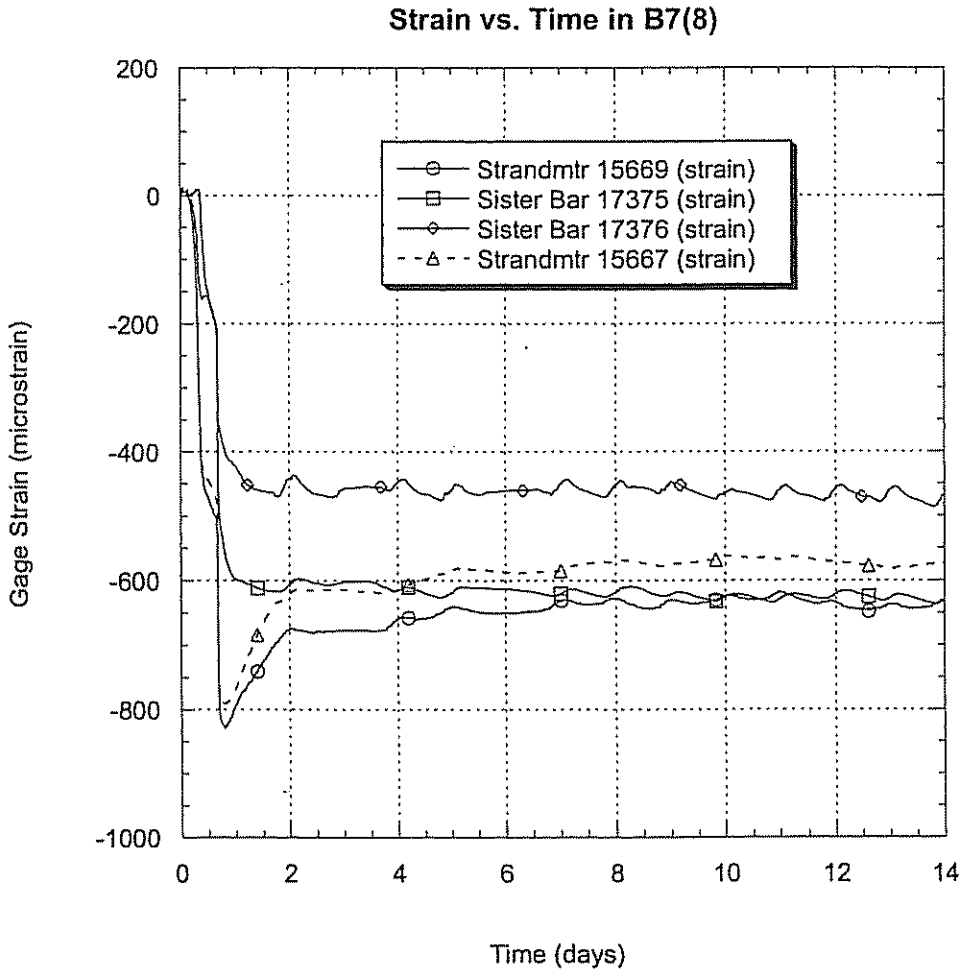

Figure 4.15 Short-Term Strain vs. Time in B7(8)

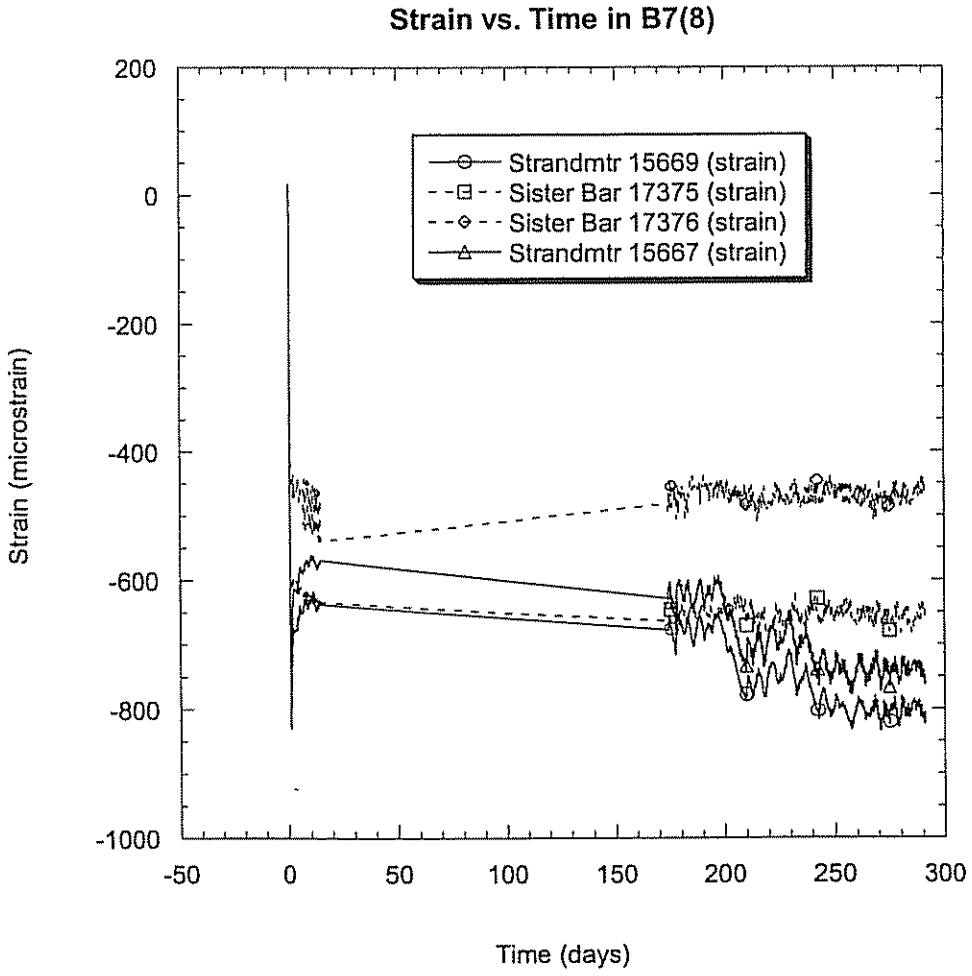

Figure 4.16 Long-Term Strain vs. Time in B7(8)

Chapter 5

METHODS TO PREDICT PRESTRESS LOSSES

5.1 Introduction

The prestress force of a prestressed concrete member continuously decreases with time. The total stress reduction during the life span of the member is called "total loss of prestress". The total loss of prestress was the primary factor that hindered the early development of prestressed concrete. It is essential to estimate the magnitude of the total loss of prestress, since it leads to the value of the effective prestressing force needed for design. The total prestress loss in prestressed beams is generally attributed to the cumulative contribution from the following sources [47]:

- Elastic shortening of the concrete. Because the concrete shortens instantaneously when the prestress force is applied to it, the tendons, already bonded to the concrete shorten, simultaneously lose part of their stress.
- Relaxation of the stressed tendons. Relaxation is a property of the steel.
- Shrinkage of the concrete. The gradual loss, with time, of free water from the concrete, called shrinkage, induces a shortening in the concrete which leads to a loss of stress in the bonded tendons.
- Creep of the concrete. Creep is caused by the compressive stresses in the concrete. It induces a shortening strain in the concrete with time in

excess of the instantaneous elastic strain. This shortening due to creep leads to a loss of stress in the bonded tendons.

Each of the above sources leads to a separate prestress loss in the tendons. Prestress losses occur either instantaneously or with time. Instantaneous losses in pretensioned members are generally reduced to the effect of elastic shortening of the members at prestress transfer. Time dependent losses include the effect of relaxation in the steel, as well as the effects of creep and shrinkage in the concrete. They affect all prestressed concrete elements [47].

It is essential to realize that time dependent losses are interdependent. The rate of stress loss due to one effect such relaxation is being continuously altered by changes in the steel stress due to the other effects such as creep and shrinkage. The rate of creep, in its turn, is simultaneously altered by the changes in the steel stress due to relaxation and shrinkage [47].

There are many methods for estimating the prestress losses in prestressed concrete beams. In this chapter, AASHTO's Lump Sum Estimate, AASHTO's Refined Estimate, AASHTO's Time Step Method, and PCI's method are presented [44,48]. Because none of these methods were developed for HPC, one important purpose of this study is to check whether they are suitable for HPC, and this will be discussed in Chapter 6.

5.2 AASHTO Approximate Lump Sum Estimate [44]

An approximate lump sum estimate of time-dependent prestress losses resulting from creep and shrinkage of the concrete and relaxation of the steel in prestressed and partially prestressed members is given by equation (5.1) for

prestensioned members stressed after attaining a compressive strength 3.5 ksi, provided that:

- The members are made from normal weight concrete (the unit weight of the concrete is about 145 lb/cu ft.),
- The concrete is either steam or moist cured,
- The prestressing is by bars or strands with low relaxation properties (Relaxation depends on type and grade of steel. For the purpose of design, prestressing steels are divided into two groups having either normal or low relaxation. Low relaxation is about 25 percent of normal relaxation.),
- Average exposure conditions and temperatures characterize the site.

Under these conditions, the total prestress losses are:

$$\Delta f_p = \Delta f_{pES} + \Delta f_{pTD} \tag{5.1}$$

where, Δf_{pES} is elastic shortening; and Δf_{pTD} is Total time dependent losses.

Total time dependent prestress loss Δf_{pTD} in box girders for low relaxtion strands is given by

$$\Delta f_{pTD}\,(Upper\ Bound) = 17.0 + 4.0\,PPR \tag{5.2}$$

$$\Delta f_{pTD}\,(Average) = 15.0 + 4.0\,PPR \tag{5.3}$$

$$PPR = (A_{ps}f_{py})/(A_{ps}f_{py}+A_s f_y)$$

where, PPR = partial prestress ratio; A_s is area of nonprestressed tension reinforcement (in^2); A_{ps} is area of prestressing steel (in^2); f_y is specified yield strength of reinforcing bars (ksi); f_{py} is yield strength of prestressing steel (ksi).

An upper bound for Δ_{fpTD} is recommended when an adverse combination of parameters, such as low concrete compressive strength, low relative humidity, and moist curing conditions exist. For box girders, I-girders, and solid rectangular beams, the effect of concrete compressive strength up to 10.0 ksi was found to be negligible.

The approximate lump sum estimates of time-dependent prestress losses reflect values and trends obtained from a computerized time step analysis of a large number of bridges and building members designed for a common range of variables, namely;

- Untimate concrete creep coefficient ranging from 1.6 to 2.4,
- Ultimate concrete shrinkage coefficient ranging from 0.004 to 0.006,
- Relative humidity ranging from 40 to 60 percent,
- Moist curing or steam curing of concrete, and
- A PPR ranging from 0.2 to 1.0.

The losses due to elastic shortening (Δf_{pES}) should be added to the time-dependent losses to determine total losses.

$$\Delta f_{pES} = (E_p/E_{ci})f_{cgp} \tag{5.4}$$

where, f_{cgp} is sum of concrete stresses at the center of gravity of prestressing tendons due to the prestressing force at transfer and the self weight of the member at the sections of maximum moment (ksi); E_p is modulus of elasticity of the prestressing steel (ksi); E_{ci} is modulus of elasticity of the concrete at transfer (ksi).

However, f_{cgp} depends on f_{pES}. In order to avoid iterative calculation, the following equation can be used [47].

$$\Delta f_{pES} = \{(f_{cgs})_{FJ}[f_{pJ} - \Delta f_{pR(t0,t)}] + (f_{cgs})_G f_{pJ}\} / [f_{pJ}/n_{pi} + (f_{cgs})_{FJ}] \quad (5.5)$$

$$F_J = A_s f_{pJ}$$

where, f_{pJ} is the stress in the tendons immediately after jacking; A_s is the total strand area; $(f_{cgs})_{FJ}$ is stress in the concrete at the centroid of the prestressing steel due to the initial prestressing force F_J; $(f_{cgs})_G$ is stress in the concrete at the centroid of the prestressing steel due to beam self weight; $\Delta f_{pR(t0,t)}$ is steel relaxation between jacking and transfer; n_{pi} is ratio of the modulus of elasticity between the prestressing steel and the concrete.

5.3 AASHTO Refined Estimate [44]

Estimates of losses due to each time-dependent sources, such as creep, shrinkage, or relaxation, can lead to a better estimate of total losses compared with the values given by the approximate lump sum estimate just discussed (Section 5.2).

In this method, the total prestress losses are given by

$$\Delta f_p = \Delta f_{pES} + \Delta f_{pSR} + \Delta f_{pCR} + \Delta f_{pR1} + \Delta f_{pR2} \quad (5.6)$$

where, Δf_{pES} is the loss due to elastic shortening; Δf_{pSR} is loss due to shrinkage; Δf_{pCR} is loss due to creep; Δf_{pR1} is loss due to steel relaxation at transfer; and Δf_{pR2} is loss due to steel relaxation after transfer. Δf_{pES} is the same as in Section 5.2.

For pretensioned members,

$$\Delta f_{pSR} = (17.0 - 0.150H) \text{ (ksi)} \quad (5.7)$$

where, H is the average annual ambient relative humidity (%).

Prestress loss due to creep may be taken as:

$$\Delta f_{pCR} = 12.0 f_{cgp} - 7.0 \Delta f_{cdp} \geq 0 \quad (5.8)$$

where, f_{cgp} is concrete stress at the center of gravity of the prestressing steel at transfer (ksi); Δf_{cdp} is change in concrete stress at the center of gravity of the prestressing steel due to permanent loads, with the exception of the load acting at the time the prestressing force is applied. Values of Δf_{cdp} should be calculated at the same section or at sections for which f_{cgp} is calculated (ksi). The "≥ 0" is needed because a negative value could result in some cases of partial prestressing, but Δf_{pCR} should not be taken as less than 0.0.

In prestressed members, the relaxation loss in low relaxation strand, initially stressed in excess of $0.50 f_{pu}$ may be taken as:

$$\Delta f_{pR1} = [log(24t)/40.0][f_{pj}/f_{py} - 0.55] f_{pj} \quad (5.9)$$

where, t is time estimated in days from stressing to transfer (days); f_{pj} is initial stress in the tendon at the end of stressing (ksi); and f_{py} is specified yield strength of the prestressing steel (ksi).

For pretensioning with stress-relieved strands, losses due to relaxation of prestressing steel may be taken as:

$$\Delta f_{pR2} = 20.0 - 0.4 \Delta f_{pES} - 0.2(\Delta f_{pSR} + \Delta f_{pCR}) \quad (ksi) \quad (5.10)$$

The estimates for relaxation are approximate for normal temperature ranges only. Relaxation losses increase with increasing temperatures.

5.4 AASHTO Time Step Method [44]

The time step method is an accurate technique to predict losses and involves mostly time dependent losses due to relaxation of the steel and creep and shrinkage of the concrete. Instantaneous losses are computed as for the other methods. In order to fully understand the time step method, it is essential to realize that time dependent losses are also interdependent. Figure 5.1 provides an overall diagram illustrating how total losses are accumulated and the interrelated causes and effects between the different sources of loss of prestress [47].

It is important to understand that the rate of stress loss due to one effect. such as relaxation is being continuously altered by changes in the steel stress due to the other effects such as creep and shrinkage. The rate of creep, in its turn, is simultaneously altered by the changes in the steel stress due to relaxation and shrinkage. To account for these interdependent effects with time, a repetitive computation procedure using successive time intervals is used. Generally, the lengths of these time intervals are not equal and vary with the age of the concrete. The stress in the steel at the beginning of any time interval is taken equal to that at the end of the preceding interval. It is assumed constant during a time interval and used to compute incremental losses during that interval. The steel stress at the end of a time interval is obtained by subtracting the incremental stress losses from the stress at the beginning of the interval. More accuracy can be obtained by increasing the number of intervals [47].

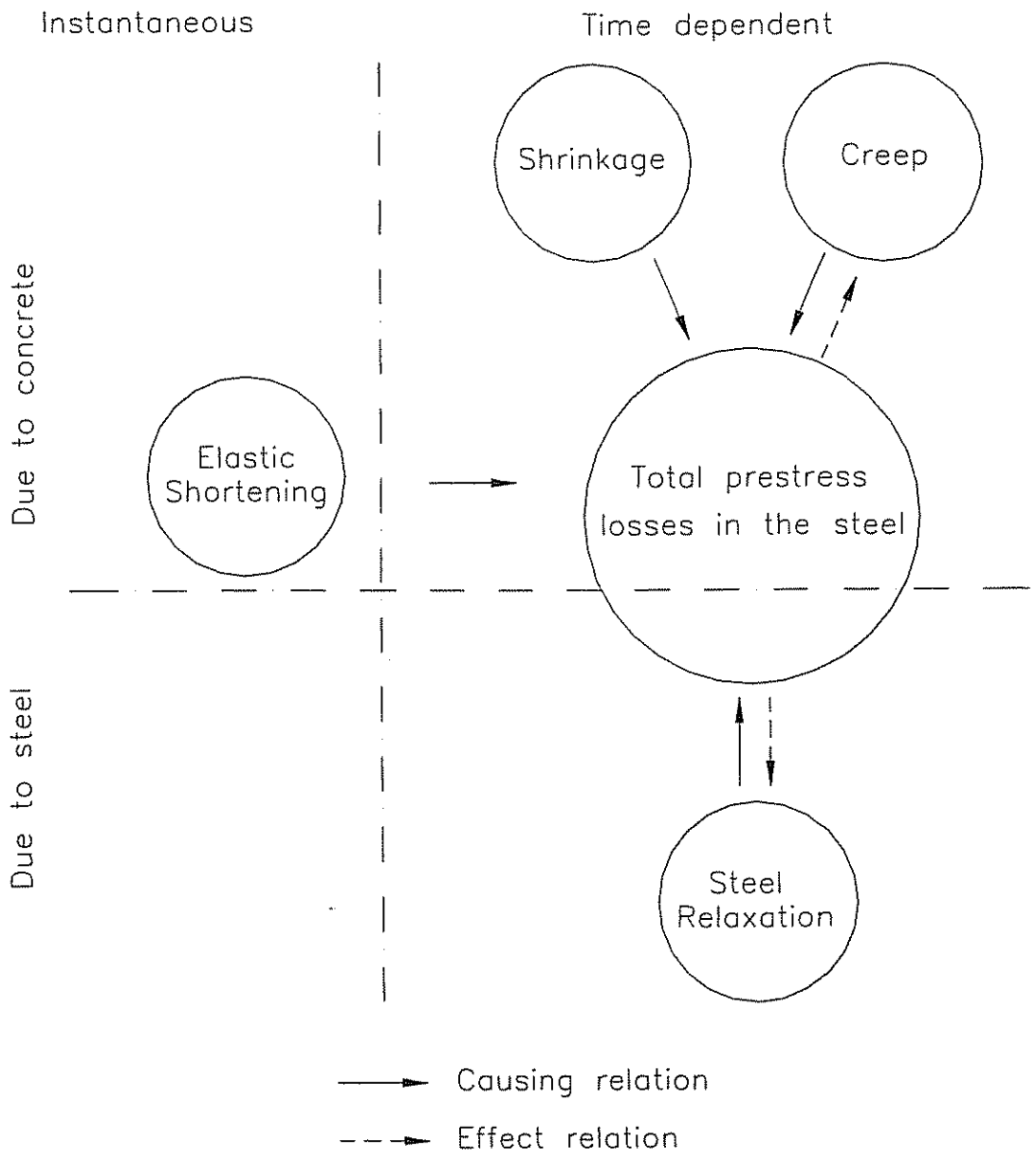

Figure 5.1 Interrelationships of Causes and Effects between Pretress Losses (Courtesy reference 47).

Before stress transfer, although the relaxation will not cause strain, it does cause prestress loss. This will have an effect on the elastic shortening and can be estimated using AASHTO 5.9.5.4.4b-2.

$$\Delta f_{PRI} = \frac{\log(24.0t)}{40}\left[\frac{f_{pj}}{f_{py}} - 0.55\right] f_{pj} \tag{5.11}$$

where, t is time estimated in days from stressing to transfer (days); $f_{pj}$is initial stress in the tendon at the end of stressing (ksi); and f_{py} is specified yield strength of prestressing steel (ksi).

AASHTO LRFD 5.4.2.3.2 gives the following equation for creep prediction.

$$\Psi(t,t_j) = 3.5 k_c k_f (1.58 - \frac{H}{120}) t_j^{-0.118} \frac{(t-t_j)^{0.6}}{10.0 + (t-t_j)^{0.6}} \tag{5.12}$$

for which,

$$k_f = \frac{1}{0.67 + (\frac{f_c'}{9})}$$

where, H is relative humidity (%); k_c is factor for the effect of the volume-to-surface ratio of the component; and k_f is factor for the effect of concrete strength.

From this formula, it can be seen that when f_c' increases, k_f goes down, and the creep coefficient Ψ goes down. As a result, the creep of HPC is much less than for conventional concrete.

AASHTO LRFD 5.4.2.3.3 gives the following equation for shrinkage prediction.

$$\varepsilon_{sh} = -k_s k_h (\frac{t}{55.0 + t}) 0.56 \times 10^{-3} \tag{5.13}$$

where, t is drying time (days); k_s is size factor; k_h is humidity factor.

From this formula, it seems ε_{sh} has no relationship with strength. If two beams made up of concrete having different compressive strengths have the same size factor and are cured and stored under the same condition, they would have the same ε_{sh}.

AASHTO LRFD does not give a formula to predict steel relaxation during a period $[t_1, t]$ after transfer. Therefore the following equation given by the PCI Committee Report is used.

$$RET = f_{st}\{[log24t - log24t1]/45\} \times [f_{st}/f_{py} - 0.55] \quad (5.14)$$

where, $f_{st}/f_{py} - 0.55 \geq 0.05$; $f_{py} = 0.9\ f_{pu}$; f_{st} is stress in prestressing steel at time t_1 (psi); f_{py} is stress at 1% elongation of prestressing steel (psi); t is time at end of time interval (days); and t1 is time at the beginning of the time interval (the time of anchorage, t_1 shall be taken as 1/24 of a day so that $\log t_1$ is zero).

Using this formula to estimate the relaxation losses before transfer, the estimated value will be 11% less than that from AASHTO LRFD. To be consistent, in this study, the PCI equation will be used to estimate the steel relaxation before and after transfer.

5.5 PCI General Method [48]

A precise determination of stress losses in prestressed concrete members is a complicated problem because the rate of loss due to one factor, such as relaxation of tendons, is continually being altered by changes in stress due to other factors, such as creep of concrete. Rate of creep is in turn altered by the change in tendon stress. It

is extremely difficult to separate the net amount of loss due to each factor under different conditions of stress, environment, loading, and other uncertain factors. In addition to the foregoing uncertainties due to the interaction of shrinkage, creep, and relaxation, physical conditions, such as variations in the actual properties of concrete made to the same specified strength, can vary the total loss. As a result, the computed values for prestress loss are only estimates and not expected to be exact. While errors in computing losses can affect service conditions such as camber, deflection, and cracking, they have no effect on the ultimate strength of a flexural member unless the tendons are unbonded or the final stress after losses is less than $0.5f_{pu}$.

The PCI general method is a time step method. It is recommended that a minimum of four time intervals be used as shown in Table 5.1. When significant changes in loading are expected, time intervals other than those recommended should be used.

Table 5.1 Minimum Time Intervals

Step	Beginning time, t1	End time, t
1	Pretensioned anchorage of prestressing steel	Age at prestressing of concrete (i.e. transfer)
2	End of step 1	Age = 30 days, or time when a member is subjected to load in addition to its own weight
3	End of step 2	Age = 1 year
4	End of step 3	End of service life

In pretensioned construction, total prestress losses

$$\Delta f_p = \Delta f_{pANC} + \Delta f_{pDEF} + \Delta f_{pES} + \Sigma (\delta f_{pCR} + \delta f_{pSH} + \delta f_{pRET}) \quad (5.15)$$

where, Δf_{pANC} is the loss of prestress due to the anchorage of prestressing steel (psi); Δf_{pDEF} is the loss of prestress due to the deflecting device in pretensioned construction (psi); Δf_{pES} is loss of prestress due to elastic shortening (psi); δf_{pCR} is loss of prestress due to creep of the concrete over time interval t1 to t4 (psi); δf_{pSH} is the loss of prestress due to shrinkage of the concrete over time interval t1 to t (psi); and δf_{pRET} is loss of prestress due to the steel relaxation over time interval t1 to t (psi).

In our study, Δf_{pANC} and Δf_{pDEF} aren't applicable. The equation can be reduced to:

$$\Delta f_p = \Delta f_{pES} + \Sigma (\delta f_{pCR} + \delta f_{pSH} + \delta f_{pRET})$$

Δf_{pES} can be found in the same way as for the other methods. The loss due to creep of concrete over each time interval is given by,

$$\delta f_{pCR} = (UCR)(SCF)(MCF)(PCR)(f_c) \quad (5.16)$$

where, UCR is ultimate loss of prestress due to creep of the concrete, (psi per psi of compressive stress in the concrete); SCF is factor that accounts for the effect of size and shape of a member on creep of concrete; MCF is factor that accounts for the effect of age at prestress and length of moist cure on creep of concrete, not applicable to accelerated concretes; PCR is amount of creep over the time interval t1 to t; and f_c is net concrete compressive stress at center of gravity of the prestressing steel (psi) at time t1, taking into account the loss of prestress force occurring over the preceding

time interval. It shall also include the change in applied load during the preceding time interval.

The ultimate creep loss for accelerated cure in normal weight concrete is

$$UCR = 63 - 20E_c/10^6 \geq 11 \tag{5.17}$$

To account for the effect of size and shape of the prestressed members, the value of SCF is given in Table 5.2,

Table 5.2 Creep Factors for Various Volume to Surface Ratios

Volume to surface ratio, in.	Creep factor SCF
1	1.05
2	0.96
3	0.87
4	0.77
5	0.68
>5	0.68

Variation of creep with time (AUC) shall be estimated by the values given in Table 5.3. Linear interpolation shall be used between the values listed.

Table 5.3 Variation of Creep with Time after Prestress Transfer

Time after prestress transfer, days	Portion of ultimate creep, AUC
1	0.08
2	0.15
5	0.18
7	0.23
10	0.24
20	0.30
30	0.35
60	0.45
90	0.51
180	0.61
365	0.74
End of service life	1.00

The amount of creep over one step (PCR) between the time interval t1 to t, is given by,

$$PCR = (AUC)_t - (AUC)_{t1} \tag{5.18}$$

And the loss due to shrinkage of the concrete over each time interval is given by

$$\delta f_{pSH} = (USH)(SSF)(PSH) \tag{5.19}$$

where, USH is ultimate loss of prestress due to shrinkage of concrete (psi); SSF is factor that accounts for the effect of size and shape of a member on concrete shrinkage; and PSH is amount of shrinkage over time interval t1 to t.

The ultimate loss due to shrinkage of concrete (USH) in normal weight concrete is given by

$$USH = 27{,}000 - 3000E_c/10^6, \text{ but not less than } 12{,}000 \text{ psi.}$$

To account for effects due to the size and shape of the prestressed member, the value of SSF is given in Table 5.4.

Table 5.4 Shrinkage Factors for Various Volume to Surface Ratios

Volume to surface ratio, in.	Shrinkage factor SSF
1	1.04
2	0.96
3	0.86
4	0.77
5	0.69
6	0.60

Variation of shrinkage with time (AUS) shall be estimated by the values given in Table 5.5. Linear interpolation shall be used between the values listed.

Table 5.5 Shrinkage Coefficients for Various Curing Times

Time after end of curing, days	Portion of ultimate shrinkage, AUS
1	0.08
3	0.15
5	0.20
7	0.22
10	0.27
20	0.36
30	0.42
60	0.55
90	0.62
180	0.68
365	0.86
End of service life	1.00

The amount of shrinkage over each step (PSH) between the time interval t1 to t is given by the following equation,

$$PSH = (AUS)_t - (AUS)_{t1} \tag{5.20}$$

Loss due to steel relaxation δf_{pRET} over the time interval t1 to t may be estimated using the following equation. (For mathematical correctness, the value for t1 at the time of anchorage of the prestressing steel shall be taken as 1/24 of a day so that logt1 at this time equals zero.)

$$\delta f_{pRET} = f_{st}\{[log24t - log24t_1]/45\}[f_{st}/f_{py} - 0.55] \tag{5.21}$$

where, f_{st} is stress in the prestressing steel at time t1 (psi); f_{py} is stress at 1 percent elongation of prestressing steel (psi); $f_{st}/f_{py} - 0.55 \geq 0.05$; $f_{py} = 0.90f_{pu}$; and f_{pu} is guaranteed ultimate tensile strength of prestressing steel (psi).

The estimated prestress loss changes with the time interval. For example, the calculated relaxation loss at the end of the service life found using one time interval may be more than twice the value using more time intervals [47].

5.6 Modified Rate of Creep Method [49, 50]

The Modified Rate of Creep Method is a time step method, similar to the AASHTO time step method. However, it takes into account the transition from non-composite to composite section and the effects of differential shrinkage between the slab and girders. The rate after slab casting is a weighted average of the slab and girder concrete properties.

The elastic shortening loss can be estimated as was done in the prior methods. The time dependent losses are given by,

$$\Delta f_{pTD} = \Delta f_{pSH} + \Delta f_{pCR1} + \Delta f_{pCR2} + \Delta f_{pRE} - \Delta f_{pEG} - \Delta f_{pCRG} - \Delta f_{pDSH} \quad (5.22)$$

where, Δf_{pSH} is the prestress loss due to girder shrinkage (It can be found using the same method as the AASHTO time step method); Δf_{pCR1} is the creep loss between time of transfer and slab casting; Δf_{pCR2} is the creep loss for any time after slab casting; Δf_{pRE} is steel relaxation; Δf_{pEG} is instantaneous prestress gain due to superimposed dead load; Δf_{pCRG} is prestress gain due to creep response caused by superimposed dead load; and Δf_{pDSH} is prestress gain due to differential shrinkage.

In the Modified Rate of Creep Method, prestress loss due to creep may be considered in two stages:

Stage 1 is the creep loss between the time of transfer and the slab casting which may be expressed as:

$$\Delta f_{pCR1} = n f_{cgp} \Psi_{t,tisc} (1 - \Delta F_{SC}/2F_o) \quad (5.23)$$

Stage 2 is the creep loss for any time after slab casting, which may be expressed as:

$$\Delta f_{pCR2} = n f_{cgp} (\Psi_{t,ti} - \Psi_{t,tisc}) (1-(\Delta F_{SC}+\Delta F_t)/2F_o) I_g/I_c \quad (5.24)$$

where, $\Psi_{t,ti}$ is creep coefficient of girder at any time; $\Psi_{t,tisc}$ is creep coefficient of girder at the time of slab casting; ΔF_{SC} = total loss at the time of slab casting minus the initial elastic shortening loss; F_o is prestressing force at transfer after elastic losses; ΔF_t is total prestress loss at any time minus initial elastic shortening loss; I_g/I_c is ratio of moment of inertia of prestressed girder to composite girder.

In the above equations, the terms $\Psi_{t,tisc}$ (1- $\Delta F_{SC}/2F_o$) and ($\Psi_{t,ti}$ - $\Psi_{t,tisc}$) (1- ($\Delta F_{SC}+\Delta F_t$)/$2F_o$) represent the effect of the variable stress history from the time of transfer to the time of slab casting and from the time of slab casting to the final conditions, respectively. The term I_g/I_c represents the effect of the composite section properties after slab casting.

The AASHTO LRFD Specifications recognize the prestress gain due to the deck weight by the term $7.0\Delta f_{cdp}$ in the creep equation. In the Modified Rate of Creep method, the creep response to slab and diaphragm dead load may be treated as a prestress gain. Part of the initial compressive strain induced in the concrete

immediately after transfer is reduced by the tensile strain resulting from permanent loads. The prestress gain due to slab dead load consists of two parts. The first part is due to instantaneous elastic prestress gain. The second part is a time-dependent creep effect. Prestress gain due to elastic and creep effect of slab casting is given by:

$$\Delta f_{pEG} = n_{SC} f_{S+D} \quad \textit{elastic prestress gain} \tag{5.25}$$

$$\Delta f_{pCRG} = n_{SC} f_{S+D} (\Psi_{t,ti} - \Psi_{t,tisc}) I_g/I_c \quad \textit{creep effect prestress gain} \tag{5.26}$$

where, n_{SC} is modular ratio at the time of slab casting; and f_{S+D} is stress in the concrete at the level of prestressing strands due to the dead load of the slab and diaphragms.

In composite prestressed girder bridges, the concrete in the girder is steam-cured while the concrete in the slab is usually cast-in-place and moist-cured. The slab concrete is also cast at a later time when the girders are in place. The free shrinkage of the slab exceeds the "unbonded" shrinkage plus creep of the top fiber of the precast beam following slab casting (which is usually the case). Due to differences in the concrete properties, curing processes, and times of casting, a prestress gain due to differential shrinkage occurs and is given by:

$$\Delta f_{pDS} = n_{SC} f_{CD} \tag{5.27}$$

where, f_{CD} is concrete stress at the level of the prestressing strands and is equal to $[\Delta\varepsilon_{S\text{-}G} A_{cSLAB} E_{cSLAB} / (1 + \Psi_{t,ti})] (y_{CS} e_c / I_c)$; $\Delta\varepsilon_{S\text{-}G}$ is differential shrinkage strain; A_{cSLAB} is area of concrete deck slab; E_{cSLAB} is modulus of elasticity of the slab; y_{CS} is distance between the c.g. of composite section and the c.g. of slab; e_c is eccentricity of the prestressing strands in composite section; and I_c is moment of inertia of the composite section.

The denominator $(1 + \Psi_{t,ti})$ approximates the long-term creep effect. Since this effect results in prestress gain, not loss, and is normally small, it can usually be neglected.

Chapter 6

COMPARISON OF MEASURED AND CALCULATED LOSSES

In order to be able to design safely and effectively using HPC, the differences between conventional concrete and HPC need to be understood. For example, design codes have not yet to incorporate formulas for the prediction of prestress losses in HPC girders. While the American Association of State Highway and Transportation Officials (AASHTO) Load and Resistance Factor Design (LRFD) bridge design code [45] can be used to design HPC bridges [50], the empirical formulas in the code were developed for conventional concrete (28-day compressive strength less than 6 ksi). To address this issue, AASHTO LRFD Section 5.4.2.1 indicates that concrete strengths above 10.0 ksi shall be used only when physical tests are conducted to establish the relationships between the concrete strength and other properties. As a result, continued research is needed to determine whether current code specifications are suitable for the prediction of prestress losses in HPC bridges, and if not, what modifications need to be made.

6.1 Background

In recent years, several experimental studies have been conducted that focus on prestress losses in HPC beams. In all of the studies, strains in the concrete were measured and used to assess the strain in the prestressing strands, and to evaluate prestress losses. While using concrete strains to assess prestress losses over the long-term is a relatively accurate method, it is difficult to investigate the short-term effect

of high heats of hydration on the prestress with this method. The difficulty arises due to the changing properties of the concrete through the curing process. It appears that prior to release, different assumptions have been made by different researchers regarding the state of stress in the strand. As a result, several researchers have evaluated short-term losses, and the data recorded during that period, quite differently. This in turn leads to inconsistent predictions of long-term prestress losses.

Two high strength concrete prestressed bridge girders were designed, instrumented, constructed and tested in Minnesota [51]. Each test girder was a 132.75 ft. long, 45 in. deep Mn/DOT 45M girder section reinforced with forty-six 0.6 in. diameter 270 ksi prestressing strands. The 28-day nominal compressive strength of the girders was 10,500 psi. Each girder was made composite with a 9-in. thick, 48-in. wide composite concrete deck cast on top of the beams with a nominal compressive strength of 4000 psi. Girder I was made from a concrete mix incorporating crushed limestone aggregate while Girder II utilized round glacial gravel aggregate in the mix with the addition of microsilica. In addition to investigating the two concrete mix designs, two different end patterns of prestressing (draping vs. a combination of draping and debonding), and two different stirrup configurations (standard Mn/DOT U vs. a modified U with leg extensions) were incorporated into the two test girders. Over 200 strain gages were imbedded in each girder during construction. After monitoring the concrete strain changes vs. time using vibrating wire strain gages, Ahlborn [52] calculated the prestress losses from the measured concrete strain. After assuming the concrete stress before release was zero, Ahlborn got the measured lower bound losses, which was regarded as measured prestress loss, shown in Table 6.1.

Table 6.1 Measured Lower Bound Losses

Time	Girder I - Limestone	Girder II - Glacial Gravel
Initial at release	15.5%	18.6%
28 days	21.6%	22.2%
Deck casting	23.9%	23.3%
Crack testing	26.6%	25.8%
Ultimate flexural test	27.2%	26.3%

French [31] also calculated the measured prestress losses from the recorded concrete strain (shown in Table 6.2) for the same beams.

Table 6.2 Measured Prestress Losses

Time	Girder I	Girder II
Release	14.5%	12.8%
28 days	20.7%	16.4%
Deck casting (200 days)	22.7%	17.7%
Cracking	25.6%	20.2%
Flexural testing	26.3%	20.7%

It can be seen that the measured prestress losses for girder II in Table 6.2 are much less than those in Table 6.1. It seems French assumed there was prestress gain in Girder II before transfer, because Girder II cracked before release. They found conventional modulus of elasticity relations overpredict the stiffness of high strength concrete which causes an underestimation of the girder elastic shortening at release.

At later ages, conventional concrete creep relations overpredict the concrete creep which results in an overprediction of the later losses.

Burns [28] et al. used vibrating wire gauges and bonded resistance strain gauges to measure concrete strain. They estimated total losses prior to release between 4% and 6%. A large component was due to the high heat of hydration. In their project, many beams remained in the casting bed for two days after casting, prior to release. They attributed the cracking prior to release to the high hydration temperature. Elastic shortening losses were significantly higher for HPC beams than for the normal concrete beams, because the HPC beams utilized a higher prestress force at release. When they calculated the prestress losses from the strain measurements, three parts were included: pre-release (estimated), elastic shortening, and long-term strain change. The measured and predicted long-term losses agreed reasonably well, with the measured losses typically being slightly lower than the predicted losses. Since almost all elastic shortening losses were higher than predicted, the prediction models must have overestimated the net time dependent losses after release. It is likely that the differences come largely from errors in estimating the material properties of the members, including modulus of elasticity and creep and drying shrinkage parameters.

Most recently, Barr et al. [53] published a report about HPC used in the Washington State SR 18/SR516 Overcrossing. Vibrating wire strain gauges were used in his project and the authors discussed the prestress loss due to temperature changes during curing. The loss was estimated to be between 3.5% and 6% of jacking stress. However, even though this loss was reported, when the total observed prestress losses were calculated, the loss due to temperature changes during curing was not taken into

account. The change in strain in the prestressing strands due to creep and shrinkage was computed by taking the average change in strain at the centroid of the prestressing strands and subtracting the strain due to elastic shortening. The total measured losses include relaxation, elastic shortening, creep and shrinkage. The observed prestress losses ranged from 12% lower to 9% higher than values calculated using the PCI method and were between 1 to 18% higher than values calculated using the AASHTO method.

All of the researchers agree that the measured prestress losses after transfer can be found by multiplying the strain change after release by the strand elastic modulus, imposing the strand relaxation. However, researchers do not agree on whether there is prestress loss due to high temperatures in addition to relaxation before transfer. Table 6.3 compares the work of the four researchers methods.

Table 6.3 Opinion Comparison About Prestress Loss Before Transfer (Except Relaxation)

Ahlborn [52]	French [31]	Burns [28]	Barr [53]
Beam cracked	Beam cracked	Beam cracked	N/A
loss ≥ 0%	No loss (gain)	Loss 4%-6%	Loss 3.5%-6%
Not included in the final measured losses	Prestress gain included in final measured losses	Included in final measured losses	Not included in final measured losses

6.2 The Sources of Prestress Losses

The accurate determination of prestress losses is important. An underestimate or overestimate of losses can affect service behavior such as camber,

deflection, and cracking, etc. In designing prestressed concrete beams, sources of prestress losses includes elastic shortening of concrete at transfer, relaxation of prestressed tendons before and after transfer, shrinkage of concrete after transfer, and creep of concrete after transfer. The AASHTO LRFD and PCI methods do not address the prestress loss caused by elevated temperature during curing.

Creep and shrinkage are not completely independent variables, but numerous investigations have indicated that considering these independently introduces only minor errors in stress prediction [54].

In this work, the time-step method for predicting prestress losses given by PCI and AASHTO LRFD was used. In every interval, creep and relaxation are taken to be independent of one another. However, between the intervals, their interdependence was taken into account.

Temperature will also cause thermal gradients. In order to minimize the effects caused by thermal gradient, in data reduction, we have chosen data at times when the temperature difference between the top and the bottom is less than 2 ^{o}F. Often it is in the early morning before sunrise.

Relaxation is defined as the loss of stress in a material that is placed under stress and held at a constant strain [55]. We have assumed that strand relaxation does not cause strain before transfer. The relaxation loss in low-relaxation steel is very low, less than 3% of the initial stress. The monitored strands were stressed 4 days before transfer. At transfer, 45% of the total estimated relaxation had taken place. Therefore, we have neglected the strain caused by relaxation after transfer.

6.3 Effect of Temperature on Prestress Losses

The plots of temperature and strain changes during curing are shown in Figure 6.1 to Figure 6.5. Note in figures that strain is on the Y1 axis (left) and temperature is on the Y2 axis (right). Recall that the gage numbers and locations are given in Fig.3.2 to Fig.3.4.

One can see that the temperature in the concrete for the beams peaked between 10 and 20 hours after the pour. It can also be seen in the plots that the strands were released at approximately 16 hours after casting, and that the concrete at that time was near its peak temperature.

It is interesting to consider the effect of the high temperature during curing. It can be seen that the stress in pretensioned strand decreases during the curing period as a result of the elevated temperature. After curing, when the heat reduces, the strands contract and regain some of the lost stress. The question that needs to be answered is, can it regain all of the losses associated with the initial high temperature during curing, or is there a permanent loss in prestress due to this process? There is a concern if the concrete has set and adhered to the steel while the temperature is still high, the strands may not be able to regain the loss caused by the thermal effects.

Podolny [56] have shown that the elevated temperatures during curing do cause short-term prestress loss (for NSC). Huang [35,57] proved that in an experiment. However, they indicated that these losses are recoverable once the temperature returns to ambient.

To understand the effect of temperature, first let us define values for the coefficient of thermal expansion for the concrete and the steel strand. According to ACI Committee 517 [58] and Khan et al. [59], the concrete coefficient of thermal

expansion varies by a factor of ten during the first few hours after casting, but decreases to be relatively stable after about 16 hours. In this study, the thermal coefficient of concrete is taken to be $5.5 \times 10^{-6}/^{\circ}F$. The coefficient of thermal expansion for steel is taken to be $6.7 \times 10^{-6}/^{\circ}F$.

To further understand the phenomena show in Figures 6.1 to 6.4, we will first consider an illustrative example in which we will plot the strand strain versus time (recall that strandmeters were used to measure strand strain versus time directly). In the example, we will assume that the strand strain is affected by temperature, elastic shortening and creep and shrinkage. We will neglect the effect of relaxation (since it is quite small). Figure 6.7 (a, b, and c) show typical strand strain response due to the important phenomena. Figure 6.7a illustrates the effect of temperature on the strand. When the temperature goes up due to hydration heat, the strand relaxes showing a decrease in tension (negative strain). The temperature recorded for beam B7(4), combined with the given coefficient of thermal expansion was used to generate this plot. Figure 6.7b illustrates the effect of elastic shortening followed by creep. For this figure, the value for elastic shortening was selected based on the measured values. Figure 6.7c shows the effect of shrinkage. The creep and shrinkage curves were based on empirical formulae developed at University of Texas at Austin [28].

Having generic strain time history response for each of the phenomena, they can now be combined to get a hypothetical total response. To illustrate the effect of temperature, we will combine the effect in two ways. First we will assume that the strands are released near the peak temperature. Next we will assume the strands are released after the concrete has cooled. In both cases, elastic shortening, creep, and shrinkage are assumed to begin immediately after release. Figure 6.7d shows the

resulting two hypothetical responses. One can see that in both cases, the losses are identical once the concrete returns to ambient temperature. If the concrete returns to ambient temperature before release (Case B, Fig. 6.7d), the effects of temperature will not affect the strain readings after transfer. However, this is not typically the case since release is performed as soon as possible. Therefore, the curve associated with release occurring near the peak temperature is more typical (Case A, Fig. 6.7d). In fact, this curve looks very similar to the data recorded by the strandmeter and shown in Figure 6.1 and Figure 6.4. In this case, the strand has a prestress loss at the time of transfer, and after the elastic shortening, actually shows a prestress gain. This gain occurs because the effects of cooling and associated re-tensioning of the strand outweigh the losses due to creep and shrinkage. As a result, one must be very careful when interpreting strain data for the purpose of determining prestress losses. Assuming that the strain at release is zero (i.e. the strand stress is the jacking stress minus relaxation) is not necessarily true. The actual strand stress at release can be far lower due to thermal effects. The thermal effects will be reversed once the beam cools, and if one assumes zero strain at release, the apparent prestress gain observed when the strand cools will lead to inaccurate loss calculations.

The illustrative example shows the usefulness of the strandmeter. Since strand strains are measured directly, the basic phenomena can easily be studied. One can easily eliminate the effects of temperature and elastic shortening. This isolates the effects of creep and shrinkage.

In terms of the sister bars, one can see that they also indicate negative strains during the time when the concrete is at elevated temperatures, and do not have a zero strain at transfer. This is likely due to the fact that as the temperature goes up,

the concrete tries to expand, but it can not, because it is confined by the forms. In cases prior to transfer when the top and bottom sister bar recorded different compressive strains (like beam B5), it was observed that temperatures recorded by the two gages varied by the amount necessary to cause the difference. For beam B7(8), where the sister bars at top and bottom showed similar compressive strains, the temperatures recorded by the two gages were very similar.

It is interesting to note that both the strandmeter and sister bar give similar strains once the concrete returns to the ambient temperature.

After studying an HPC bridge located in Kent, Washington, Stanton et al. [25] believed that the temperature changes during fabrication may cause a permanent prestress loss. In that case, the strands were stressed in cold weather, then they were heated by the curing of the surrounding concrete, which must have caused the strand stress to drop. During the time at high temperature, the strand bonded to the concrete, after which the concrete and steel cooled and shortened together. If the two materials have the same coefficient of thermal expansion, no mechanical strain change, and therefore no stress change, would be induced by cooling. Therefore, temperature changes during fabrication would induce a permanent prestress loss. The thermal loss was estimated to exceed both the relaxation and shrinkage losses.

Stanton et al. did not have sufficient measurements to verify a thermal loss. Our test results agree with the conclusions of Huang and Podolny that the thermal loss is recoverable. Current design procedures seem to back up this hypothesis in that they do not account for such loss.

It appears that some researchers have assumed that the strand and concrete have the same strain change after transfer. In making this assumption one can reach

the wrong conclusion that the thermal losses are not recoverable. When temperature changes, the strand and concrete do not have the same strain change.

Now another question arises. If the thermal loss is recoverable when the temperature goes down, when temperature goes up, shouldn't the loss occur again? In other words, does the prestress loss change with the ambient temperature? In fact, it is true and is verified by the test data. In Figure 6.2, 6.3, and 6.6, this phenomenon can be seen very clearly. In September, October and April, the ambient temperature was relatively stable. However in May (May 1 was the 210^{th} in B7(4) and 200^{th} in B7(8)), the temperature went up dramatically and causing a prestress loss. However, the strain from the sister bar wasn't effected by the temperature change. In strandmeter 15670 in B7(4), when the temperature increased from 53 °F to 78 °F, the strain decreased from –455 ppm to –573 ppm. This means that a 25 °F elevated temperature caused a 118 ppm. Every elevated degree caused about 4.7 ppm compressive strain. Likewise, in strandmeter 15669 and 15667 in B7(8), 28 °F and 29 °F increase in temperature caused 129 ppm and 135 ppm compressive strain respectively. Every temperature change caused about 4.7 ppm strain. One may say that this change in strain is caused by the difference of thermal coefficients between strandmeter and strand. However, the maximum coefficient difference is less than 1.7 ppm/ °F (in fact, this difference has been taken into account in data reduction). Therefore, there must be other reasons.

In the strands in B7(8), at about 195 days, the measured strain and temperature from strandmeter 15667 are –605 ppm and 47.8 °F respectively. At about 209 days, the measured strain and temperature are –740 ppm and 77 °F respectively. Every increased degree caused about 4.7 ppm compressive strain in the strand. However, the strain from the sister bar was not affected by the temperature changes.

The assumption that after transfer the strand and the concrete are bonded together and have the same strains does not match the test results.

From the test data, every degree of increased temperature can causes about 4.7 ppm compressive strain. Assuming the biggest temperature change from the winter to the summer is 70 °F, then the prestress loss in summer is about 9.5 ksi ($70\times4.7\times29000\times10^{-6}$) less than that in the winter. Under the same condition, the temperature can cause a 2.4% average pretress loss variation.

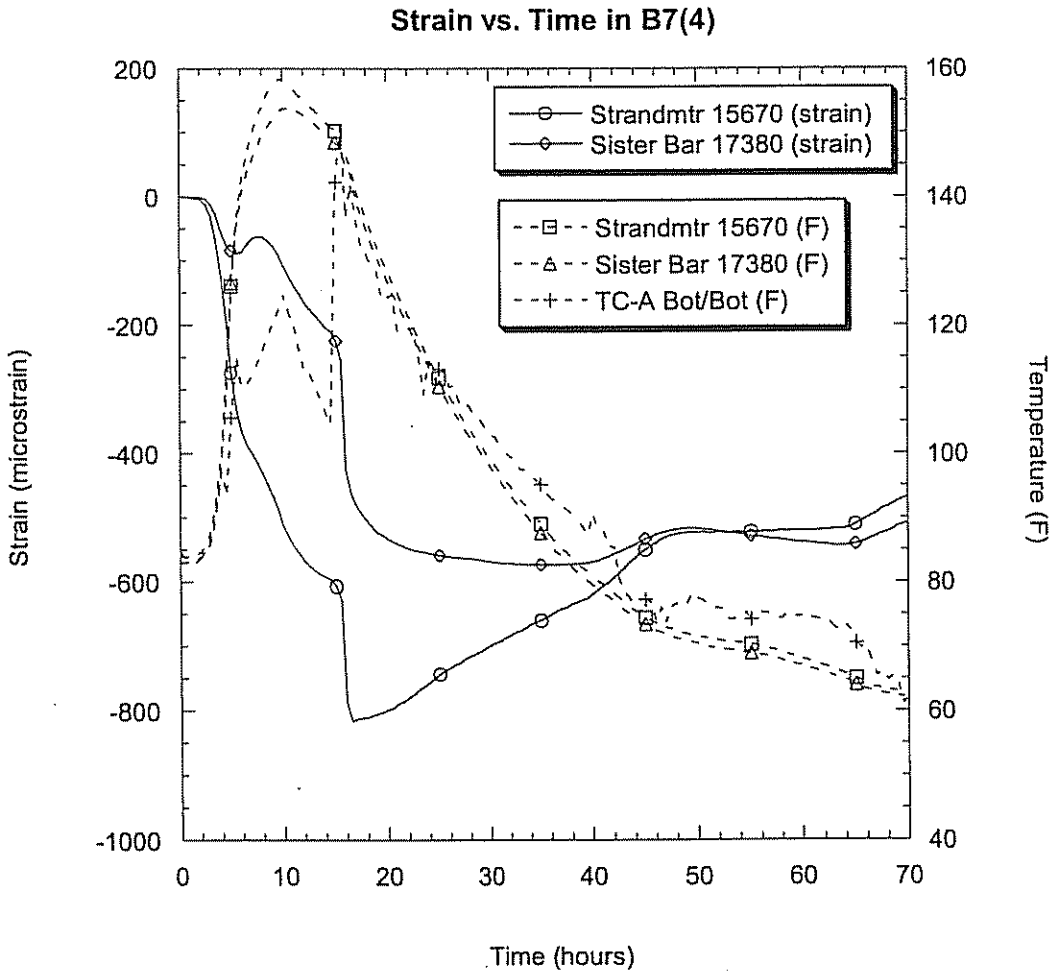

Figure 6.1 Strand Strain and Temperature vs. Time in B7(4) (A)

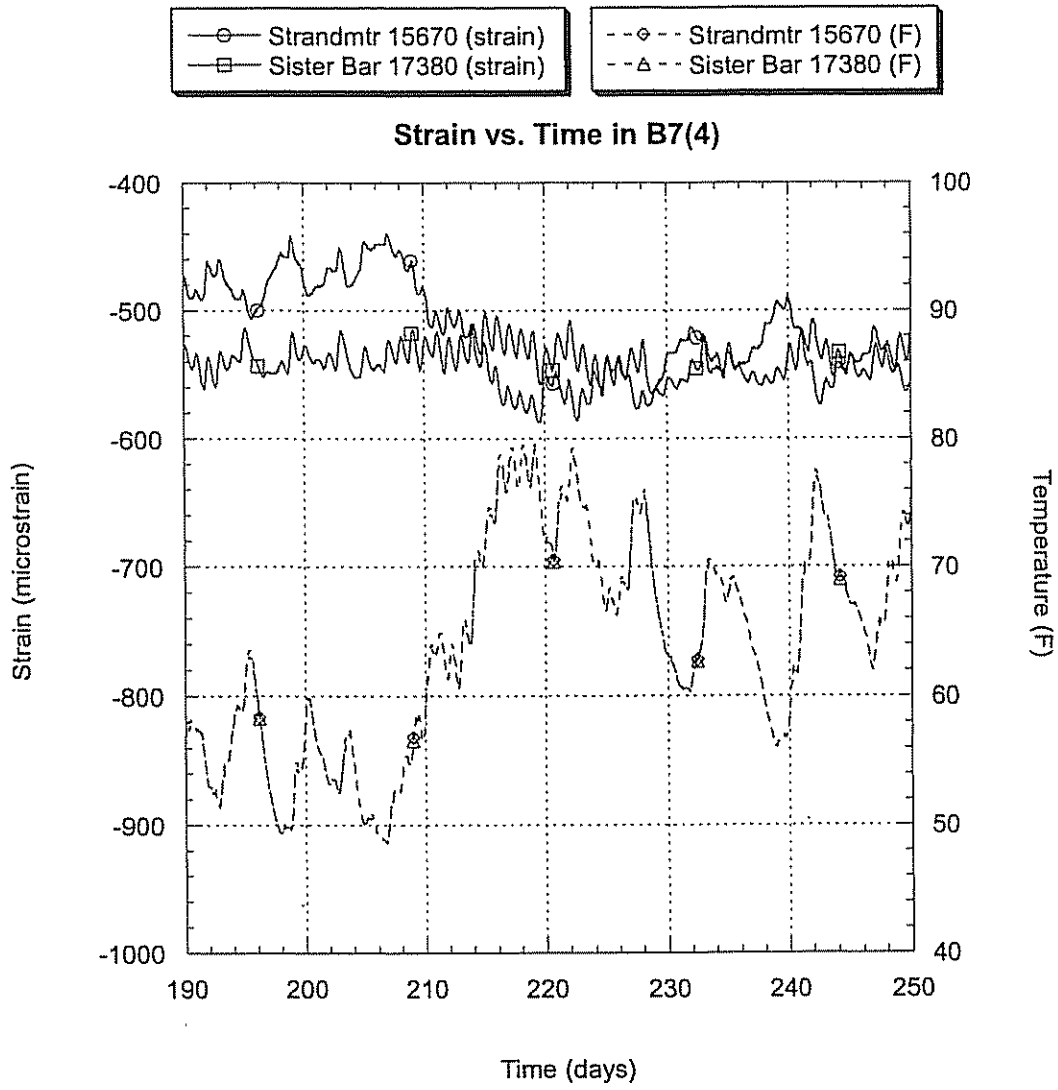

Figure 6.2 Strand Strain and Temperature vs. Time in B7(4) (B)

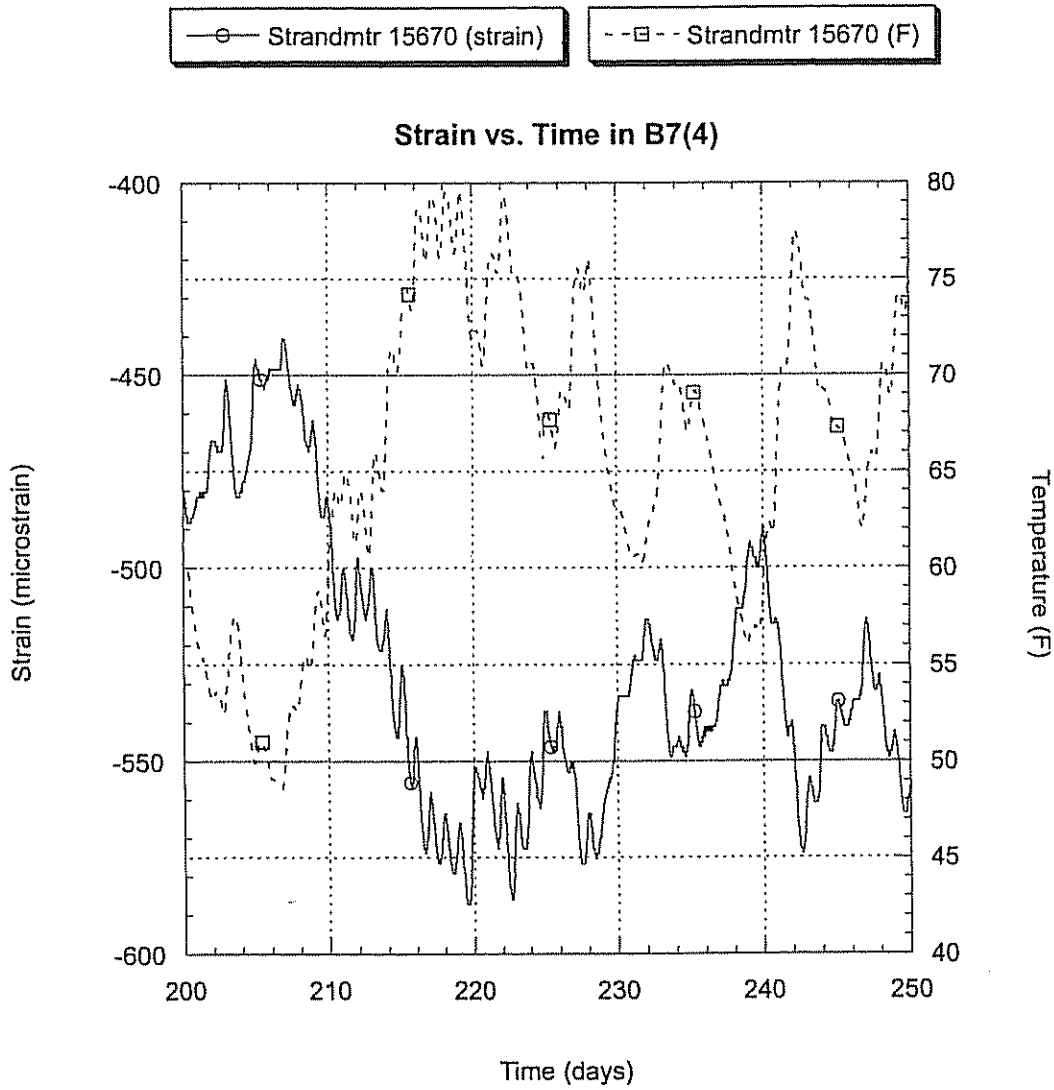

Figure 6.3 Strand Strain and Temperature vs. Time in B7(4) (C)

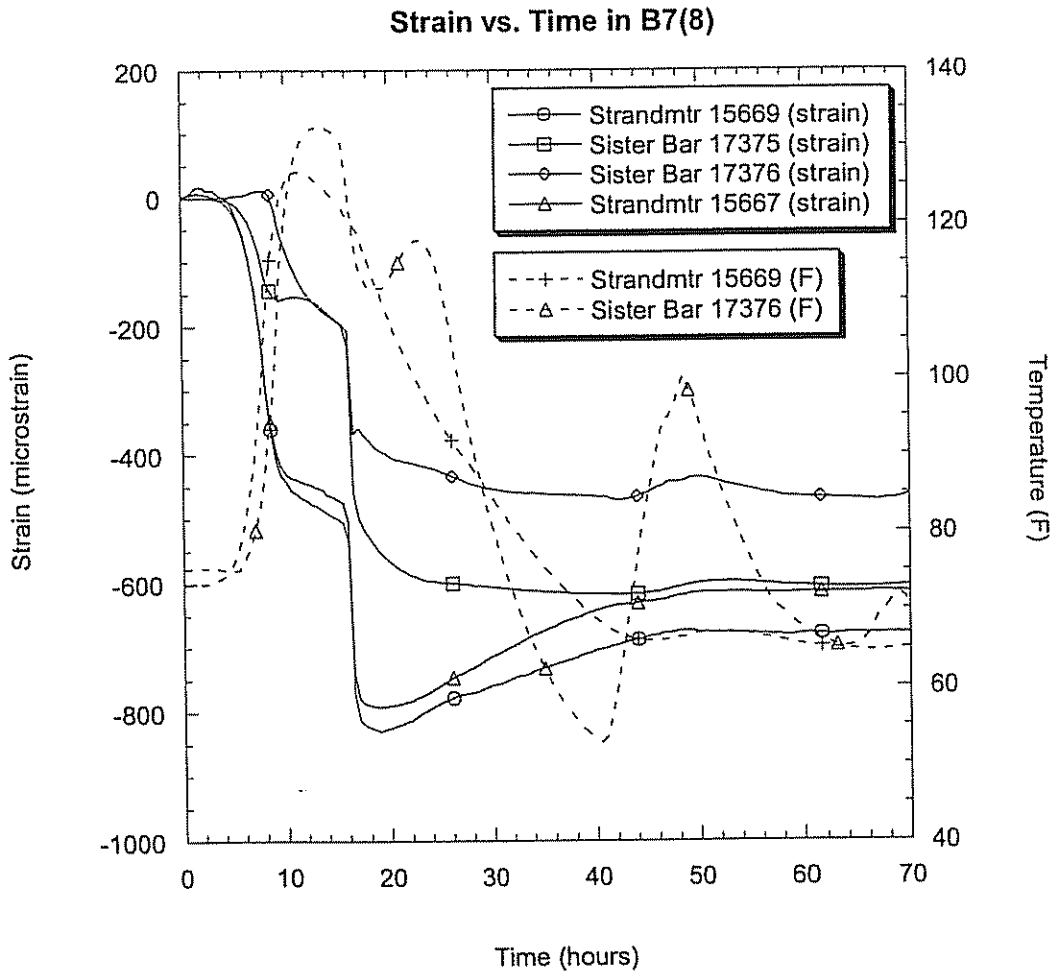

Figure 6.4 Strand Strain and Temperature vs. Time in B7(8) (A)

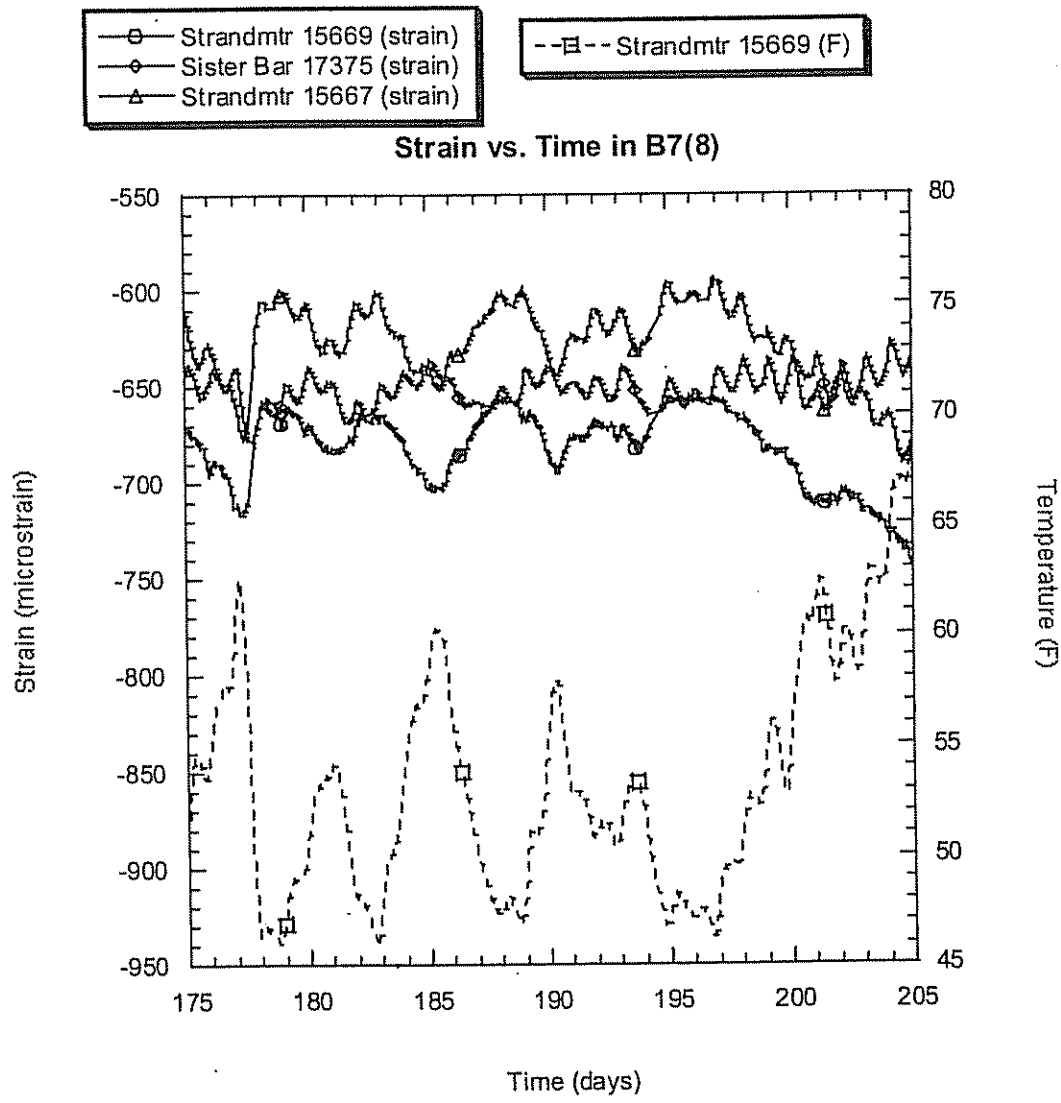

Figure 6.5 Strand Strain and Temperature vs. Time in B7(8) (B)

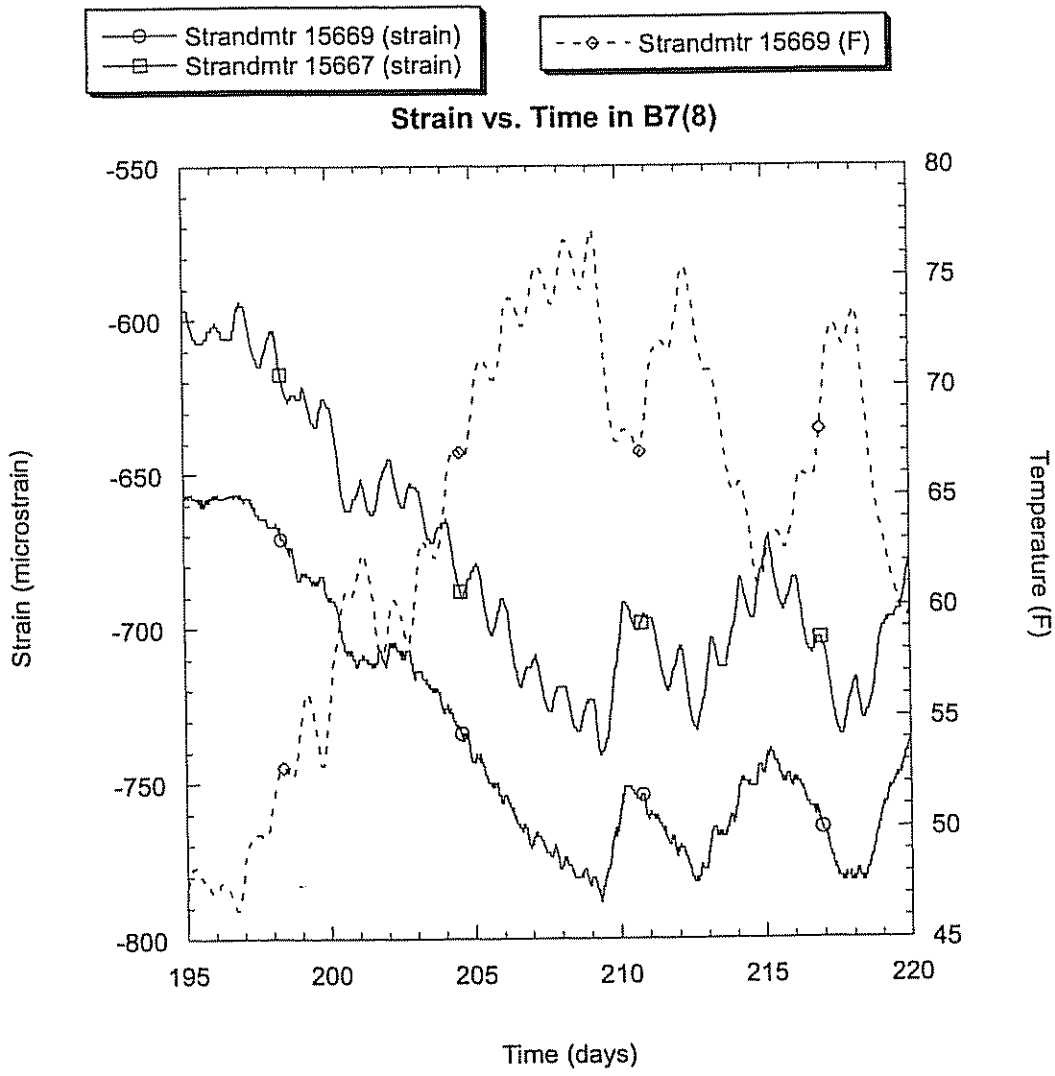

Figure 6.6 Strand Strain and Temperature vs. Time in B7(8) (C)

a)

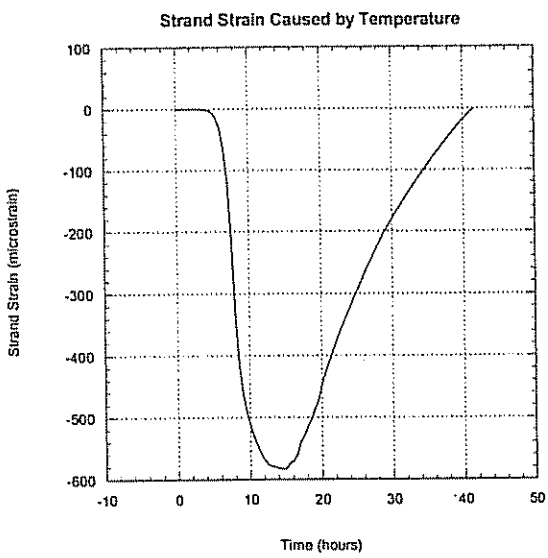

b)

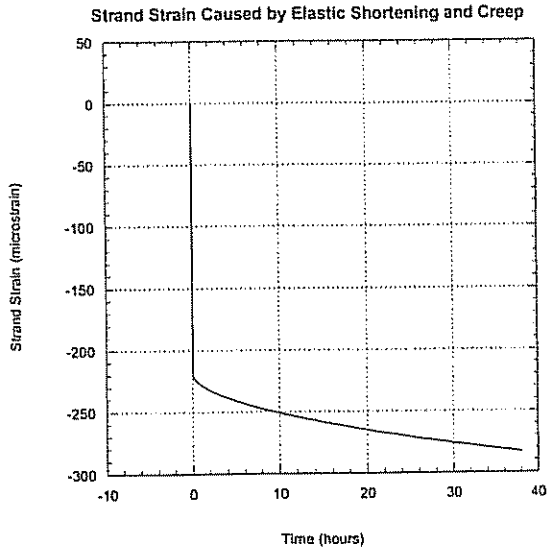

c)

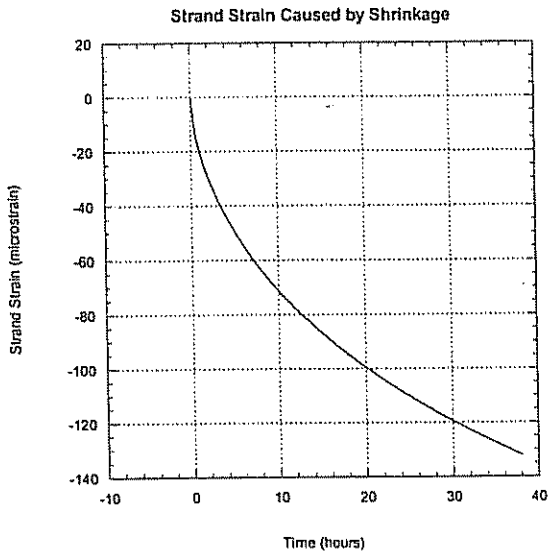

d)

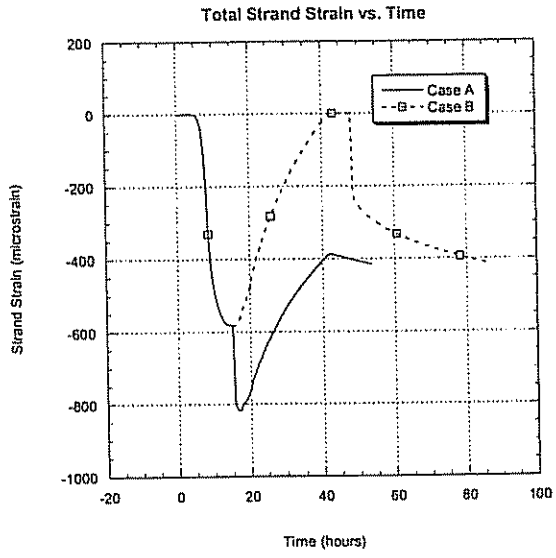

Figure 6.7 a) Strand Strain Caused by Temperature; b) Strand Strain Caused by Elastic Shortening and Creep; c) Strand Strain Caused by Shrinkage; d) Total Strand Strain vs. Time

6.4 Prestress Losses

One can calculate the prestress losses by multiplying the average measured strain by the elastic modulus of the steel, and imposing the steel relaxation. In low relaxation strands, the prestress loss caused by relaxation is very small. Any prediction method will introduce little difference in the total calculated prestress losses. The elevated temperature during curing has been shown to cause a prestress loss, but it is recoverable when the temperature goes down. Therefore, when calculating the prestress losses from measured strains, one should use all measured strain, including the strain before release. If not, one may underestimate the prestress losses, because the strain after transfer includes the recovery strain caused by the lowering tempearture.

AASHTO LRFD doesn't give a formula to predict steel relaxation during a period [t_1, t] after transfer. So the following equation given by the PCI Committee Report [48] is used.

$$RET = f_{st}\{[log24t - log24t1]/45\} \times [f_{st}/f_{py} - 0.55] \quad (6.1)$$

where, $f_{st}/f_{py}-0.55 \geq 0.05$; $f_{py} = 0.9\ f_{pu;}$; f_{st} is stress in prestressing steel at time t_1 (psi); f_{py} is stress at 1% elongation of prestressing steel (psi); t is time at end of time interval (days); t1 is time at beginning of time interval (at the time of anchorage; t_1 shall be taken as 1/24 of a day so that $logt_1$ is zero) (psi).

Using this formula to estimate the relaxation losses before transfer, the estimated value will be 11% less than that from AASHTO LRFD. In order to be consistent, Equation 6.1 is used to estimate steel relaxation before and after transfer.

The measured and predicted prestress losses at different times are shown in Table 6.4.

Table 6.4 Comparison of Prestress Losses at Different Times (ksi)

Beam	Items	Elastic Shortening	After Transfer	7 days	14 days	28 days	180 days	240 days	365 days	End of life
B5	PCI	6.7	9.2	14.1	15.5	17.5	23.3	24.3	26.5	31.3
	AASHTO (step by step)		9.2	11.6	12.9	14.9	23.2	24.4	26.0	31.8
	AASHTO (refined)		9.5	...	...	...	...	...	...	32.7
	B5 (measured)	**	**	20.9	22.5	23.0	**	24.1	**	**
B7	PCI	5.8	8.3	12.9	14.3	16.1	21.7	22.6	24.6	29.3
	AASHTO (step by step)		8.3	10.5	11.8	13.7	21.6	22.8	24.4	30.0
	AASHTO (refined)		8.6	...	...	...	...	...	...	30.3
	B7(4) (measured)	6.5	26.1*	17.6	**	**	19.1	**	**	**
	B7(8) (measured)	6.8	24.4*	20.6	21	**	22.9	**	**	**

- * The strandmeter and sister bar yielded significantly different strains. These values were calculated based on the strains from strandmeter.
- ** No measured data is available.

Let us now discuss the results shown in Table 6.4. First, we should recall that the initial jacking stress for the strands was 202.5 ksi. Comparing the losses in Table 6.4, we can see that the elastic shortening loss is on the order of 3% of the initial stress and is relatively well predicted for the HPC beams (within 15% of the measured value). Immediately after transfer, the predicted loses are due to a combination of relaxation and elastic shortening. However, unlike the predicted values, the temperature effects affect the measured values. As a result of the short-term losses

due to thermal effects, the measured losses just after transfer (approximately 25 ksi or a loss of 12%) are much larger than the predicted values (approximately 8.3 ksi or a loss of 4%). Between the time of transfer and 28 days, the concrete quickly returns to ambient temperature and the associated thermal losses are recovered. Over this time segment, the significant losses are due to creep and shrinkage. It can be seen that during this time, both the AASHTO and PCI equations underestimate the prestress losses. At 28 days, the measured losses are roughly 22 to 23 ksi which corresponds to a loss of 11% while the predicted losses range from 14 to 17 ksi which corresponds to losses ranging from 7 to 9%. It is interesting to note that even the predicted AASHTO and PCI values differ significantly from each other.

The larger than predicted losses during the first 28 days may be due to the observation that creep and shrinkage of HPC occurs much faster than it does for conventional concrete. While these effects occur more quickly, it has also been observed that HPC has almost the same long-term shrinkage as conventional concrete [2].

After approximately one half a year, the AASHTO and PCI equations give nearly identical predicted values, and these values match the measured values quite well. For beam B5, at 240 days, the measured loss is 24.1 ksi or a loss of 12%. The predicted values from PCI and AASHTO are 24.3 ksi and 24.4 ksi respectively (difference of only 1%). For the B7 beams, at 180 days, the average measured loss is 21 ksi or a loss of 10%. The predicted values from PCI and AASHTO are 21.7 ksi and 21.6 ksi or a loss of 11%.

Chapter 7

CONCLUSION AND RECOMMENDATION FOR FUTURE WORK

7.1 Conclusions

Compared with conventional concrete, HPC has many advantages. It is stronger, allowing bridges to have longer spans and fewer girders. Increasing the span length can reduce the number of piers and foundations, thereby reducing the substructure cost. Superstructure costs are minimized through the use of fewer girders. Furthermore, HPC is more durable than conventional concrete primarily because it is less permeable, making bridges more resistant to damage caused by freeze-thaw cycles, deicing salts, etc. According to the Federal Highway Administration (FHWA), the average service life of all types of bridges is 42 years. It has been estimated that HPC bridges may last 75 to 100 years with fewer repairs and thus reduced life-cycle costs. The project discussed herein has been studying an HPC bridge and attempts to validate some of the attributes of HPC, and to see whether existing codes can be used to design HPC bridges, or should be modified.

7.1.1 Material Properties

Based on the test data in this project, the following conclusions can be drawn.

- The test results of compressive strength were compared to predictions made using ACI 209R-92. It is found that ACI 209 does a good job of predicting the HPC strength.

- The elastic modulus test results were compared with the predictions made using AASHTO and ACI 363R-92 formulae. ACI 363R-92 agrees better with the test results than does the AASHTO formulae which overestimate the value of the elastic modulus. It should be noted that in other state projects, ACI 318 was more accurate in some cases, while ACI 363 was more accurate in other cases. Sometimes neither gave good prediction. This may be because the modulus of elasticity of concrete is not a function of compressive strength alone. Other effects on the modulus of elasticity included the type of aggregates and the percentage of coarse aggregates.
- Modulus of rupture test results were compared with predications made using AASHTO and ACI 363R-92 formulae. In this case the ACI equation proved to be fairly accurate while the AASHTO formula underestimated the modulus of rupture for the HPC.
- The equation for the prediction of the splitting tensile strength from AASHTO and ACI 363R-92 both overestimated the splitting tensile strength from 16% to 52%.
- Low permeability and high strength concrete can be obtained in Delaware with locally available materials.
- Ongoing corrosion monitoring will help to establish the long-term durability of the HPC.

7.1.2 Structural Behavior

The elevated temperature during curing causes the strand stress to decrease significantly. However, the loss was shown to be recoverable upon cooling. Adherence of the concrete to the strand in a precast girder does not prevent the steel from regaining its thermal loss of stress upon cooling.

The effect on strain measurements of the hydration heat depends upon when the strands are released relative to the heating and cooling cycle.

The strand stress was shown to change with the temperature. In summer, the temperature goes up, and the stress goes down; in winter, the temperature goes down, and the stress goes up. Given the same condition, the thermal loss variation may reach ±2.4%.

In terms of short-term losses (less than 28 days), current AASHTO and PCI equations for conventional concrete underestimated the prestress losses. This may be because creep and shrinkage occur much faster for HPC than they do for conventional concrete.

In terms of long-term losses (after half a year), AASHTO and PCI equations for conventional concrete yield very accurate loss predictions. In the study reported, the losses occuring after one-half a year were measured to be between 10 to 12%, reasonably closed to the predicted losses (11%).

Vibrating wire strandmeters seemed to be a very effective method for monitoring both short- and long-term prestress losses.

7.2 Recommendation for Future Work

From the test result in this case, it can be seen that the thermal loss caused by the elevated temperature during curing is recoverable, and ambient temperature changes can cause fluctuation in losses over time. This phenomenon isn't well understood and needs to be investigated further.

Many of the design provisions in the AASHTO Standard Specifications for Highway Bridges are based on knowledge and experience with normal concrete. With the introduction of high performance concrete, the applicability of these provisions needs to be reassessed. Items that can be investigated with live load tests include impact factors, lateral load distribution, shear lag, and vertical deflections.

In order to make a comparison between the life cycle costs of conventional concrete bridges and HPC bridges, the continued monitoring of Bridge 8F is necessary.

For HPC to be used more extensively, information about HPC and Bridge 8F needs to be widely disseminated.

Increasing emphasis is being placed on the durability of HPC and not on high strength. In many applications, high strength concrete is used only because of its high durability quality rather than the need for its strength. There has been an enormous amount of research performed on durability of concrete, but without much correlation largely because the properties are "material specific" and dependent on test methods. There is an urgent need for new and improved test methods that would provide more consistent correlation between the laboratory and field results so that the data on durability can be better quantified. More research is needed to develop a rational design methodology for durability [2].

In New York State, all new and replacement bridge decks built using the HPC concrete from 1995 through early 1998 were inspected. The result revealed that 51 percent of the 84 inspected decks exhibited cracking. Of these cracked decks, over fifty percent began cracking within 14 days of the concrete placement [60]. Deck cracking is common in all of the states. There are also many cracks in the deck of Bridge 8F. The reasons for the deck cracking need to be investigated and something needs to be done to help reduce or eliminate the cracking.

Appendix: Static Truck Load Test on Bridge 8F

One static load test was conducted on the bridge 8F in Frederica on the morning of August 2, 2001. The Strandmeters and Sister Bars installed in three beams (labeled B5, B7(4), and B7(8)) during fabrication were used to measure the strain changes. A DataTaker 615 and a laptop were used to collect the test data.

Load Cases

2 DelDot trucks filled with sand were used to load the bridge. The weight and dimensions of each truck were measured prior to the test (see Fig. 1). To examine various responses, different truck positions were implemented. For single-lane loading, 4 different load cases were used. For two-lane loading, 3 loading cases were used. The different load cases are shown in Fig. 2 and the positions of the gages in the three monitored beams are shown in Fig. 3.

Test Results

In every load case, the strain in every gage was measured three times. And their average values are shown in Table 1. B7(4) is the middle beam. Because of symmetry, strains in B7(4) meet Case 1=Case 4, Case 2=Case 3, Case 5=Case 7. Considering the elastic shortening at stress transfer was over 200 microstrain, the strains caused by the trucks were small. It is reasonable to assume that the strains were in beam elastic range. So superposition of strains is applicable. From Fig. 2, it can be seen that the superposition of Case 1 and 2 is Case 5. The superposition of Case 3 and 4 is Case 7. And the superposition of Case 2 and 3 is Case 6. Their comparison is shown in Table 2. The values from superposition are very close to the direct test results. So the superposition is justified.

At the same location, Strandmeter and Sister Bar gave a little different reading. It may be due to system error. In calculating the neutral axis (N.A.) and distribution factor (D.F.), their average (shown in Table 3) will be used. From Case 1 to Case 7 the ratios of bottom to top strain are reasonable close. Since small strains are susceptible to

experimental error. When the strain is less than 3 microstrain, it will not be taken into account in calculating the average ratio. From plane assumption, in B5, the measured neutral axis is 19.3 in. from the section bottom. The theory value is 17.4 in. It may be due to the concrete parapet. It causes the N.A. to move up. In B7(8), the measured neutral axis is 20.3 in. from the section bottom. The expected value is 20.6 in. They are very close. So the plane assumption is justified. It should be noted that the bridge deck was cast-in-place. In calculating the theoretical locations of neutral axis and moment of inertia, the full composite effect was considered.

The measured distribution factor is the ratio of the maximum measured moment in a girder during a pass divided by the maximum theoretical moment determined by applying the trucks per lane to a single girder. The measured moment M can be got from the following equation,

$$M = E I \varepsilon / y$$

Where, E is the measured concrete elastic modulus at 28 days; I is the moment of inertia of composite beam; ε is the measured average concrete strain; y is the distance between neutral axis and the gages.

The comparison between measured D.F. and calculated D.F. from LRFD is shown in Table 4 and Table 5. It should be noted that Table 4 is for single-lane loading, and Table 5 is for two-lane loading. It can be seen that the LRFD overestimates the D.F. under single-lane and two-lane loading.

From an engineer's judgment, the maximum D.F. should be from Case 8. But for the reason of bridge safety, the case was not conducted. It has just been proved that the superposition is applicable. Case 8 can be got by the sum of Case 1, 4 and 6 or the sum of Case 5 and 7. The results of superposition are shown in Table 6. They are very close. Their average value will be used to calculate D.F. under multi-lane loading. The comparison between measured and calculated D.F. is shown in Table 7. It can be seen that under multi-lane loading the measured and calculated D.F. are reasonable close for interior beams. But for exterior beams, LRFD is conservative.

Using the D.F. from LRFD, one can also get the theory strains under single-lane and multi-lane loadings. The comparisons between measured and calculated strains are shown in Table 8. In estimating the strains caused by single-lane loading, the LRFD is conservative. But it doesn't matter. The controlling case is multi-lane loading. In interior beams, the calculated maximum strain is 53 microstrain. The maximum test value is 43 microstrain. They are reasonably close. In exterior beam, the expected value is 103 microstrain. The test value is 43 microstrain. It may be due to the participation of the concrete parapet.

Conclusion

Based on the test results, the following conclusions can be drawn.

1. The stress caused the passing trucks is in the elastic range. The bridge behaved linearly. So strain superposition is applicable.
2. The measured and calculated neutral axis in interior beam are very close. The difference in exterior beam may be due to the concrete parapet.
3. Under multi-lane loading, in interior beams the measured D.F. is reasonably close to the D.F. from LRFD. For other cases, the LRFD is conservative.

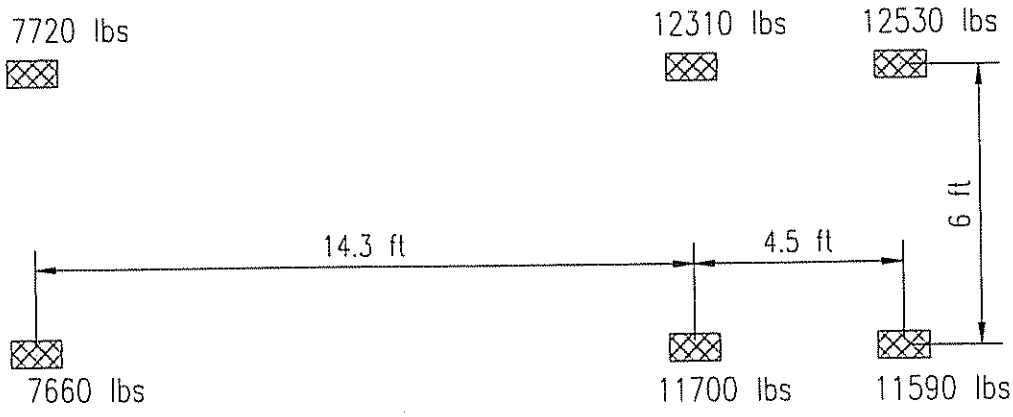

Dimension and weight of truck 2736
(Total weight 63510 lbs)

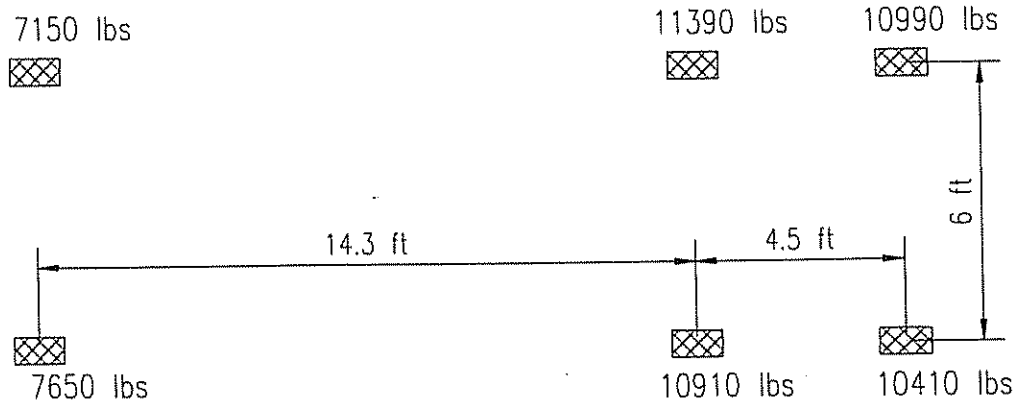

Dimension and weight of truck 2846
(Total weight 58500 lbs)

Figure 1 The Dimensions and Weights of Trucks

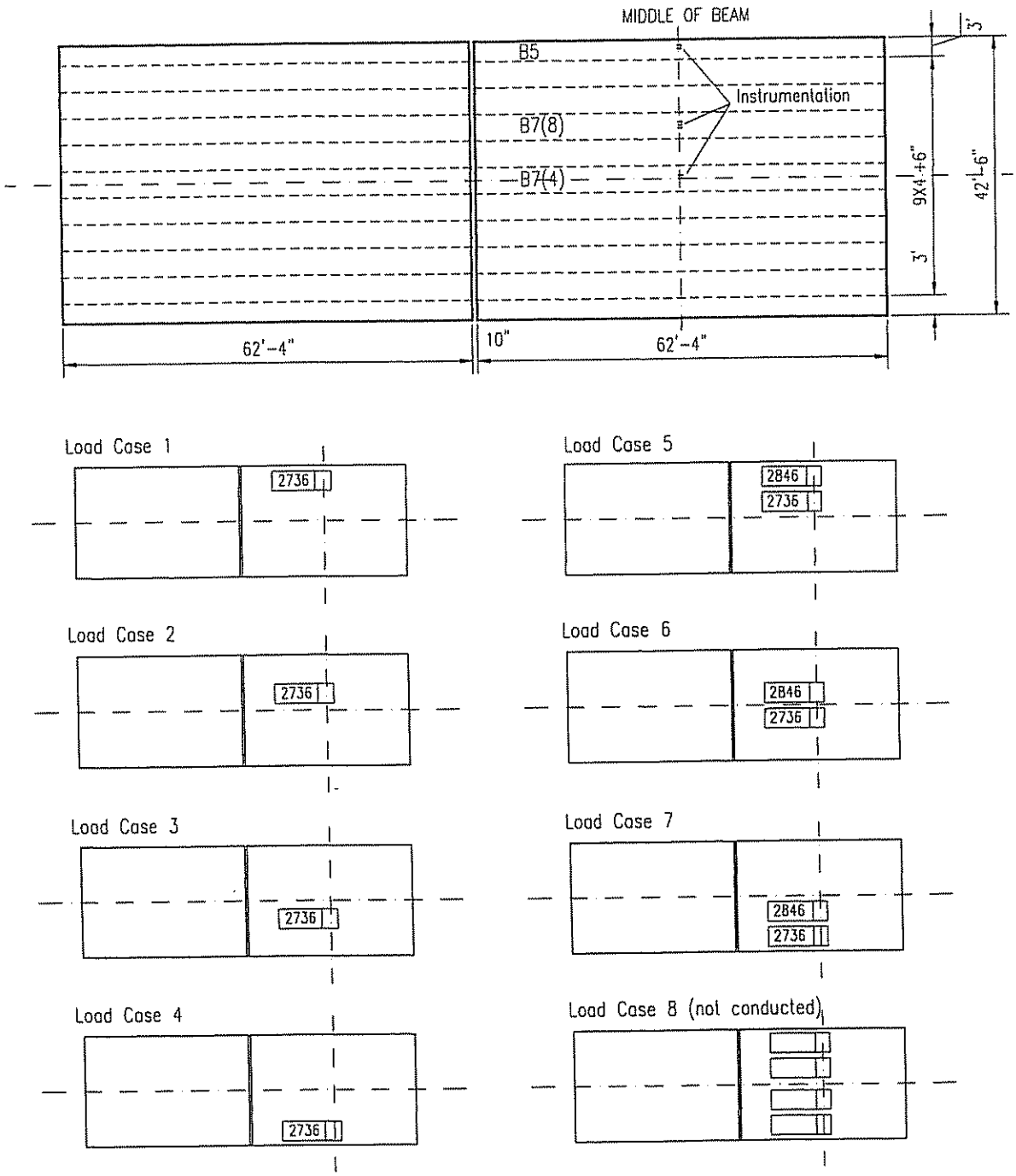

Figure 2 Truck Locations during Load Tests

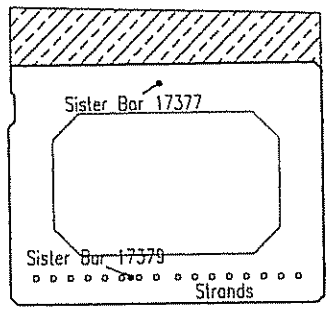

Positions of Sister Bars in B5

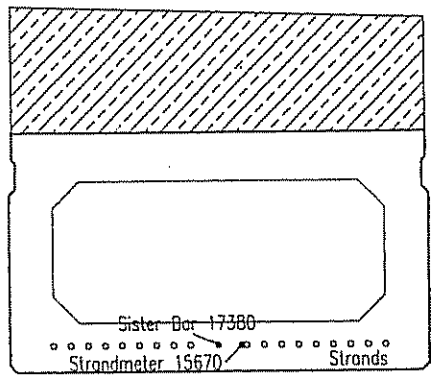

Positions of Strandmeter and Sister Bars in B7(4)

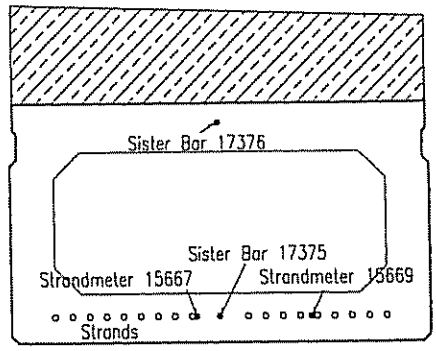

Positions of Strandmeters and Sister Bars in B7(8)

Figure 3 Positions of Gages

APPENDIX

Programs Used in DataTaker 615

The program used to monitor girder B5 is shown below:

```
;P31=2
;P36=1
;D=\D
;T=\T
;BEGIN
; RA30M
; 6TT("AMBIENT")
; 1FW 1+YS05("STRANDMTR 15668")
; 2FW 2+YS05("SISTER BAR 17379")
; 3FW 3+YS05("SISTER BAR 17377")
; 4TT("B5 CYL POUR2")
; 5TT("B5 CYL POUR3")
; 10-TT("TC-A BOT/BOT")
; 10+TT("TC-B TOP/BOT")
; 10*TT("TC-C BOT/BOT")
; 9TT("TC-D TOP/TOP")
; 8V("CORROSION")
;END
;LOGON
```

;G

The program used to monitor girder B7(4) is shown below:

;P31=2

;P36=1

;D=\D

;T=\T

;BEGIN

;RA30M

; 4TT("AMBIENT")

; 1FW 1+YS05("STANDMTR 15670")

; 2FW 2+YS05("SISTER BAR 17378")

; 3FW 3+YS05("SISTER BAR 17380")

; 5TT("B5 CYL POUR2")

; 6TT("TC-A BOT/BOT")

; 7TT("TC-B TOP/BOT")

; 8TT("TC-C BOT/TOP")

; 9TT("TC-D TOP/TOP")

; 10V("CORROSION")

;END

;LOGON

The program used to monitor girder B7(8) is shown below:

;P31=2

```
;P36=1
;D=\D
;T=\T
;BEGIN
;RA30M
; 1FW 1+YS05("STANDMTR 15569")
; 2FW 2+YS05("SISTER BAR 17375")
; 3FW 3+YS05("SISTER BAR 17376")
; 4FW 4+YS05("STANDMTR 15667")
; 5V("CORROSION")
; 6TT("TC-A BOT/BOT") CYLINDER
; 7TT("TC-B TOP/BOT")
; 8TT("TC-C BOT/TOP")
; 9TT("TC-D TOP/TOP")
; 10TT("AMBIENT")
;END
;LOGON
```

After all of the three beams were cast and removed from the bed, they were moved and stored at the CBS yard next to each other. Each beam was supported on two wood beams and simultaneously monitoring of all three beams began. Because the number of channels in the DataTaker being used was limited to ten channels, only strandmeters and sister bars were monitored during the time they were in the yard. The program used is shown below:

;P31=2

;P36=1

;D=\D

;T=\T

;BEGIN

; RA30M

; 1FW 1+YS05("B5 STRAND 15668")

; 2FW 2+YS05("B5 SISTER 17379")

; 3FW 3+YS05("B5 SISTER 17377")

; 4FW 4+YS05("B7(4) STRAND 15670")

; 5FW 5+YS05("B7(4) SISTER 17378")

; 6FW 6+YS05("B7(4) SISTER 17380")

; 7FW 7+YS05("B7(8) STRAND 15569")

; 8FW 8+YS05("B7(8) SISTER 17375")

; 9FW 9+YS05("B7(8) SISTER 17376")

; 10FW 10+YS05("B7(8) STRAND 15667")

;END

;LOGON

Delaware Center for Transportation
University of Delaware
Newark, Delaware 19716